UNC-5086

MINIMUM WEIGHT SHIELD SYNTHESIS FOR SPACE VEHICLES

F. R. Nakache
A. D. Krumbein
J. Celnik
J. Certaine

A. D. Krumbein: Project Scientist

May 20, 1964

Work Performed under UNC Project 2195
Contract No. NAS 8-5277 with
George C. Marshall Space Flight Center
NASA, Huntsville, Alabama

GPO PRICE $ _____

OTS PRICE(S) $ _____

Hard copy (HC) 4.00

Microfiche (MF) 1.00

UNITED NUCLEAR CORPORATION
DEVELOPMENT DIVISION
5 New Street
White Plains N Y

UNC-5086

MINIMUM WEIGHT SHIELD SYNTHESIS FOR SPACE VEHICLES

F. R. Nakache
A. D. Krumbein
J. Celnik
J. Certaine

A. D. Krumbein: Project Scientist

May 20, 1964

Work Performed under UNC Project 2195
Contract No. NAS 8-5277 with
George C. Marshall Space Flight Center
NASA, Huntsville, Alabama

UNITED NUCLEAR CORPORATION
Development Division
White Plains, New York

ABSTRACT

12169

The proton shield synthesis technique for spherical geometry has been extended to include a number of dose constraints and analytic expressions have been derived to calculate doses behind given spherical shields in particular proton environments. The theory of shield optimization for generalized convex enclosures has likewise been extended and calculations carried out which give shield compositions and layer thicknesses over a wide range of parameters. The secondary neutron portion of the optimization theory has also been extended to include new materials and more complex shields.

Author

CONTENTS

TABLES

FIGURES

1. INTRODUCTION AND SUMMARY

The major objective of the program described in this report is the extension and generalization of the proton shield synthesis technique originally developed for the NASA Marshall Space Flight Center.[1] This technique allows the shield designer to determine which materials and/or mixtures should go into a minimum weight proton shield for a space vehicle. It also enables him to specify the thickness of each material or mixture and the order of these regions in the complete shield.

The proton shield optimization theory for the spherical case has been extended to include minimum weight shields for a variety of dose constraints, whereas, in the previous work, the only constraint allowed was that the shield was to eliminate all protons below a given energy. The dose constraints incorporated into the theory thus far are: (1) specified dose in a small spherical tissue sample at the center of the shield with no self-shielding, (2) specified dose at that point with self-shielding by a spherical tissue model, (3) specified average body dose, (4) specified dose at any depth, and (5) application of two of the above constraints simultaneously. In addition, the special case in which the tissue model completely fills the cavity to be shielded has been studied. This case is of interest because it is applicable to the design of local body shields. A complete solution has been obtained for this case.

In Reference 1, the formulation of an approach to proton shield optimization of a convex, nonspherical void assuming normal proton incidence was begun. In the

present work, this approach is extended and calculations are carried out from which the local compositions and layer thicknesses of a minimum weight shield for any convex void can be obtained. It is then possible, in many cases, to approximate a complete minimum weight shield for a realistic convex void by defining the optimized shield at specific points.

A feasible approach to synthesizing an entire minimum weight shield analytically for symmetrical convex voids has been found. This method considers, for any point on the shield, a minimum equivalent shield thickness and requires that all possible proton paths through the shield at that point, for any direction of incidence, provide at least that much shielding. From a family of surfaces which satisfy this condition, the one which minimizes the shield weight is chosen. The mathematical formulation of this approach is not as yet complete, but, if successfully carried out, it should have wide application for the optimization of space shields of any symmetric vehicle.

The data on secondary neutron production and attenuation required for the proper inclusion of these parameters in the shield synthesis theory have been revised according to the latest calculations[2,3] and experimental results.[4] The resulting secondary neutron parameters have been extended to new materials and to additional proton spectra. Based on these new results, a generalized four parameter Young diagram has been calculated. The parameters include not only material density and proton attenuation, but also secondary neutron production and attenuation. Since there are four parameters involved, a four-dimensional "diagram" results. Therefore, it is not possible to construct such a diagram for visual representation. From the mathematical analysis, however, a number of conclusions can be drawn as to the proper shielding materials and their order in a shield optimized for both primary protons and secondary neutrons. Although no unique material sequence can be specified for a case of this complexity, shields made of given materials can be

optimized. Several optimized shields have been synthesized using the results of this extended analysis.

The results obtained using the extensions to the shield optimization theory described in this report verify our original finding that substantial weight savings are possible in certain cases by the use of the shield synthesis technique. Further extensions of the technique are deemed desirable, and recommendations for such new work are included in this report.

2. PROTON SHIELD OPTIMIZATION WITH DOSE CONSTRAINTS – SPHERICAL GEOMETRY

In previous work[1] a shield optimization technique was developed which leads to minimum weight spherical proton shields, given the constraint that the shield should stop all protons below a given cutoff energy. In this section, relationships are developed which permit the determination of minimum weight spherical shields given various specified dose rate constraints. These relationships are based on a realistic analytical expression for the incident proton spectrum.

Analytical expressions are given for point dose, average body dose, depth dose, and surface dose for a spherical man model at the center of the shielded enclosure (the maximum dose location). An optimization procedure is then presented which leads to the determination of the minimum weight shield for specified values of any of these dose values or for a combination of dose constraints. In this section, only the direct dose from protons is considered. Secondary neutron dose is considered in Section 4.

2.1 STATEMENT OF PROBLEM AND ASSUMPTIONS MADE

In the energy range up to about 300 Mev, the proton attenuation in aluminum can be represented by a single power fit of the form[1]

$$\frac{dE}{dr} = \alpha E^{-n} \tag{2.1}$$

Values for n of 0.786 and for α of 569 afford a satisfactory fit to the Bethe stopping power equation,[5] and to experimental results up to about 300 Mev. Above 300 Mev, another single power fit appears to be necessary.

If aluminum is chosen as a reference material, an approximate expression for the rate of energy loss per cm in a given material can be written as

$$\frac{dE}{dr} = A_i \, \alpha E^{-n} \tag{2.2}$$

where A_i is called the proton relative stopping power of material i and is defined as the ratio of the proton energy loss per unit distance in the i^{th} material to the energy loss in aluminum.

In Reference 1, calculations of proton relative stopping powers of various materials and compounds of possible interest to space shielding were made at a number of energies. It was shown that A_i is practically constant from 500 Mev down to at least 50 Mev for most materials. Thus, for space shielding purposes, A_i can be considered energy independent.

Now consider a spherical shield consisting of concentric shells of radii $r_0, r_1, \ldots, r_j$ where r_0 is the radius of the void to be shielded. The shield materials have proton relative stopping powers $A_1, A_2, \ldots, A_j$. Assume that a man can be represented by a sphere of radius, e, such that $e \leq r_0$. The proton relative stopping power of tissue, A_T, and its density, ρ_T, are given. The man can occupy any position inside the void.

A proton flux, representative of a flare or the Van Allen belt spectrum, is considered to impinge on the outer surface of the spherical shield. What is required now is the minimization of the shield weight, subject to the condition that the energy deposition (primary dose) in the crew model is less than or equal to a specified

value and also subject to the restriction that shielding materials be chosen from those of a given set.

The choice of shielding materials is made according to the Young prescription which has been given in a previous report.[1] Fig. 1 shows the Young plot which is used in this study. The materials at the vertices of this Young diagram are polyethylene (CH_2), carbon, nickel, and tungsten.

These materials will be used in that order from the outside shield layer in. Often, only part of this sequence need be used. For instance,for most reasonably sized voids and shield thicknesses, tungsten will not be used. Thus, given this sequence of materials, the problem is actually to find what number of materials and set of layer thicknesses will minimize the proton shield weight while satisfying the prescribed dose constraint.

The calculations will also assume that the expression for the incident proton flux at the outside of the spherical shield can be written as follows:

$$P(E) = \frac{C_1}{E^{+m} + C_2} \tag{2.3}$$

where m, C_1 and C_2 are constants determined by the particular proton environment. Such a single power fit appears to be valid for most flares over a large energy range, as can be seen in Fig. 2.

It is important, however, to remark that in all cases C_2 becomes negligible compared to E^m when the proton energy reaches the order of 50 Mev. Since one expects that the shield will stop protons below that energy, it is reasonable to use the following expression in the calculations:

$$P(E) = C_1 E^{-m} \tag{2.4}$$

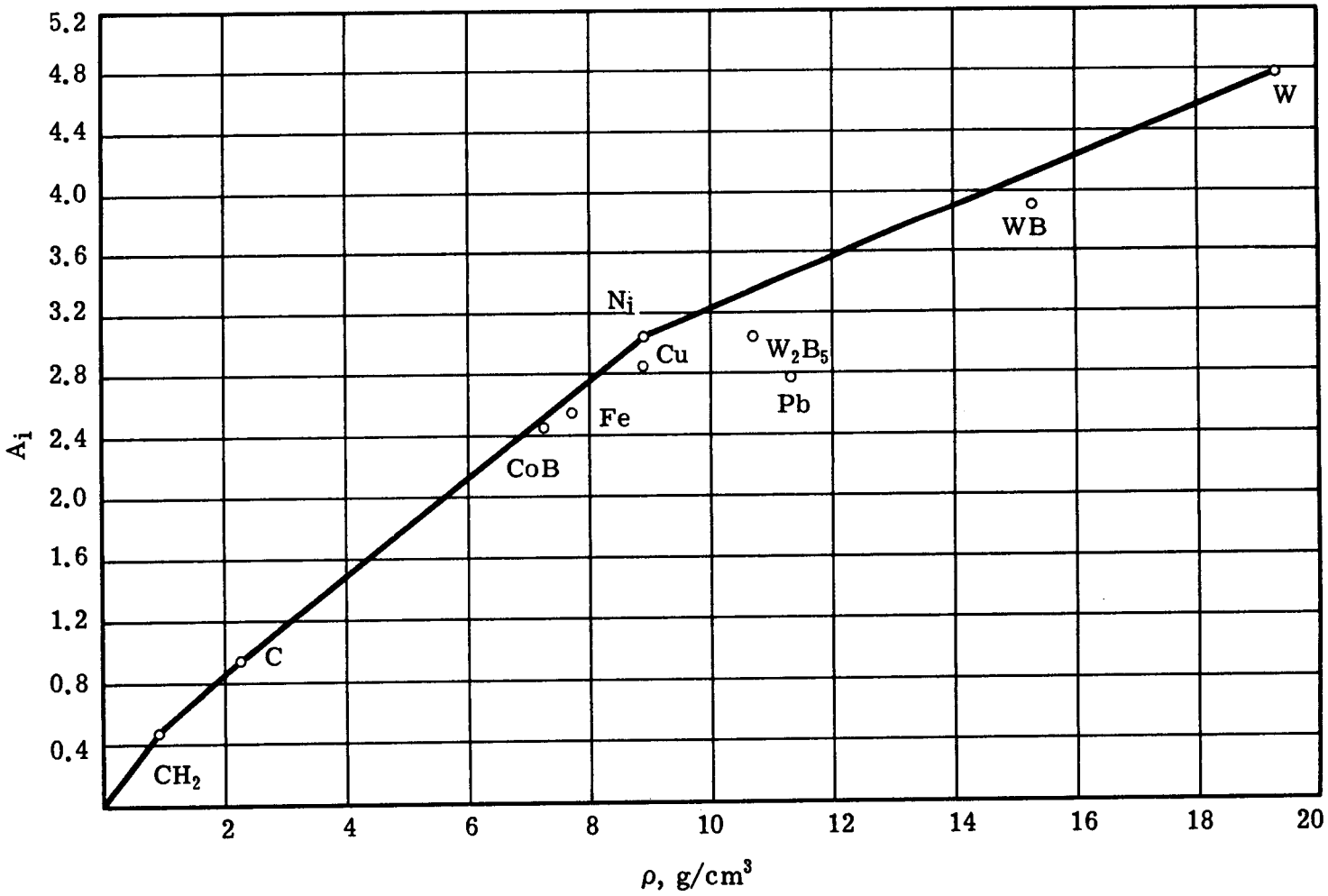

Fig. 1 — Young diagram for proton shielding materials

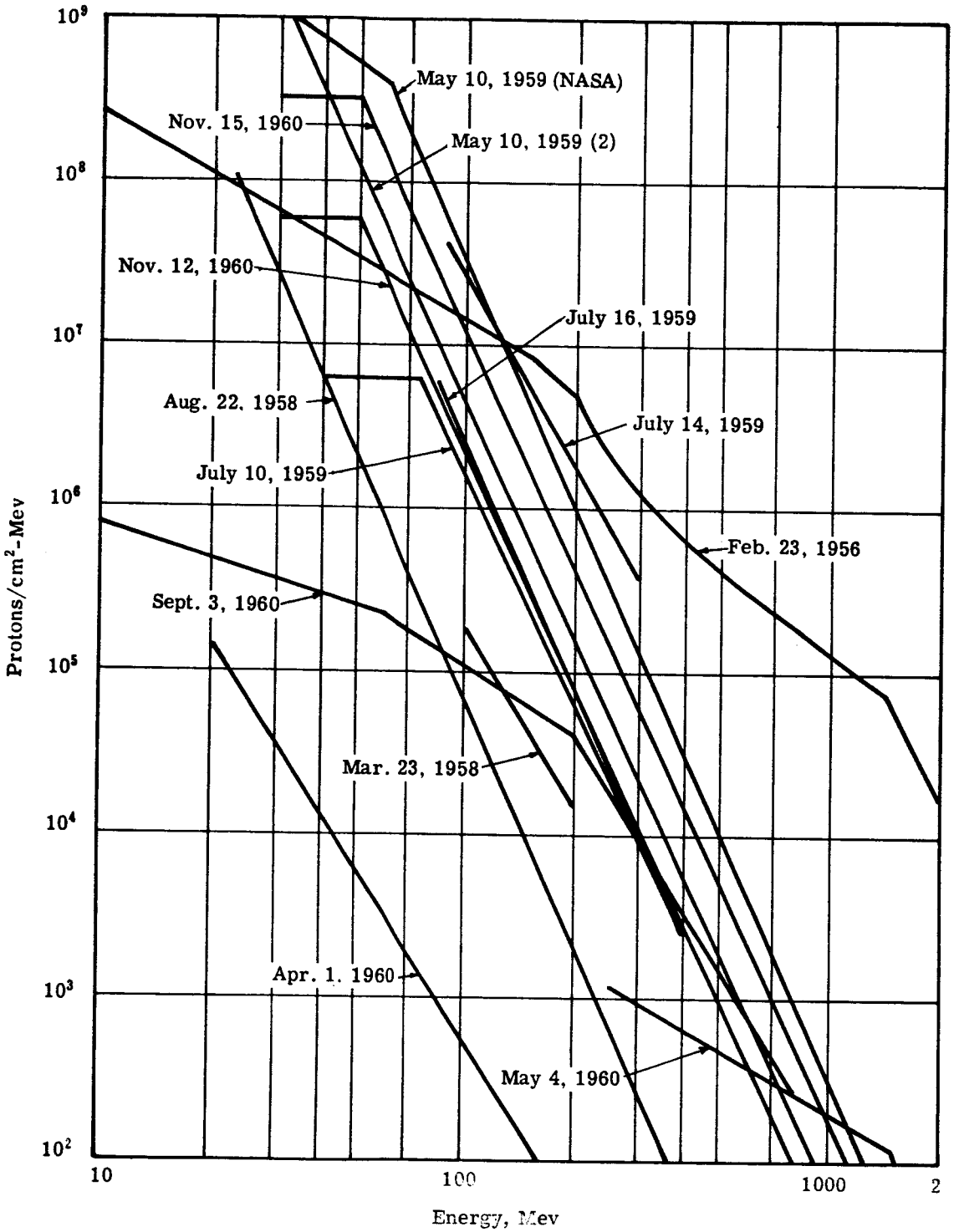

Fig. 2 — Time integrated differential energy spectra for several solar proton events

which is sometimes called the Winckler spectrum[6] for the particular flare.

A better representation of the energy distribution of proton flares is to use several power fits, each valid in given energy ranges.

$$P_j(E) = C_1^j E^{-m_j} \tag{2.5}$$

where

$$E_{j-1} < E < E_j, \qquad j = 1, 2 \ldots$$

Table 1 shows some power fits for selected spectra.

A property of these spectra which will be used in subsequent approximations is that the number of protons of energy E impinging on the shield decreases rapidly with increasing energy.

Table 1 — Sample Proton Spectra, $P(E) = C_1 E^{-m}$*

	Energy Range, Mev	C_1	m
May 10, 1959 Flare	10 - 60	1.90×10^{11}	1.5
	60 - 780	3.19×10^{17}	5
Sept. 3, 1960 Flare	10 - 60	4.03×10^{6}	0.7
	60 - 200	8.0×10^{7}	1.43
	200 - 780	7.87×10^{12}	3.6
Feb. 23, 1956 Flare	10 - 150	8.5×10^{9}	1.5
	150 - 400	5.0×10^{12}	2.65
	400 - 780	2.0×10^{10}	1.73
Van Allen Belt – Freden and White Spectrum	10 - 80	1.55×10^{2}	0.72
	80 - 400	7.33×10^{3}	1.60
	400 - 700	1.02×10^{5}	2.04

*P(E) is in protons/cm^2/Mev except for the Van Allen Belt where P(E) is in protons/cm^2/sec/Mev.

The incident proton flux is further assumed to be isotropic in space. This is a good approximation when considering time-average flux since the shielded void represents a space vehicle which is free to move and rotate. Thus, the impinging proton flux per unit solid angle and per unit energy is given by

$$P(E,\Omega)d\Omega dE = \frac{1}{4\pi} P(E)dEd\Omega = \frac{d\Omega}{4\pi} \left[\sum_j C_1^j E^{-m_j} \right] dE \qquad (2.6)$$

Since the proton flux is isotropic, the number of protons of energy dE about E that are incident on the element of surface dA with angle $d\varphi$ about φ (where φ is the angle with the normal to the surface), is given by

$$P(E,\varphi)d\varphi dAdE = \frac{P(E)}{2} \sin \varphi \cos \varphi \, d\varphi dAdE \qquad (2.7)$$

Finally, use is made of the fact that the energy deposited in a spherical phantom is greatest if its center coincides with the void center. In our analysis it is then possible to consider only phantoms which are concentric with the void since, if the primary dose constraint is satisfied for that crew model position, it will be satisfied for any other position of the man inside the void.

This simplification is valid because when the phantom is displaced from the center of the void the rays which are incident on the phantom have, in general, a longer path length through the shield than when the phantom is at the center. Therefore, the proton cutoff energy for these rays is higher. Since the proton flux incident on the shield decreases rapidly with increasing energy, the higher cutoff energy causes less energy to be deposited in the phantom.

2.2 DOSE CALCULATION – ANALYTICAL TECHNIQUE

A number of important relationships have been developed which are useful in the calculation of the dose received by a spherical model inside a multilayer shield. In many cases, these expressions represent advances over previous work in that

they are more general or more accurate. Therefore, they are of interest in themselves and provide a basis for the shield optimization relationships developed in Section 2.3. The dose relationships are summarized in this section and some numerical results are given. Derivations are given in the Appendices.

2.2.1 Nomenclature

A	proton stopping power relative to aluminum
A_i	proton relative stopping of the i^{th} shielding material
ΔA_i	$A_i - A_{i+1}$
A_T	proton relative stopping power of tissue
a	$\frac{1}{n+1} + 2$
$B(a,b)$	complete beta function
b	$\frac{m-n-3}{n+1}$
C_1, C_2	constants in the expression for the proton dose, functions of the particular proton spectrum
C	$\beta B(a,b)$
C'	$[b(b+1)\ A_T C]^{-(b+2)}$
$D(r)$	local dose or dose rate per unit isotropic proton flux per gram of tissue
$D(0)$	dose or dose rate at void center
D_v	average body dose or dose rate per unit isotropic proton flux per gram of tissue
$D_p(e')$	depth dose or dose rate in phantom at radius e' per unit isotropic proton flux per gram of tissue
$\overline{D}$	specified value of local dose
$\overline{D}_v$	specified value of average body dose
$\overline{D}_p(e')$	specified value of depth dose
E	energy of incident proton

E'	energy of proton after attenuation by the shield
E''	energy of proton leaving the phantom
E'_0	proton energy corresponding to R'_0
E'_m	proton energy corresponding to R'_m
e	radius of spherical man model or phantom
e'	radius of a given shell in the phantom where $0 \leq e' \leq e$
F_v	energy deposition or deposition rate per unit isotropic proton flux per unit phantom mass
$f(K_0, K_m)$	$\frac{K_0^{-b} - K_m^{-b}}{K_m - K_0} - \frac{K_m^{-b} - (2A_T e + K_0)^{-b}}{K_0 + 2A_T e - K_m}$
$\overline{f}$	$\frac{e\overline{D}}{C}$
$g(K'_0, K'_m)$	function in brackets in Eq. 2.22
$\overline{g}$	$\frac{3\,\overline{D}_0(e')}{A_T\,C}$
h	function of ν and η
K or $K(\varphi)$	the angle dependent equivalent aluminum path length through the shield in units of cm of aluminum or g/cm^2 of aluminum
K_0	minimum equivalent aluminum path length through the shield
K_1	angle independent coefficient in the expression for K
K_m	maximum equivalent aluminum path length through the shield
K_T	total equivalent aluminum path length through both shield and phantom
$\overline{K}_0$	$C'\overline{D}^{(b+2)}$
L	Lagrangian
m	exponent of E in the expression for the proton flux
n	exponent of E in the proton attenuation expression for aluminum
P(E)	isotropic proton flux in protons per cm^2 per Mev or protons per cm^2 per Mev per sec
R	range of protons incident on the shield in units of cm of aluminum
R'	range of protons incident on the phantom

R''	range of protons emerging from the phantom
R'_0	$R - K_0$
R'_m	$R - K_m$
$R(\nu,\eta)$	$f - \overline{f}$
r_0	radius of the spherical enclosure or void to be shielded
r_i	radius of the i^{th} shielding layer
$S(\nu,\eta)$	$\nu \frac{\partial f}{\partial K_m} - \eta \left(\frac{\partial f}{\partial K_m} + \frac{\partial f}{\partial K_0} \right)$
W	total weight of the shield
Z_1	K_m/K_0
Z_2	$\frac{K_m}{K_0 + 2A_T e}$

Greek Symbols

α	constant in the proton attenuation expression for aluminum
β	$\frac{3C_i}{4\rho_T} \frac{[\alpha(n+1)]^{-\frac{m+2}{n+1}}}{n+2}$
ϵ	$\frac{3}{4e\rho_T} \left(\frac{n+1}{n+2} \right)$
η, μ, ν'	Lagrange multipliers
ν	$\nu' + \eta$
φ	angle of incidence of the proton on the phantom
φ_0	minimum angle of incidence of proton on the phantom for which all incident protons are stopped in the shield
ρ_i	density of the i^{th} shielding material
ρ_T	density of tissue
$\Delta\rho_i$	$\rho_i - \rho_{i+1}$

2.2.2 Equivalent Aluminum Thickness of Shield

The equivalent aluminum thickness seen by a ray penetrating a shield of inner radius, r_0, incident on the spherical phantom of radius, e, at angle φ with the normal direction at the phantom surface is

$$K = -A_1 (r_0^2 - e^2 \sin^2\varphi)^{1/2} + \sum_{i=1}^{j} (A_i - A_{i+1}) (r_i^2 - e^2 \sin^2\varphi)^{1/2} \tag{2.8}$$

with the convention that $A_{j+1} = 0$.

The minimum attenuation is given when $\varphi = 0$

$$K_0 = - A_1 r_0 + \sum_{i=1}^{j} (A_i - A_{i+1}) r_i = \sum_{i=1}^{j} A_i (r_i - r_{i-1}). \tag{2.9}$$

If K is expanded in series in the form

$$K = K_0 + K_1 \sin^2 \varphi + K_2 \sin^4 \varphi \ldots \tag{2.10}$$

then

$$K_1 = \frac{e^2}{2} \left(\frac{A_1}{r_0} - \sum_{i=1}^{j} \frac{A_i - A_{i+1}}{r_i} \right) . \tag{2.11}$$

Since the coefficients K_i decrease rapidly, a good approximation to K is

$$K = K_0 + K_1 \sin^2 \varphi . \tag{2.12}$$

2.2.3 Energy of Protons Attenuated by the Shield and Incident on the Phantom

The energy, E′, of a proton of energy E penetrating the shield and incident on the phantom at angle φ is

$$\frac{E'^{n+1}}{(n+1)\alpha} = \frac{E^{n+1}}{(n+1)\alpha} - K(\varphi)$$

if

$$\frac{E^{n+1}}{(n+1)\alpha} - K(\varphi) > 0$$

otherwise

$$E' = 0 . \tag{2.13}$$

2.2.4 Energy, E'', of Protons Leaving the Phantom

The relationships which apply are summarized in Table 2. The formulas are given in terms of the range of the protons. The range is related to the energy by the approximate relationship, obtained by integrating the equation

$$R = R(E) = \frac{E^{n+1}}{(n+1)\alpha} \tag{2.14}$$

An interesting fact to note from Table 2 is that, if for a given E (or R), there exists an angle $\varphi = \varphi_0 < \pi/2$ for which a proton (which otherwise would strike the phantom) is stopped by the shield, then all protons of energy E which emerge in the void ($\varphi < \varphi_0$) are stopped by the tissue. A proton can emerge from the phantom only if its incident energy, E, is high enough to permit it to penetrate the shield and strike the phantom at any angle.

2.2.5 Energy Deposition in the Phantom for Monoenergetic Protons

The relationships which apply to the average body energy deposition rate are summarized in Table 3. Numerical results for a typical case (K_0 =10 g/cm^2 of Al, r_0 = 50 cm, e = 26 cm) are given in Fig. 3.

2.2.6 Energy Deposition in the Phantom for Given Proton Spectra

If the proton spectrum is represented by a single power fit, the average body dose or dose rate per unit proton flux is given by

Table 2 — Range of Protons Incident and Emerging from the Phantom as a Function of R and φ

Range of Protons Incident on the Shield, R	Range of Protons Incident on the Phantom, R′	Range of Protons Emerging from Phantom, R″	Comments
$R \leq K_0$	0	0	For all incidence angles
$K_0 \leq R \leq K_m$	$R' = R - K(\varphi)$, $0<\varphi\leq\varphi_0$ $R' = 0$ $\varphi_0<\varphi$	0 for $0 < \varphi \leq 1/2$	$R = K_0 + K_1 \sin^2 \varphi_0$ (Eq. 7.6)
$K_m \leq R \leq K_T(0)$	$R' = R - K(\varphi)$, $0<\varphi\leq\pi/2$	$R''=R-K_T(\varphi)$, $\varphi_1<\varphi<\pi/2$ $R''=0$ $0<\varphi\leq\varphi_1$	$R=K_m + [K_T(0) - K_0]\cos \varphi_1 - (K_m - K_0)\cos^2 \varphi_1$ (Eq. 7.13)
$R > K_T(0)$	$R' = R - K(\varphi)$	$R'' = R - K_T(\varphi)$	For all incidence angles

Table 3 — Average Body Energy Deposition Rate per Unit Mass of Tissue per Unit Proton Flux as a Function of Range in Aluminum of the Incident Protons

Proton Range, R(E)	$F_V(E)$	Comments
$R(E) \leq K_0$	0	$R = \frac{E^{n+1}}{(n+1)\alpha}$
$K_0 < R < K_m$	$\epsilon \frac{E_0' R_0'}{K_m - K_0}$	$R_0' = R - K_0$
$K_m < R < K_T(0)$	$\epsilon \left[\frac{E_0' R_0' - E_m' R_m'}{K_m - K_0} - \frac{E_m' R_m'}{K_T(0) - K_m} \right]$	$R_m' = R - K_m$
$R > K_T(0)$	$\epsilon \left[\frac{E_0' R_0' - E_m' R_m'}{K_m - K_0} - \frac{E_m' R_m' - E_0'' R_0''}{K_T(0) - K_m} \right]$	$R_0'' = R - K_T(0)$

where $\epsilon = \frac{3}{4e\rho_T} \left(\frac{n+1}{n+2} \right)$

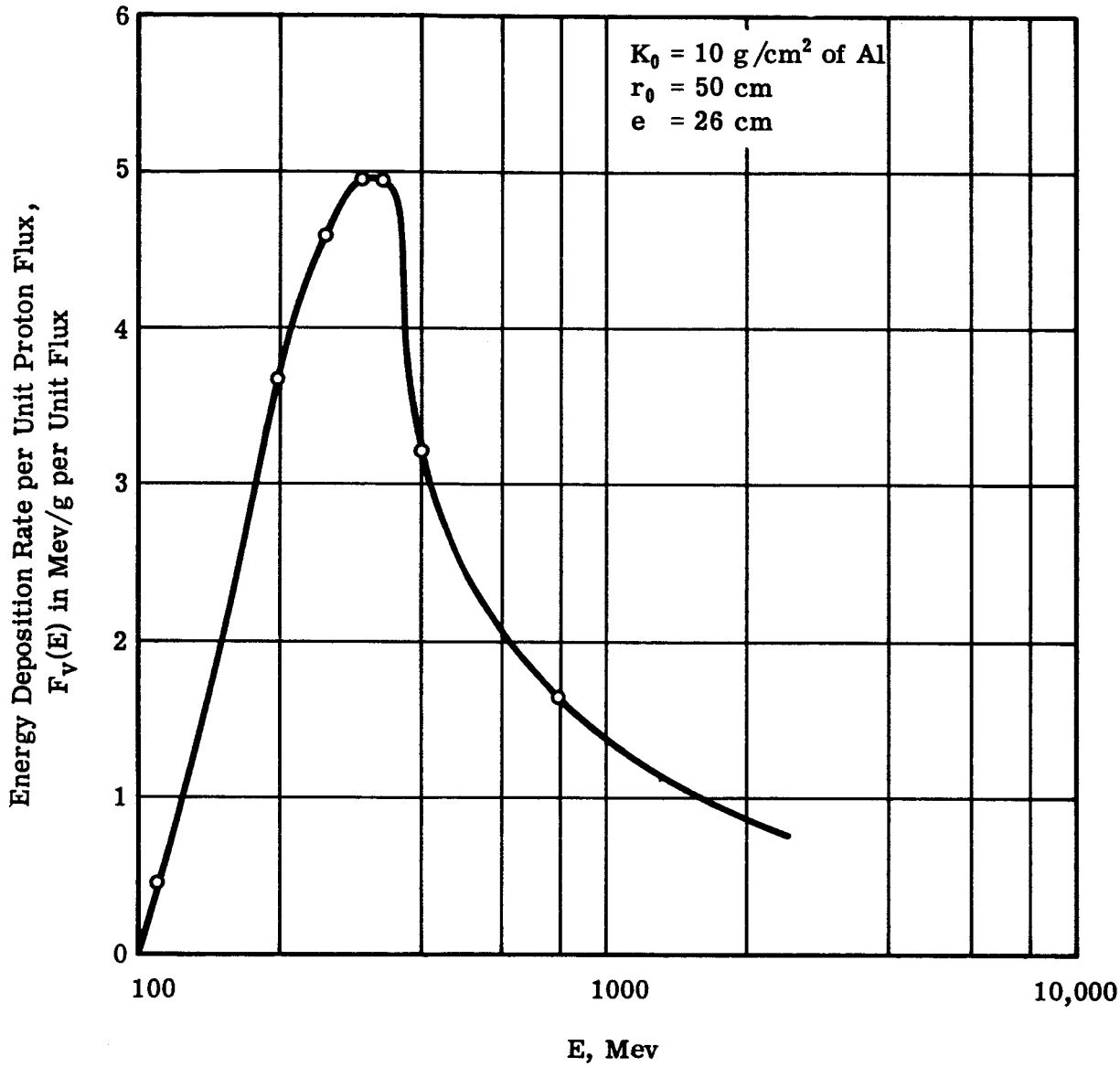

Fig. 3 — Energy deposition rate vs energy of incident protons

$$D_V = \frac{\beta B(a,b)}{e} \left[\frac{K_0^{-b} - K_m^{-b}}{K_m - K_0} - \frac{K_m^{-b} - K_T(0)^{-b}}{K_T(0) - K_m} \right] \tag{2.15}$$

where $b = (m - n - 3)/(n + 1)$, or

$$D_0 = \frac{\beta}{e} \frac{\log K_m/K_0}{K_m - K_0} - \frac{\log K_T(0)/K_m}{K_T(0) - K_m} \tag{2.16}$$

for $b \to 0$, or

$$D_{-1} = (a - 1) D_0 = \frac{n+2}{n+1} D_0 \tag{2.17}$$

for $b \to -1$.

The units of D are in Mev/g-sec if a time dependent proton flux is given, and in Mev/g if a time-integrated proton flux is used.

If the spectrum is represented by a combination of power fits, the average body dose or dose rate per unit proton flux is given by

$$D_V = \frac{1}{e} \sum_{j=1}^{1} \beta_j f_j(K_0, K_m) \tag{2.18}$$

where f_j is a combination of incomplete beta-functions and is given in Section 7 (Eq. 7.29).

These relationships have been applied to the calculation of the average body dose for particular flare spectra as a function of shield thickness and void radius. Results are shown in Figs. 4 and 5.

The first flare considered is that of May 10, 1959. Two different spectra have been postulated for this flare. The NASA integral spectrum is matched by suitably choosing two differential spectra that join at 60 Mev. These are given in Table 1.

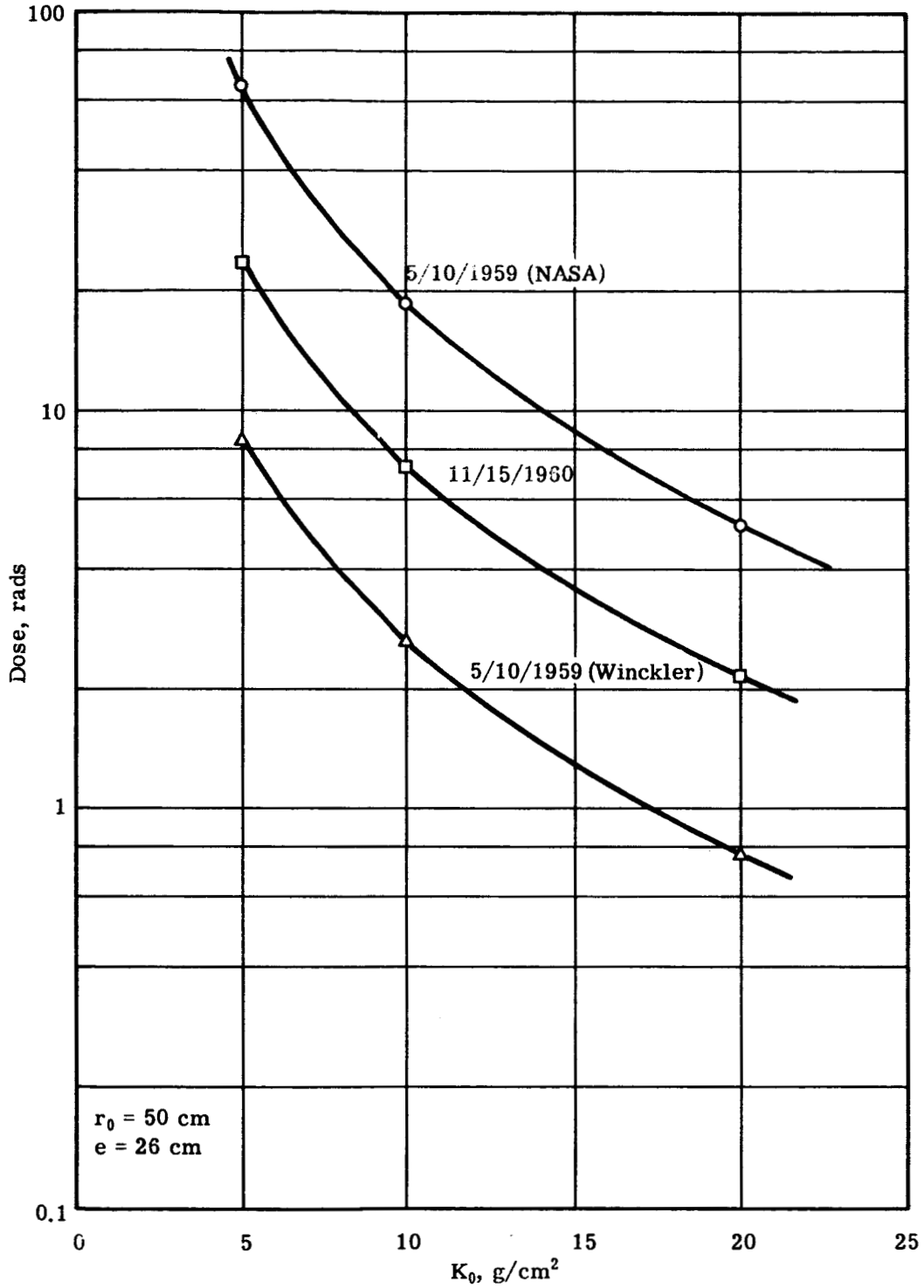

Fig. 4 — Average body dose vs aluminum equivalent shield thickness, K_0. Flares of May 10, 1959 and November 15, 1960.

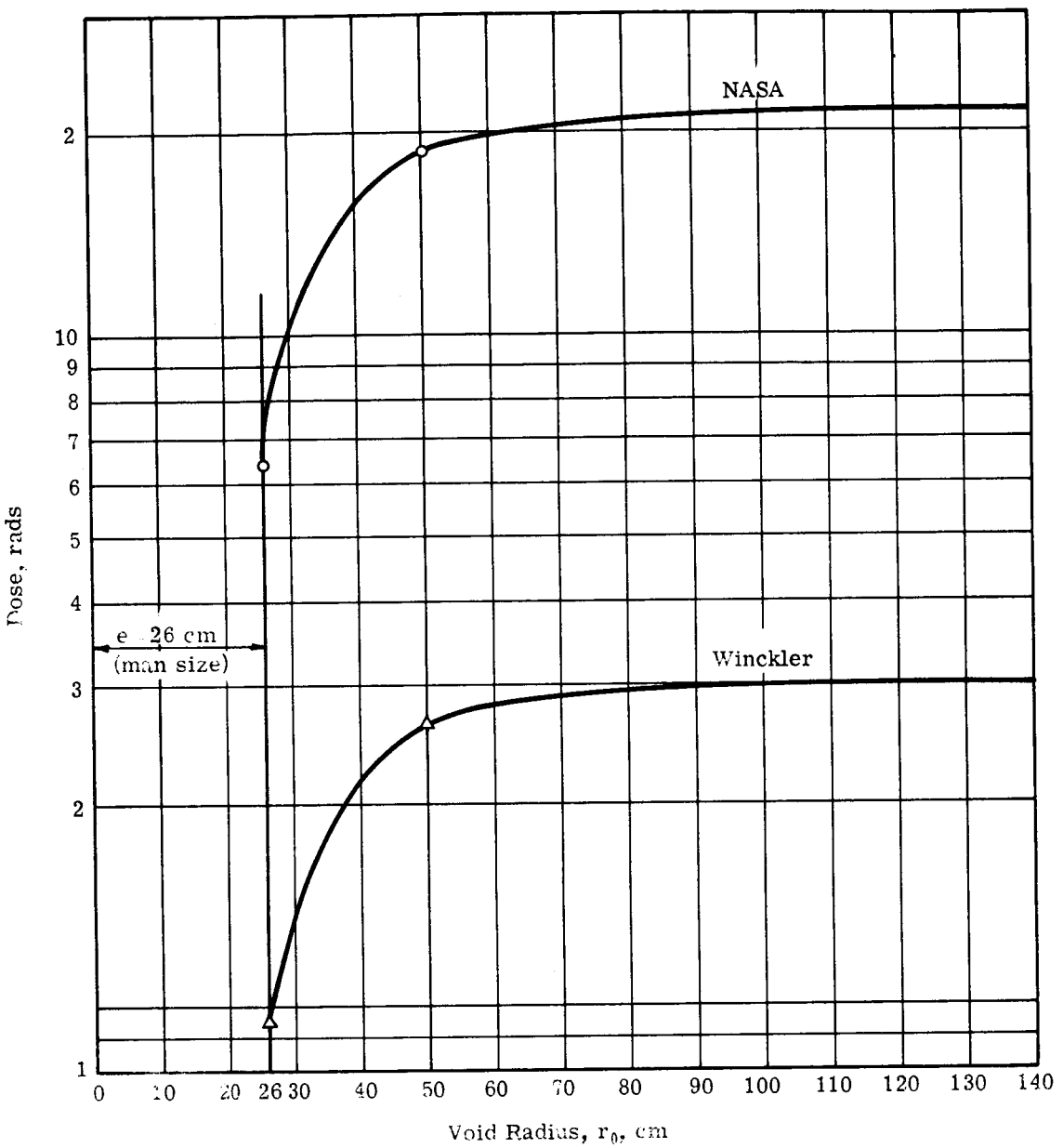

Fig. 5 — Average body dose vs void radius, r_0, for a shield of 10 g/cm^2 of Al – flare of May 10, 1959

The Winckler spectrum is given by a single power fit for $30 < E < 1000$ Mev, namely

$$P(E) = 1.672 \times 10^6 \, E^{-4.8} . \tag{2.19}$$

A phantom of radius e = 26 cm is used. This represents approximately an average man since the weight of the model is about 73.5 kg or 162 lb.

For a void radius, r_0, of 50 cm, the average body dose vs aluminum shield thickness in g/cm^2 is plotted in Fig. 4 for the NASA and Winckler spectra. A similar plot for the November 15, 1960 flare is also given. These results have been compared to other numerical dose calculations performed at United Nuclear by E. Greuling, et al., in which protons were assumed to be isotropically incident on the phantom (rather than on the shield). The agreement is very good because the man-to-void size ratio is small ($\approx 1/2$). As the ratio e/r_0 increases, the average body dose becomes smaller because many of the protons which reach the phantom now penetrate the shield at a flatter angle and thus have a large path length through the shield.

In Fig. 5, the average body dose vs the void radius is shown, assuming an aluminum shield thickness of 10 g/cm^2. When r_0 becomes very large, all protons which contribute to the energy deposition in the body can be considered as normally incident on the shield. Note that the average body dose increases rather rapidly when r_0 increases from $r_0 = e = 26$ cm to $r_0 = 50$ cm, and then increases very slowly to the asymptotic value given when all protons are normally incident on the shield.

2.2.7 Dose at the Phantom Center without Self-Shielding

The dose or dose rate per unit flux at the void center for a point detector is given by

$$D = D(0) = b(b+1)A_T \frac{C}{K_0^{b+2}} \tag{2.20}$$

Results for the flare of May 10, 1959 are given in Fig. 6. As expected, the dose at the center point without self-shielding is much larger than the average body doses previously given.

2.2.8 Dose at the Phantom Center with Self-Shielding

The dose or dose rate per unit flux at the center of the spherical phantom is given by

$$D(\text{center}) = b(b+1)\,\beta\,A_T\,\frac{B(a,b)}{(K_0 + A_T e)^{b+2}} \tag{2.21}$$

If we compare the values of dose obtained by use of this equation to those shown in Figs. 4 and 5, we find that the dose at the phantom center, when self-shielding is taken into account, is small compared to the average body dose for a phantom 26 cm in radius. Most of the average body dose is contributed by radiation deposited in the outer portion of the phantom.

2.2.9 Depth Dose

The proton energy per gram of tissue deposited in an infinitesimally thin tissue shell at a given depth in the spherical man model is of special interest. Since the energy deposited will depend on the location of the shell with respect to the surface of the man, it is called depth dose. In particular, the energy per gram of tissue deposited in a shell located at the phantom surface is called the skin dose.

It is likely that, for shielding purposes, a depth dose constraint rather than an average body dose constraint will be imposed because the permissible doses to certain vital organs such as eyes, kidneys, etc., are smaller than the permissible average body dose.

The energy deposition or rate of deposition per unit flux per gram of tissue in a shell of thickness de' located at radius e' in the phantom is given by

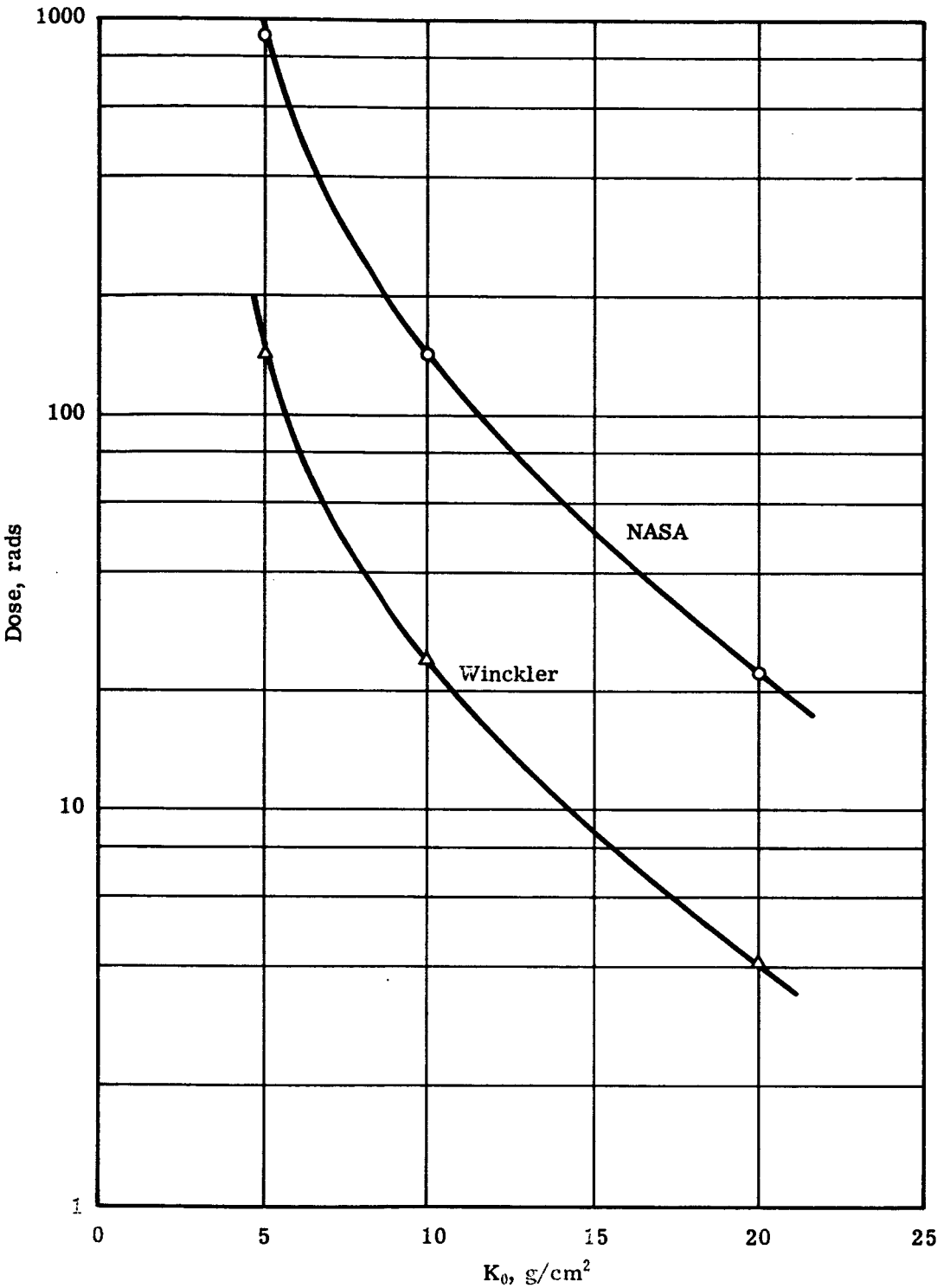

Fig. 6 — Center void dose vs aluminum shield thickness, K_0.
May 10, 1959 flare – O NASA spectrum; Δ Winckler spectrum

$$D_p(e') = \frac{A_T C}{3} \left[\frac{K_0^{-b} - K_m'^{-b}}{(K_m' - K_0')^2} - \frac{K_m^{-b} - (K_0' + 2A_T e')^{-b}}{(K_0' + 2A_T e' - K_m')^2} \right]$$

$$+ b \left[\frac{K_0'^{-(b+1)} - 2K_m'^{-(b+1)}}{K_m' - K_0'} + \frac{2K_m'^{-(b+1)} - (K_0' + 2A_T e')^{-(b+1)}}{K_0' + 2A_T e' - K_m'} \right] \qquad (2.22)$$

The particular case of $e' = e$ is of interest since, in this case, Eq. 2.22 reduces to $D_p(e)$, the skin dose. In Figs. 7 and 8, the depth dose distribution vs e' is plotted for the NASA and Winckler spectra of the flare of May 10, 1959. The parameters used are

$e = 26$ cm

$r_0 = 50$ cm

$K_0 = 5$ g/cm^2, 10 g/cm^2, 20 g/cm^2 of aluminum.

As the depth in tissue increases (i.e., as e' decreases), the depth dose decreases from a maximum on the skin to a minimum at the center of the spherical man. For relatively thin shields, D_p decreases rapidly near the skin. As the thickness of the shield increases, the reduction in dose becomes less important and the dose remains practically constant.

In Fig. 9, the doses are normalized to the skin dose. Thus, for $K_0 = 5$ g/cm^2 of aluminum, the relative dose decreases from 1.0 on the skin to 0.347 at the center, while for $K_0 = 20$ g/cm^2 of aluminum, it decreases only from 1.0 to 0.81. The curves of Fig. 9 have the same shape and otherwise compare very well with the single curve given by Schaefer.[7]

2.3 THE OPTIMIZATION PROBLEM

In this section, a method is developed for determining the minimum weight proton shield in spherical geometry subject to various dose constraints and a computer approach to the solution of the resulting equations is described.

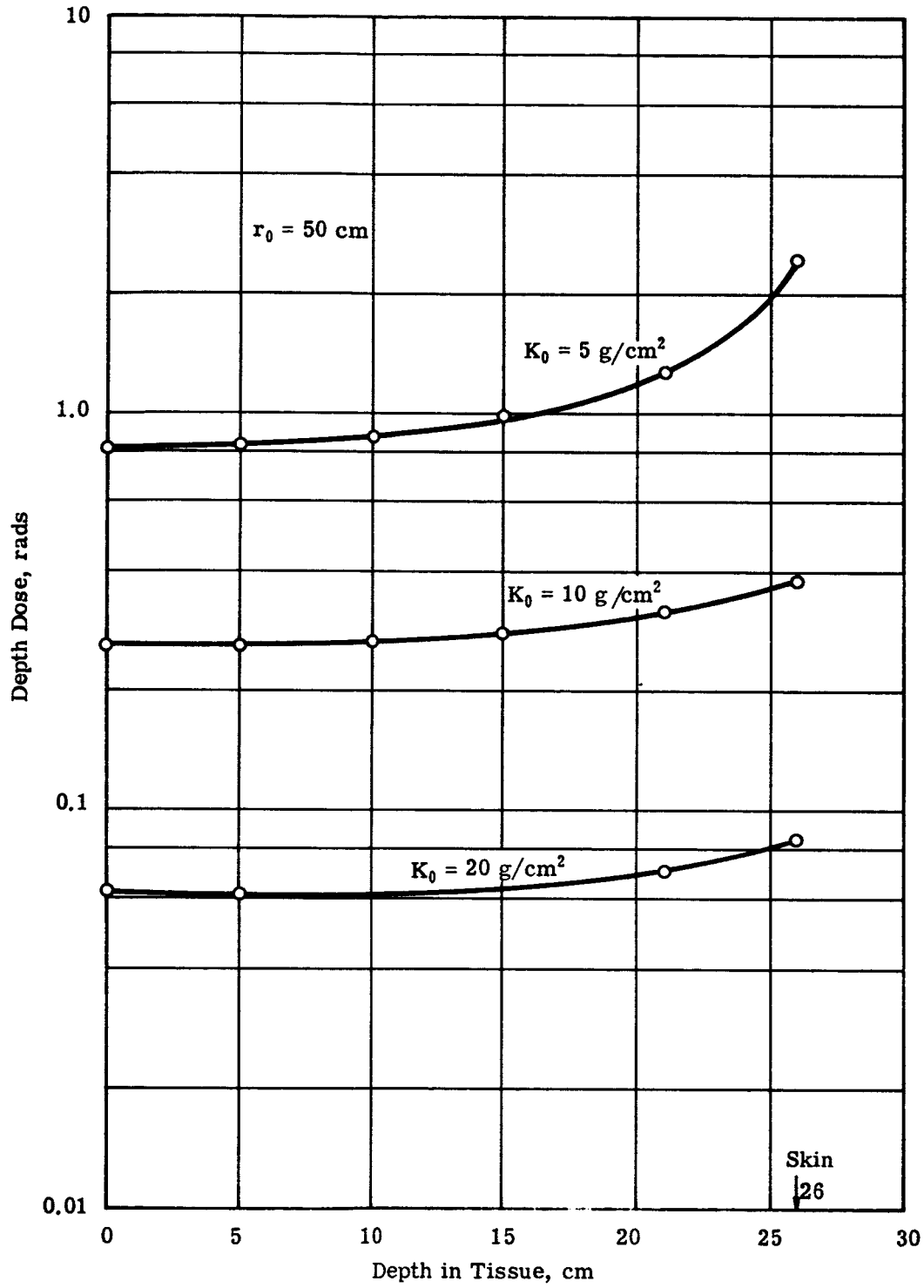

Fig. 7 — Depth dose vs depth in tissue for a 52-cm diameter sphere – NASA spectrum of flare of May 10, 1959

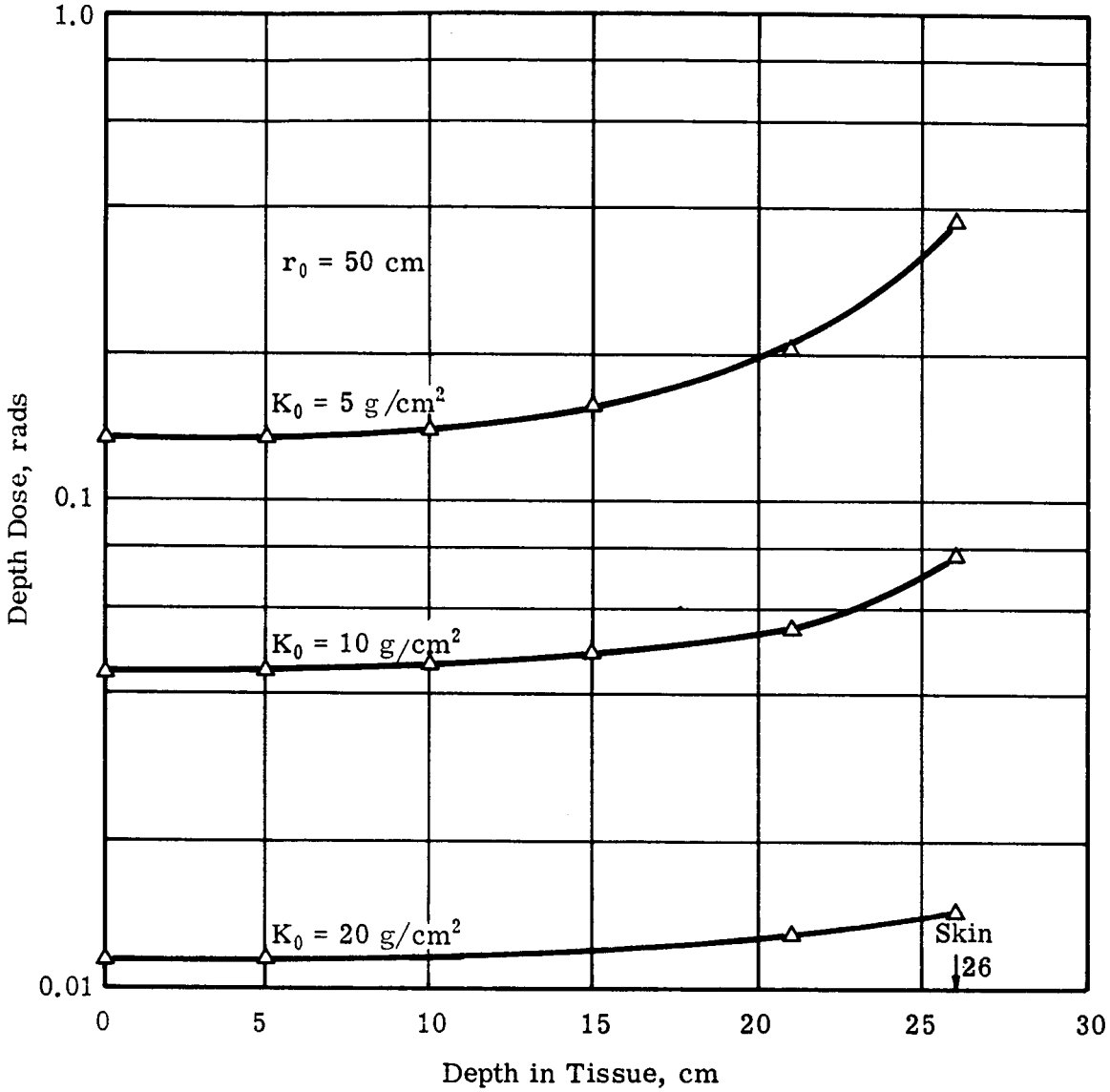

Fig. 8 — Depth dose vs depth in tissue for a 52-cm diameter sphere – Winckler spectrum of flare of May 10, 1959

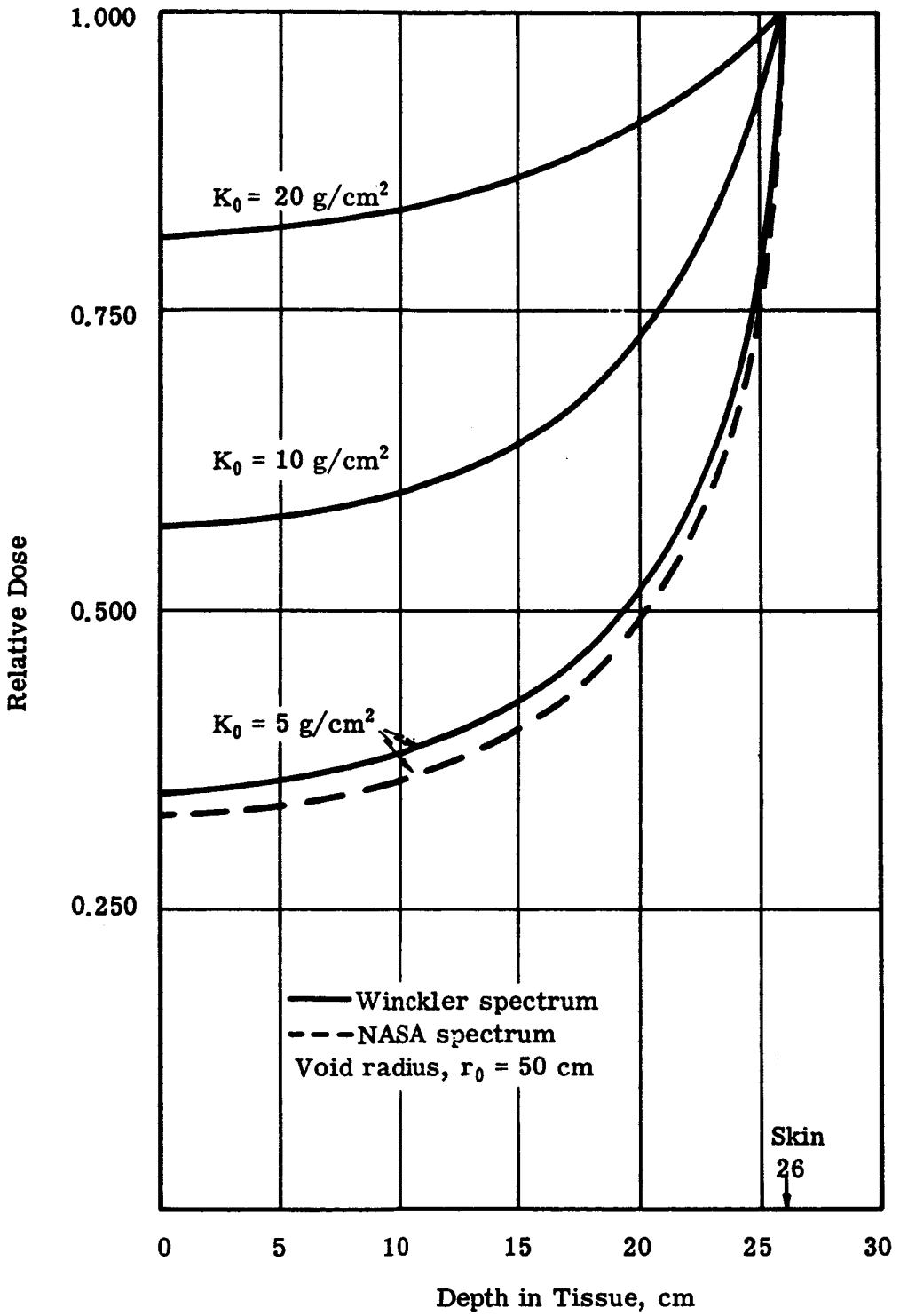

Fig. 9 — Relative proton depth dose vs depth in tissue for a 52-cm diameter tissue sphere for various Al shields for the flare of May 10, 1959

2.3.1 Average Body Dose

The weight of the shield is given by

$$W = \frac{4\pi}{3} \sum_{i=1}^{j} \rho_i \, (r_i^3 - r_{i-1}^3)$$

or

$$\frac{W}{4\pi} = \sum_{i=1}^{j} \Delta\rho_i \frac{r_i^3}{3} - \rho_1 \frac{r_0^3}{3} \tag{2.23}$$

where ρ_i represents the density of the i^{th} material; $\Delta\rho_i = \rho_i - \rho_{i+1}$, with the convention that $\rho_{j+1} = 0$.

The constraint is that the average body dose must be less than or equal to a specified value, $\overline{D}$. As shown in Section 7 (Eq. 7.26), it is necessary that

$$f(K_0, K_m) = \frac{e\overline{D}}{C} = \overline{f} \tag{2.24}$$

where $f(K_0, K_m)$ is given by Eq. 7.27.

K_0 and K_m are functions of the shell radii and are given in Eqs. 2.9 and 7.6 as

$$K_0 = \sum_{i=1}^{j} \Delta A_i r_i - A_1 r_0$$

and

$$K_m = \sum_{i=1}^{j} \Delta A_i \, (r_i^2 - e^2)^{1/2} - A_1 (r_0^2 - e^2)^{1/2}$$

where $\Delta A_i = A_i - A_{i+1}$

with the convention $A_{j+1} = 0$.

To minimize the weight W given by Eq. 2.23 subject to Eqs. 2.24, 2.9, and 7.6, we construct the Lagrangian

$$L = \frac{W}{4\pi} + \mu\,[\bar{f} - f(K_0, K_m)] + \nu' \left(K_0 - \sum_{i=1}^{j} \Delta A_i r_i + A_1 r_0 \right)$$

$$+ \eta \left[K_m + A_1 (r_0^2 - e^2)^{1/2} - \sum_{i=1}^{j} \Delta A_i \, (r_i^2 - e^2)^{1/2} \right] \tag{2.25}$$

where μ, ν', and η are Lagrange multipliers.

According to Slater,[8] the minimum weight is achieved if the following conditions are satisfied.

$$1.\ f - \bar{f} = 0;\ \mu > 0$$

$$2.\ K_0 = \sum_{i=1}^{j} \Delta A_i r_i - A_1 r_0;\ \nu' > 0$$

$$3.\ K_m = \sum_{i=1}^{j} \Delta A_i \, (r_i^2 - e^2)^{1/2} - A_1 \, (r_0^2 - e^2)^{1/2};\ \eta > 0 \tag{2.26}$$

$$4.\ \frac{\partial L}{\partial K_0} = \nu' - \mu \frac{\partial f}{\partial K_0} = 0$$

$$5.\ \frac{\partial L}{\partial K_m} = \eta - \mu \frac{\partial f}{\partial K_m} = 0$$

$$6.\ \frac{\partial L}{\partial r_i} = \Delta\rho_i r_i^2 - \nu' \Delta A_i - \eta \Delta A_i \frac{r_i}{\sqrt{r_i^2 - e^2}} = 0; \qquad i = 1, 2, 3, \ldots, j.$$

Let us define a new Lagrangian factor

$$\nu = (\nu' + \eta) > \eta > 0. \tag{2.27}$$

Eliminating μ in Eq. 2.25, the system of equations in ν, η, and r_i to be solved becomes

$$r_i^2 - \nu \frac{\Delta A_i}{\Delta \rho_i} - \eta \frac{\Delta A_i}{\Delta \rho_i} \left(\frac{r_i}{\sqrt{r_i^2 - e^2}} - 1 \right) = 0; \qquad i = 1, 2, \ldots, j \tag{2.28a}$$

$$\frac{\partial f}{\partial K_m} - \eta \left(\frac{\partial f}{\partial K_0} + \frac{\partial f}{\partial K_m} \right) = 0 \tag{2.28b}$$

$$f - \overline{f} = 0 \tag{2.28c}$$

An important point to note is that if e becomes very small, then Eq. 2.28a reduces to

$$r_i^2 - \frac{\Delta A_i}{\Delta \rho_i} = 0; \qquad i = 1, 2, \ldots, j.$$

Further, in Section 7.4.3 it is found that for $e \ll 1$, $f(K_0, K_m)$ reduces to a function of K_0 only. Therefore, the solution of the optimization problem is similar to that given in Reference 1, if one first finds the normal shielding attenuation, K_0, corresponding to the specified dose using Eq. 7.33. Then

$$r_i^2 - \nu \frac{\Delta A_i}{\Delta \rho_i} = 0; \qquad i = 1, 2, \ldots, j$$

$$K_0 - \sum_{i=1}^{j} \Delta A_i r_i + A_1 r_0 = 0$$

which yields

$$r_i = \frac{K_0 + r_0 A_1}{\sum_{i=1}^{j} \frac{(\Delta A_i)^{3/2}}{(\Delta \rho_i)^{1/2}}} \times \left(\frac{\Delta A_i}{\Delta \rho_i} \right)^{1/2}$$

in accord with Eq. 11 of Reference 1.

It is readily seen from Eq. 2.28a that

$$r_i^2 \geq \nu \frac{\Delta A_i}{\Delta \rho_i} \tag{2.29}$$

since ν and η are positive numbers and $0 \leq e \leq r_i$. In order to obtain r_i from Eq. 2.28a one has to solve cubic equations in r_i^2. In Appendix D it is shown that one and only one solution of these equations satisfies the inequality (2.29). Further, since r_i must be positive, one obtains the shell radii by taking the positive square root of the solution. Hence, the shell radii, r_i, are obtained as a function of the two Lagrange multipliers and, of course, depend on the values of e and $\Delta A_i/\Delta \rho_i$, i.e.,

$$r_i = h_i(\eta,\nu). \tag{2.30}$$

Thus, the problem is to find a set of Lagrange multipliers, η and ν, which satisfies the system

$$r_i = h_i(\eta,\nu) \qquad i = 1, 2, \ldots, j \tag{2.31}$$

$$\nu \frac{\partial f}{\partial K_m} - \eta \left(\frac{\partial f}{\partial K_0} + \frac{\partial f}{\partial K_m} \right) = 0$$

$$f - \overline{f} = 0$$

The method of solution is based on a rule of false position iteration for the values of ν and η.[9] In this method, a guessed value for the set (ν,η) provides us with a set of shell radii, r_i. Once r_i has been obtained the following quantities can be computed successively.

$$K_0 = \sum_{i=1}^{j} \Delta A_i \, h_i(\eta,\nu) - A_i r_0$$

$$K_m = \sum_{i=1}^{j} \Delta A_i \{[h_i(\nu,\eta)]^2 - e^2\}^{1/2} - A_1 (r_0^2 - e^2)^{1/2}$$

$$Z_1 = \frac{K_m}{K_0} > 1 \text{ and } Z_2 = \frac{K_m}{K_0 + 2A_T e} < 1$$

$$f = \frac{1}{K_m^{b+1}} \left[\frac{Z_1}{Z_1 - 1} (Z_1^b - 1) - \frac{Z_2}{Z_2 - 1} (Z_2^b - 1) \right]$$

$$\frac{\partial f}{\partial K_m} = \frac{1}{K_m^{b+2}} \left[- \frac{Z_1^2}{(Z_1 - 1)^2} (Z_1^b - 1) + \frac{Z_2^2}{(Z_2 - 1)^2} (Z_2^b - 1) + \frac{bZ_1}{Z_1 + 1} - \frac{bZ_2}{Z_2 + 1} \right]$$

$$\frac{\partial f}{\partial K_m} + \frac{\partial f}{\partial K_0} = \frac{1}{K_m^{b+2}} \left[\frac{Z_1^{b+2} + Z_1}{1 + Z_1} - \frac{Z_2^{b+2} + Z_2}{1 + Z_2} \right]$$

$$R(\nu,\eta) = f - \overline{f}$$

$$S(\nu,\eta) = \nu \frac{\partial f}{\partial K_m} - \eta \left(\frac{\partial f}{\partial K_m} + \frac{\partial f}{\partial K_0} \right)$$

Given three linearly independent sets (ν_ℓ, η_ℓ) the corresponding values R_ℓ and S_ℓ can be computed. A rule of false position iteration for the value of ν and η which satisfies $R(\nu,\eta) = S(\nu,\eta) = 0$ is given by

$$X = \frac{\begin{vmatrix} X_1 & R_1 & S_1 \\ X_2 & R_2 & S_2 \\ X_3 & R_3 & S_3 \end{vmatrix}}{\begin{vmatrix} 1 & R_1 & S_1 \\ 1 & R_2 & S_2 \\ 1 & R_3 & S_3 \end{vmatrix}} \qquad (2.32)$$

where $X = \nu$ or η.

A corresponding set of r_i and R and S are then computed and the following inequalities are tested

$$\begin{aligned} R &\leq \delta \\ S &\leq \delta \end{aligned} \tag{2.33}$$

where δ is a very small number.

If the inequalities (2.33) are satisfied, then the values of ν and η are accepted as solutions. If they are not satisfied, the procedure is repeated by replacing one set (ν_ℓ,η_ℓ) by the new computed set. This is done until the convergence of R and S to 0 is accepted for the computed values of ν and η.

The procedure outlined was programmed for the CDC-1604-A, but to date this portion of the overall optimization code, MOPS, has not been completely checked out. It is difficult to predict what the value of δ must be in the inequalities (2.33) for which the values of η and ν are acceptable. Initial guesses of the three sets (η,ν) must be based on physically meaningful quantities and the convergence will be attained rapidly if one starts with good sets (ν,η). However, machine experiments with the code will be necessary before a practical procedure can be determined.

2.3.2 Depth Dose

To optimize the shield weight subject to a given depth dose at r = e′ within the spherical man, the approach outlined for the average body dose constraint is followed.

If the depth dose can be written as (see Eq. 2.22)

$$D_p(e') = \frac{A_T C}{3}\, g(K_0', K_m') \tag{2.34}$$

then the system of equations in the Lagrangian factors ν and η and the shield

layer radii, r_i, to be solved are

$$r_i^2 - \nu \frac{\Delta A_i}{\Delta \rho_i} - \eta \frac{\Delta A_i}{\Delta \rho_i} \left[\frac{r_i}{(r_i^2 - e'^2)^{1/2}} - 1 \right] = 0; \qquad i = 1, 2, \ldots, j$$

$$\nu \frac{\partial g}{\partial K'_m} - \eta \left(\frac{\partial g}{\partial K'_0} + \frac{\partial g}{\partial K'_m} \right) = 0$$

$$g - \bar{g} = 0 \tag{2.35}$$

$$K'_0 = \sum_{i=1}^{j} \Delta A_i r_i - A_1 r_0 + A_T (e - e')$$

$$K'_m = \sum_{i=1}^{j} \Delta A_i (r_i^2 - e'^2)^{1/2} - A_1 (r_0^2 - e'^2)^{1/2} + A_T (e^2 - e'^2)^{1/2}$$

where

$$\bar{g} = \frac{3 \bar{D}_p(e')}{A_T C}$$

and $\bar{D}_p(e')$ is the given constraint.

Of course, we also must have

$$r_0 < r_1 < r_2 \ldots < r_j.$$

Note that if $e' \to 0$, the optimization problem becomes trivial since the constraint can be replaced by a given aluminum equivalent shield thickness, K_0. This case has been treated in Reference 1.

The method of solution is also based on a rule of false position iteration for the values of the Lagrangian factors ν and η. The steps to be followed are:

1. Guess a set of values for ν and η

2. Obtain r_i in terms of ν and η
3. Compute K_0' and K_m'
4. Using these values of K_0' and K_m', evaluate $g(K_0',K_m')$ and $\partial g/\partial K_0'$ and $\partial g/\partial K_m'$
5. Evaluate the remainders

$$R(\nu,\eta) = g(K_0',K_m') - \bar{g}$$

$$S(\nu,\eta) = \nu \frac{\partial g}{\partial K_m'} - \eta \left(\frac{\partial g}{\partial K_m'} + \frac{\partial g}{\partial K_0'} \right)$$

6. Repeat steps 2 through 5 with two other guesses for the set (ν,η)
7. Compute a new set (ν,η) by solving the following equation

$$x = \frac{\begin{vmatrix} x_1 & R_1 & S_1 \\ x_2 & R_2 & S_2 \\ x_3 & R_3 & S_3 \end{vmatrix}}{\begin{vmatrix} 1 & R_1 & S_1 \\ 1 & R_2 & S_2 \\ 1 & R_3 & S_3 \end{vmatrix}}$$

where $x = \nu$ or η

8. Repeat the process until the computed remainders R and S are less than or equal to a very small number, δ.

Once the false position iteration procedure has been worked out successfully for the average body dose constraint, the solution of the depth dose problem should follow in a straightforward manner.

2.3.3 Particular Case of the Completely Filled Void

If the crew model fills the available space inside the shield completely, i.e., if $e = r_0$, then it can be shown that all the materials available on the Young diagram

must be used in the minimum weight shield. To do this, it must be shown that all the optimized shield layer radii $r_1 \ldots r_n$ are greater than r_0, i.e., that

$$r_0 < r_1 < r_2 < \ldots < r_n \quad \text{for } r_0 = e.$$

In Section 2.3.1, the system of equations to be solved in order to obtain the minimum shield layer radii, r_i, is given in Eq. 2.28. If the set of Lagrange multipliers in Eq. 2.28, $\nu > 0$ and $\eta > 0$, is determined, then r_i values are obtained by solving the following equation

$$r_i^2 - \frac{\Delta A_i}{\Delta \rho_i}\left[\nu' + \eta \frac{r_i}{(r_i^2 - r_0^2)^{1/2}}\right] = 0; \qquad i = 1, 2, \ldots, n \tag{2.36}$$

where n represents the total number of materials on the Young diagram. Here we revert to the multiplier ν' and the definition given in Eq. 2.27 is used.

Let us define x_i, by $x_i = r_i - r_0$, and then let us show that a unique positive solution, x_i, to the equation exists.

$$(x_i + r_0)^2 - \frac{\Delta A_i}{\Delta \rho_i}\left[\nu' + \eta \frac{x_i + r_0}{(2x_i r_0 + x_i^2)^{1/2}}\right] = 0 \tag{2.37}$$

If the positive values of x_i, which satisfy Eq. 2.37, exist, they are given by the intersection of two curves which are defined by the following equations:

$$y_1 = (x + r_0)^2 \qquad x > 0 \tag{2.38}$$

$$y_2^i = \frac{\Delta A_i}{\Delta \rho_i}\left[\nu' + \eta \frac{x + r_0}{(2xr_0 + x^2)^{1/2}}\right] \qquad x > 0 \ .$$

But as x increases from 0 to infinity, y_1 increases from r_0^2 to ∞ while y_2^i decreases from ∞ to

$$\frac{\Delta A_i}{\Delta \rho_i}(\nu' + \eta)$$

(see Fig. 10). Hence, there is one and only one intersection point of the two curves in the first quadrant ($x > 0$, $y > 0$).

Therefore one, and only one, value of x_i exists which satisfies Eq. 2.37 and is positive. Since

$$x_i > 0$$

$$\therefore \quad r_i > r_0.$$

Since the Young curve is increasing and concave downward (see Fig. 1)

$$0 < \frac{\Delta A_1}{\Delta \rho_1} < \frac{\Delta A_2}{\Delta \rho_2} \ldots < \frac{\Delta A_i}{\Delta \rho_i} \ldots < \frac{\Delta A_n}{\Delta \rho_n}.$$

Then, from Eq. 2.38, given x, we have

$$y_2^1 < y_2^2 < \ldots < y_2^i < \ldots < y_2^n \qquad 0 < x < \infty$$

Thus, it is shown in Fig. 10 that x_i must satisfy the inequality:

$$0 < x_1 < x_2 < \ldots < x_i < \ldots < x_n$$

and therefore

$$r_0 < r_1 < r_2 < \ldots < r_n.$$

Thus, all the materials on the Young diagram must be used in order to obtain a minimum weight shield for this case.

This result is of particular interest in the design of space suits where the astronaut completely fills the "shielded void." In addition, even for a space vehicle, if the man can and does move around inside the crew compartment, he can be viewed as being uniformly distributed in the available space.

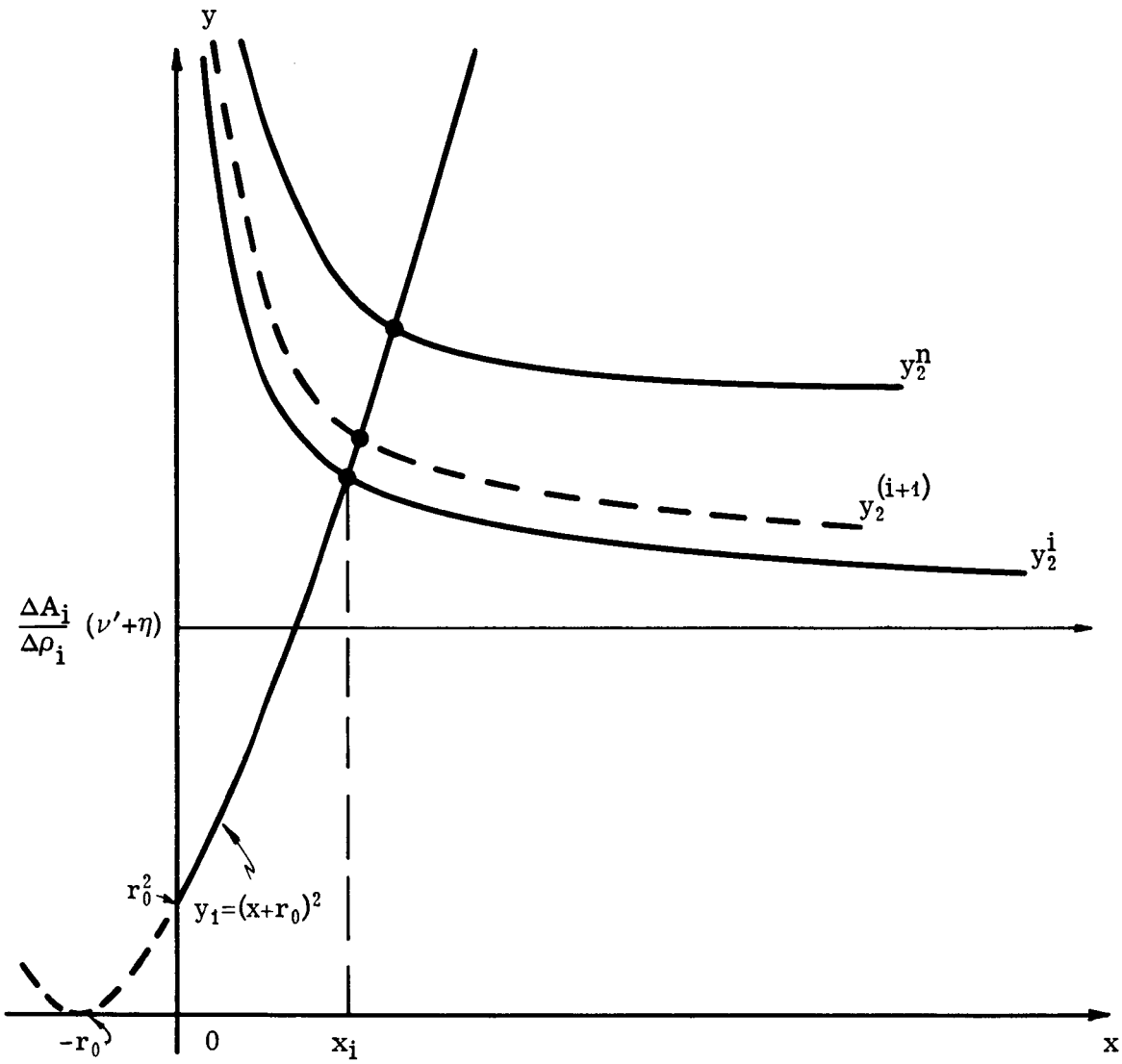

Fig. 10 — Intersection of the curves defined by Eq. 2.38

2.3.4 Simultaneous Application of Two Dose Constraints

In Section 2.3.1 we considered the constraint that the average body dose D_V, in the spherical phantom must be less than a specified dose, $\overline{D}_V$. In this section, we add the additional constraint that nowhere inside the void can the local dose D(r) exceed another specified value, $\overline{D}$.

Since the local dose is a maximum at the void center, as shown in Section 2.2.7, it is sufficient that the void center dose, D(0), be less than $\overline{D}$. From Eq. 2.20

$$D(0) = b(b+1)\, A_T \frac{C}{K_0^{b+2}}$$

What is required then is that

$$K_0 \leq C' \overline{D}^{b+2}$$

where

$$C' = \left[b(b+1)\, A_T C\right]^{-(b+2)} \tag{2.39}$$

A trivial solution is obtained if the specified values of the dose constraint are such that

$$\overline{D} \leq \overline{D}_V \tag{2.40}$$

Then, since the local dose at the center is always greater than the average body dose (when e > 0) for a given shield, if we obtain the minimum weight shield subject only to the constraint that

$$K_0 = \overline{K}_0 = C' \overline{D}^{(b+2)} ,$$

this shield will satisfy the two dose constraints in the problem. This case has been solved in Reference 1.

In general, however,

$$\overline{D} > \overline{D}_V \tag{2.42}$$

Then the procedure to obtain the minimum weight proton shield subject to the two prescribed constraints is as follows:

1. Compute the minimum weight proton shield subject only to the constraint that

   $K_0 = \overline{K}_0 = C'\overline{D}^{(b+2)}$.

   Once the number of shield materials and the set of shell radii have been determined, calculate the average body dose in the given crew model, D_V. Test if D_V is less than or greater than $\overline{D}_V$. If less, the solution of the problem has been obtained. If greater, proceed to step 2.

2. Compute the minimum weight proton shield subject only to the constraint that $D_V \leq \overline{D}_V$. Do this by using the technique outlined in Section 2.3.1. Once the number of shield materials and set of shell radii have been determined, compute K_0 and test if K_0 is less than or greater than $\overline{K}_0$. If less, the solution of the problem has been found. If greater, proceed to step 3.

3. Since the average body dose is a function of K_0 and K_m, compute $\overline{K}_m$ for a given dose, $\overline{D}_V$, and a given normal shield attenuation, $\overline{K}_0$.

   Then, construct the Lagrangian

   $$L = \frac{W}{4\pi} + \mu\,(\overline{K}_0 - K_0) + \eta\,(\overline{K}_m - K_m) \tag{2.43}$$

   where μ and η are positive Lagrange multipliers. The optimum weight shield is then achieved if the following conditions are satisfied.

$$\bar{K}_0 - K_0 = 0;\ \mu > 0.$$

$$\bar{K}_m - K_m = 0;\ \eta > 0.$$

$$\frac{\partial L}{\partial K_i} = \Delta\rho_i r_i^2 - \mu\Delta A_i - \eta\,\Delta A_i \frac{r_i}{\sqrt{r_i^2 - e^2}} = 0; \qquad i = 1, 2, \ldots, j. \tag{2.44}$$

The method of solution by iteration described in Section 2.3.1 must be used to solve the system of equations (Eq. 2.44).

3. PROTON SHIELD OPTIMIZATION FOR CONVEX VOLUME VOIDS

3.1 METHOD OF LOCAL OPTIMIZATION

In Reference 1, the analysis of the technique of spherical shield optimization was extended to the more general case of convex voids under the assumption that the shield must eliminate all normally incident protons below a specified energy. This analysis resulted in an equation for the local layer thicknesses in the optimized shield given as Eq. 22 of Reference 1. This theory has now been put in slightly different form and has been applied to the calculation of local minimum shields for convex voids.

3.1.1 Theory

The problem is to find the initial material sequence and layer thicknesses of the minimum weight shield surrounding an elementary surface, dS, about each point P on S. If the void has rotational symmetry, dS is taken as an infinitesimally thin ring about the axis of revolution.

The surface element, ds, is characterized by its two principal radii of curvature. All distances are measured from one of the curvature centers, the positive direction being the normal outwards. Then the local weight is

$$\Delta W = \sum_{i=1}^{n} (\rho_i - \rho_{i+1}) \left(\frac{s_i^3}{3} - \sigma \frac{s_i^3}{2} \right) - \rho_1 \left(\frac{s_0^3}{3} - \sigma \frac{s_0^3}{2} \right) \qquad (3.1)$$

where n = number of shield materials

ρ_i = density of i^{th} material with $\rho_{n+1} = 0$

s_i = distance to the outer surface of the i^{th} shield layer from the major center of curvature of the local section considered

s_0, $s_0 + \sigma$ = principal radii of curvature of the local section, σ assumed to be finite.

The aluminum equivalent thickness of the local shield is given by

$$K = \sum_{i=1}^{n} (A_i - A_{i+1}) s_i - A_1 s_0 \tag{3.2}$$

where A_i is the proton relative stopping power of the i^{th} material with $A_{n+1} = 0$.

To minimize W subject to Eq. 3.2, we construct the Lagrangian

$$L = \Delta W + \mu \left[K - \sum_{i=1}^{n} (A_i - A_{i+1}) s_i + A_1 s_0 \right] \tag{3.3}$$

where μ is a Lagrange multiplier.

The distances, s_i, of the minimum weight shield, are then obtained by minimizing L with respect to each s_i. Hence,

$$s_i = \frac{\sigma}{2} \left[1 \pm \left(1 + \frac{4\mu}{\sigma^2} \frac{A_i - A_{i+1}}{\rho_i - \rho_{i+1}} \right)^{1/2} \right] \tag{3.4}$$

where the sign $\pm$ depends on the sign of σ in order for s_i to be positive. Substituting Eq. 3.4 into Eq. 3.2 yields an equation in μ.

With this general expression it is possible to synthesize the minimum weight shield for any convex void by breaking it up into local volumes, each of which has designated values of s_0, σ, and K. The local void volumes which can be treated include a sphere (for which $\sigma = 0$), a cone, and a cylinder. The latter

two special cases (for which σ becomes infinite) are treated in detail in Section 4.2 of Reference 1. Once the local shield layers have been determined, the weights of each layer can be calculated by numerical integration over the shield surface and the total weight of the optimized shield can be obtained.

3.1.2 Numerical Results

In order to investigate the application of the theory, the dimensionless parameters K/s_0 and σ/s_0 are used to show how different materials enter the local minimum weight shield. Fig. 11 shows how the number of materials to be used in the local optimized shield varies as a function of the two parameters. In the regions between the curves, the designated materials make up the local minimum weight shield. It is interesting to note that the ordinate in Fig. 11, i.e., $\sigma = 0$, gives the results for the spherical case.

Sets of curves which give the thicknesses of each shield layer have been constructed. A separate curve is required for each combination of materials specified by Fig. 11. These curves are shown in Figs. 12 through 15. The parameters used are s_i/σ and $(K+A_j s_0)/\sigma$, where A_j is the relative stopping power of the innermost material of that particular sequence. The thickness of any given layer is then equal to $(s_i - s_{i-1})$.

3.2 SHIELD OPTIMIZATION FOR COMPLETE CONVEX VOIDS

In the last section, it is shown how it is possible to synthesize a minimum weight shield for a convex void on a piecewise basis. In that method, normal incidence of the incident proton radiation was assumed. In this section, an approach to synthesizing a complete minimum weight shield analytically for a symmetrical convex void and at the same time removing the normal incidence restriction will be outlined.

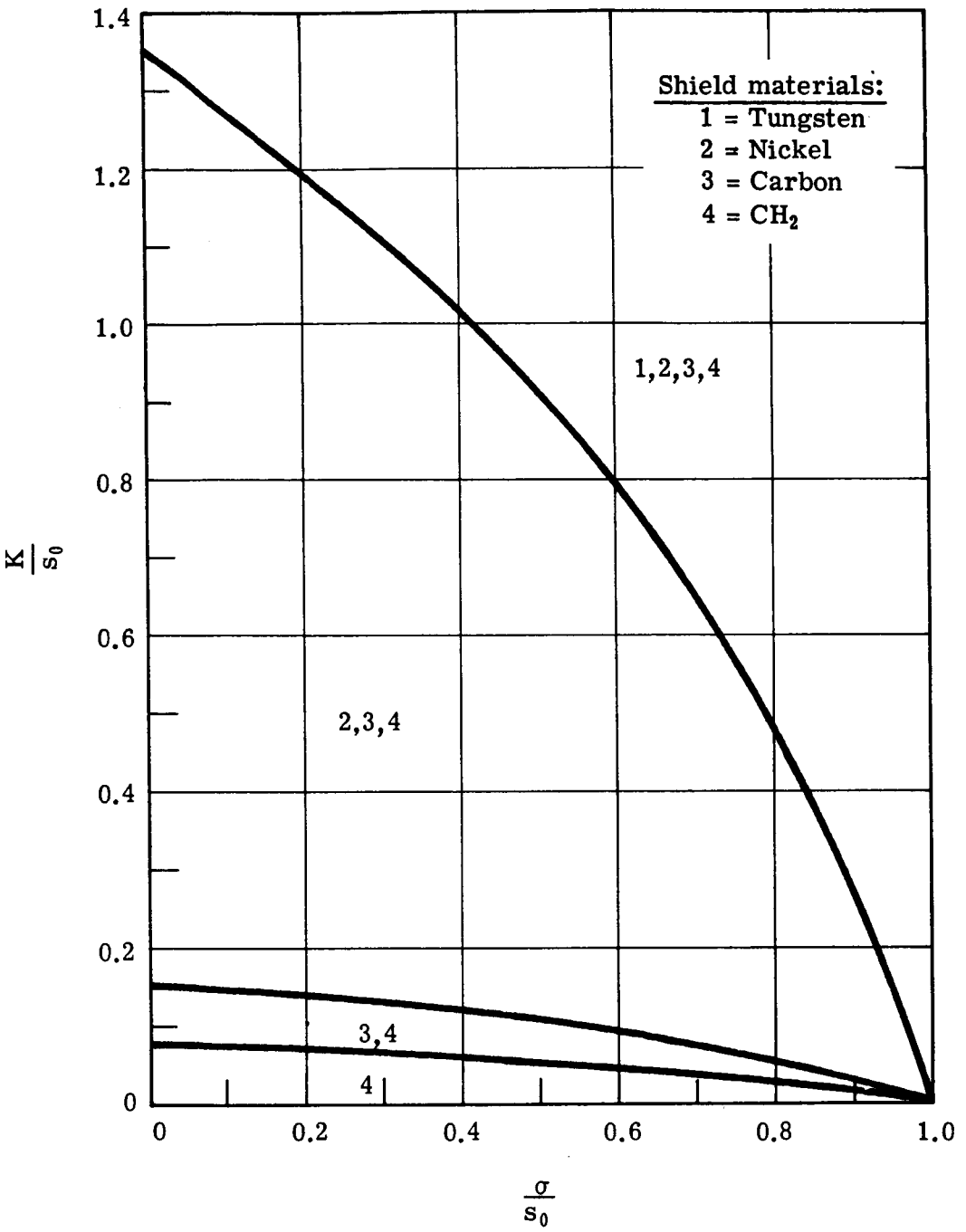

Fig. 11 — Materials to be included in an optimized shield as a function of K/s_0 and σ/s_0

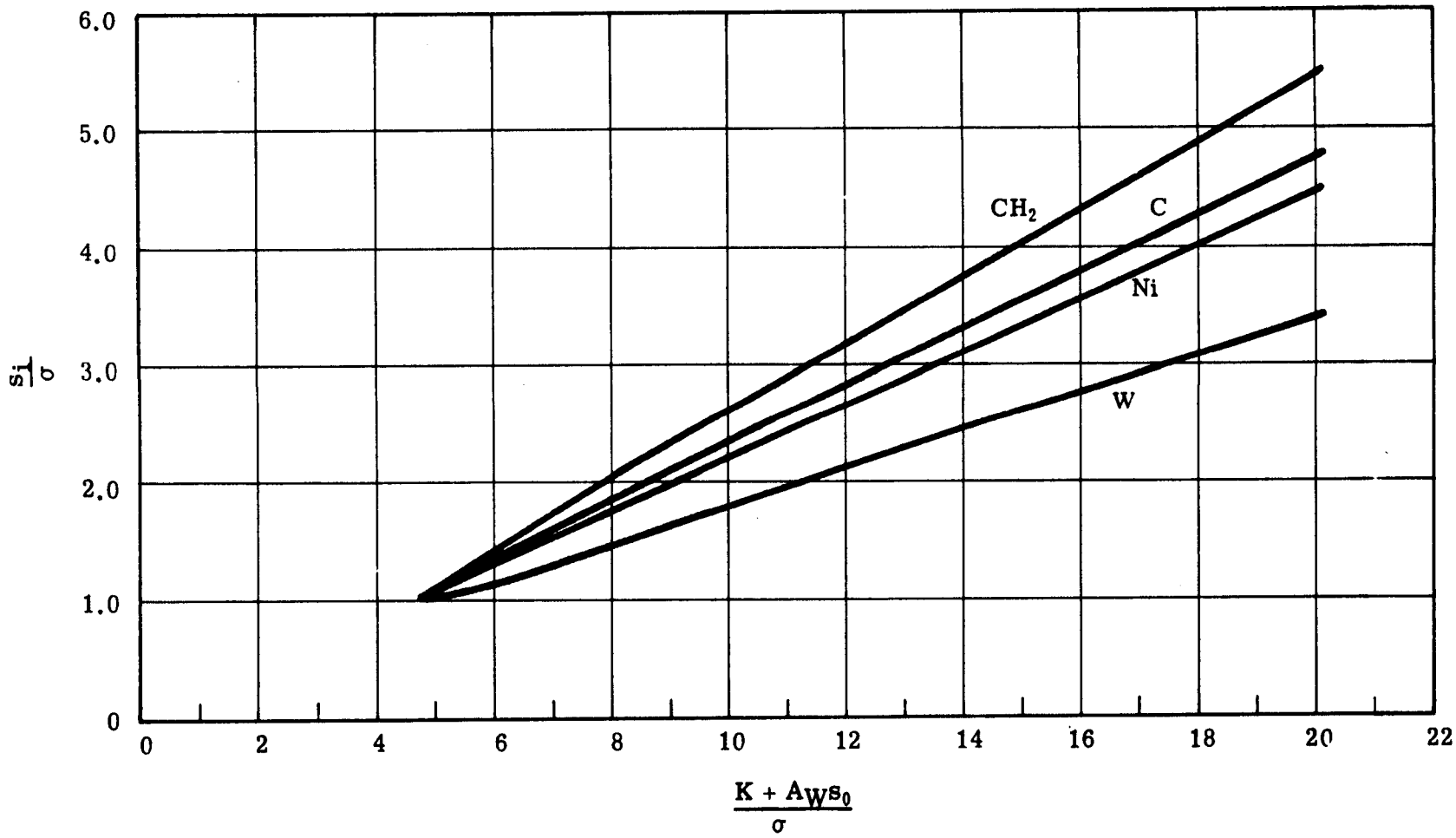

Fig. 12 — Distances to the outer surfaces of the various shield layers for a four-material shield as a function of s_i/σ and $(K+A_W s_0)/\sigma$

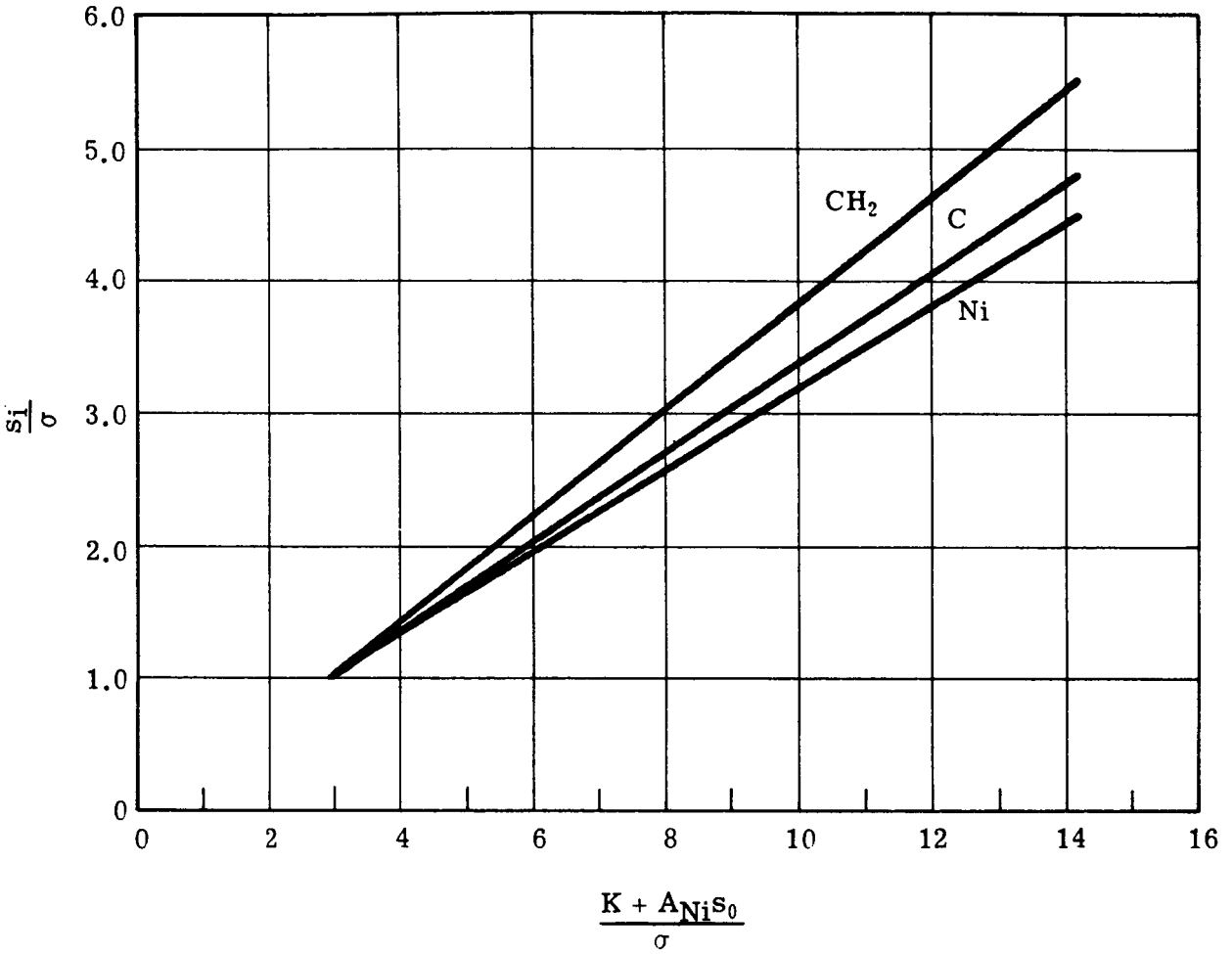

Fig. 13 — Distances to the outer surfaces of the various shield layers for a three-material shield as a function of s_i/σ and $(K+A_{Ni}s_0)/\sigma$

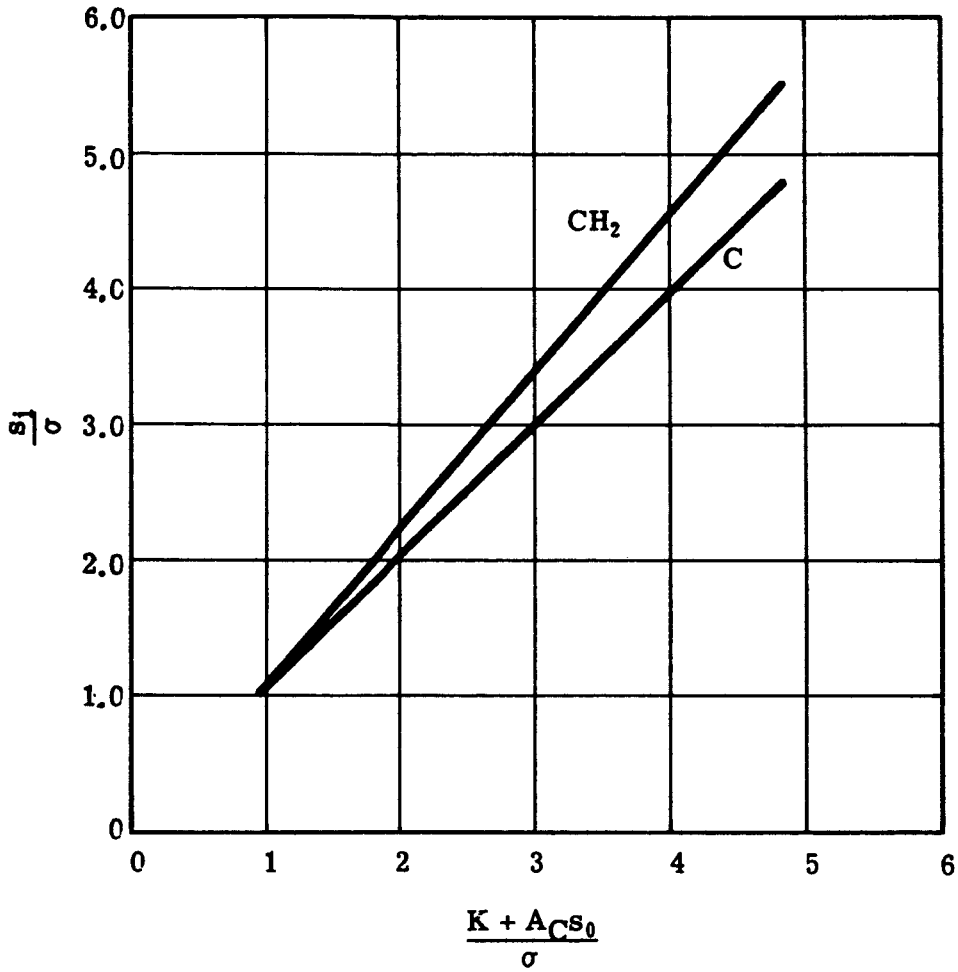

Fig. 14 — Distances to the outer surfaces of the various shield layers for a two-material shield as a function of s_i/σ and $(K+A_C s_0)/\sigma$

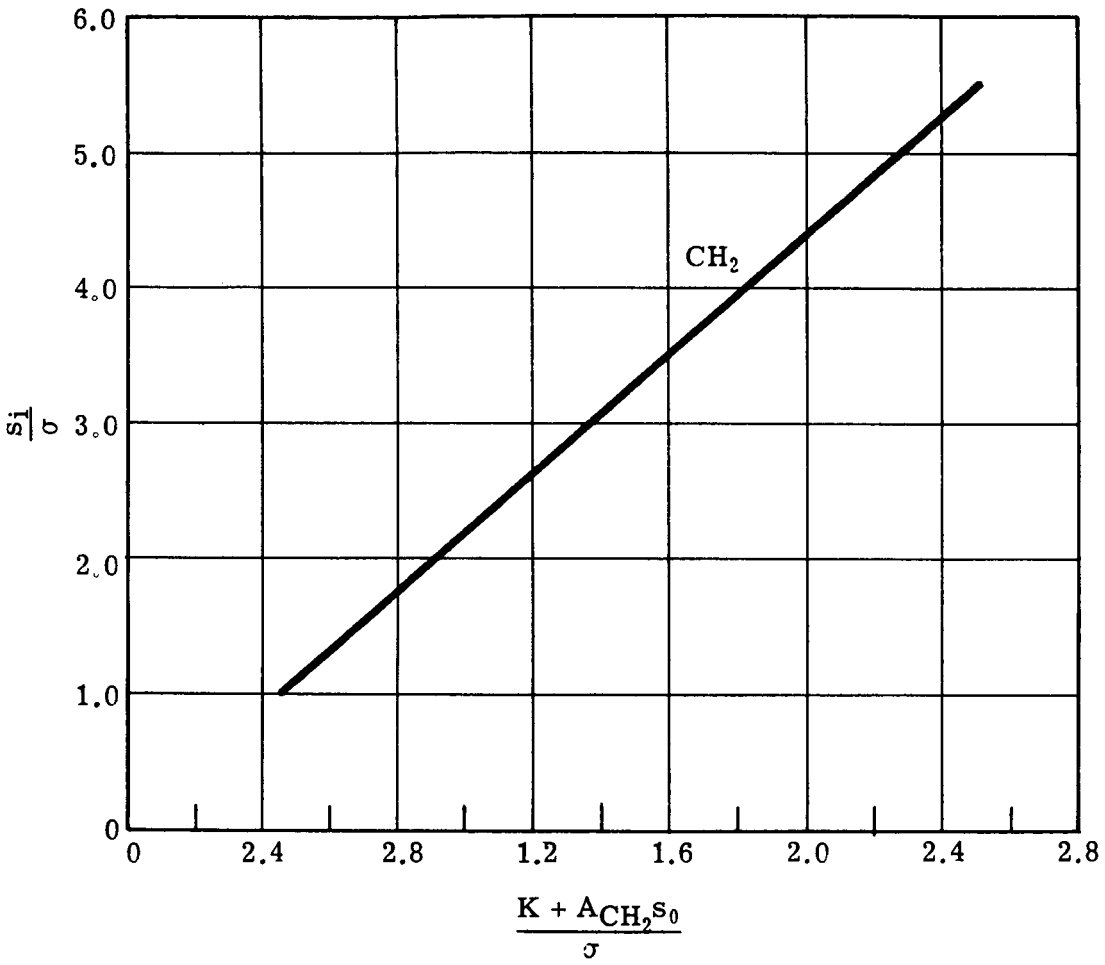

Fig. 15 — Distances to the outer surface of a one-material shield as a function of s_i/σ and $(K+A_{CH_2}s_0)/\sigma$

3.2.1 Statement of Problem and Assumptions Made

Given a convex void enclosed by a surface of revolution, the optimization problem concerns itself with determining surfaces which define layers of surrounding shield materials (obtained from a Young diagram) such that protons of energy less than a given cutoff energy, E_0, have an aluminum equivalent range which does not exceed a given constant, K, for any direction of proton incidence. Then, for a given family of surfaces which satisfy this condition, the one which minimizes the weight of the shield is chosen.

The other assumptions made are:

1. Besides requiring that a surface of revolution enclose the void, the surfaces of the surrounding shield layers are taken to be surfaces of revolution about the axis of the void.
2. The void surface is defined in terms of a parametric representation using as a parameter the distance, s, measured from an origin which is the intersection of the axis and the void surface (Fig. 16).
3. The void is defined as having a continuously turning normal at all points on its surface. This assumption makes it possible to define the shield layer surfaces in terms of the void surface itself and the distance along

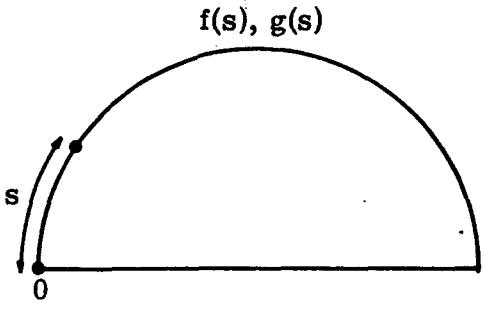

Fig. 16 — Parametric representation of the void surface

the normal from the void to the surface in question. This assumption is not absolutely necessary to the theory , but it has the advantage of enabling us to define the shield layers in terms of a single, uniquely determined, normal thickness function, t(s).

4. A further simplification is made in the formulation by permitting the void surface cross section to be defined in terms of straight line segments and/or arcs of circles. However, this should be sufficiently general to handle most shapes of interest.

3.2.2 Theory

In terms of the foregoing assumptions the equation of the void surface in cylindrical coordinates (R,Z) may be obtained by eliminating s from the equations

$$R(s) = f(s)$$
$$Z(s) = g(s) \qquad (3.5)$$

for $0 \leq s \leq S$ = total surface length.

The equation of each shield layer of normal thickness, t(s), can then be obtained by eliminating s from the equations

$$R(s) = f(s) - t(s)\, f'(s)$$
$$Z(s) = g(s) + t(s)\, g'(s) \qquad (3.6)$$

where the functions must satisfy the conditions

$$g'(0) = 0 = g'(S) \qquad (3.7a)$$

$$g'(s) \geq 0 \qquad \text{if } 0 \leq s \leq S \qquad (3.7b)$$

$$\frac{dZ}{dR} = \frac{f'(s)}{g'(s)} \qquad \text{must be continuous if } g' \neq 0 \tag{3.7c}$$

$$\frac{d^2Z}{dR^2} = \frac{g'(s)\, f''(s) - f'(s)\, g''(s)}{[g'(s)]^3} \leq 0 \text{ if } g' \neq 0 \tag{3.7d}$$

The singly and doubly primed functions have the usual meaning of first and second derivatives.

If the void surface is defined in terms of straight line segments, the equations for the straight line between (g_1,f_1) and (g_2,f_2) where $g_1 < g_2$ and (g_1,f_1) corresponds to $s = s_1$ are given by

$$g(s) = g_1 + \frac{(g_2-g_1)(s-s_1)}{\sqrt{(g_2-g_1)^2 + (f_2-f_1)^2}}$$

$$f(s) = f_1 + \frac{(f_2-f_1)(s_2-s_1)}{\sqrt{(g_2-g_1)^2 + (f_2-f_1)^2}} \tag{3.8}$$

It is clear that all the conditions of Eq. 3.7 are satisfied along the portion of the surface defined by the straight line.

The alternate formulation is to define the void surface by a circular arc with center (α,β) and radius r passing through (g_1,f_1) at $s = s_1$, where (g_1,f_1) is the left-most point on the arc. It should be noted that f(s) must exceed β for all s on the arc since the arc must be concave downward (see Fig. 17). The equations for the circular arc defined in this manner are

$$g(s) = \alpha + (g_1-\alpha)\cos\left(\frac{s-s_1}{r}\right) - (f_1-\beta)\sin\left(\frac{s-s_1}{r}\right)$$

$$f(s) = \beta - (g_1-\alpha)\sin\left(\frac{s-s_1}{r}\right) - (f_1-\beta)\cos\left(\frac{s-s_1}{r}\right) \tag{3.9}$$

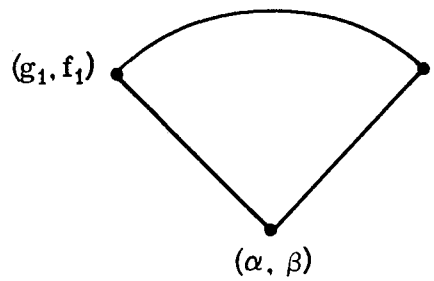

Fig. 17 — Circular arc definition of the void surface

Along the portion of the surface defined by the circular arc the following conditions hold

$$g'(s) = \frac{[f(s) - \beta]}{r} \geq 0$$

$$f'(s) = -\frac{[g(s) - \alpha]}{r}$$

$$g''(s) = -\frac{[g(s) - \alpha]}{r^2}$$

$$f''(s) = -\frac{[f(s) - \beta]}{r^2} \qquad (3.10)$$

Therefore, the conditions of Eq. 3.7 are also satisfied for this formulation.

The equations for the shield layers in the two cases are the following:

Straight Line Segment

$$Z(s) = g_1 + \frac{(f_2 - f_1)(s - s_1) - t(s)(f_2 - f_1)}{\sqrt{(g_2 - g_1)^2 + (f_2 - f_1)^2}}$$

$$R(s) = f_1 + \frac{(f_2 - f_1)(s - s_1) + t(s)(g_2 - g_1)}{\sqrt{(g_2 - g_1)^2 + (f_2 - f_1)^2}} \qquad (3.11)$$

Circular Arc

$$Z(s) = \alpha + \left[\frac{r+t(s)}{r}\right]\left[(g_1-\alpha)\cos\left(\frac{s-s_1}{r}\right) - (f_1-\beta)\sin\left(\frac{s-s_1}{r}\right)\right]$$

$$R(s) = \beta - \left[\frac{r+t(s)}{r}\right]\left[(g_1-\alpha)\sin\left(\frac{s-s_1}{r}\right) + (f_1-\beta)\cos\left(\frac{s-s_1}{r}\right)\right] \qquad (3.12)$$

The calculation of the distance from the void surface to any shield layer surface now can be derived. By virtue of the cylindrical symmetry an arbitrary point on the void surface may be chosen. This will be the point with coordinates $f(s_0),0, g(s_0)$. Let $(\Omega_x,\Omega_y,\Omega_z)$ be a unit vector at this point which makes an angle of not more than 90° with the outward normal. Then $(\Omega_x,\Omega_y,\Omega_z)$ must satisfy

$$\Omega_x^2 + \Omega_y^2 + \Omega_z^2 = 1$$

and

$$\Omega_x \geq \frac{f_0'}{g_0'}\,\Omega_z$$

or

$$\Omega_x g_0' \geq \Omega_g f_0', \text{ since } g_0' \geq 0.$$

Consider the point

$$(f_0,0,g_0) + T(\Omega_x,\Omega_y,\Omega_z).$$

If this point is to lie on the surface defined by Eq. 3.6, or one of its specialized forms (Eqs. 3.11 or 3.12) it must be possible to determine s', lying in the proper range, so that the corresponding R and Z satisfy the equations

$$Z(s') = g_0 + T\Omega_z$$

$$R(s') = \sqrt{f_0^2 + 2f_0\Omega_x T + (1-\Omega_z^2)\,T^2} \qquad (3.13)$$

It is possible to introduce a new set of variables for the angular dependence, which will satisfy conditions with fixed limits, independently of the value of the parameter s_0. Let

$$\Omega_1 = g_0'\Omega_X - f_0'\Omega_Z$$
$$\Omega_2 = f_0'\Omega_X + g_0'\Omega_Z \tag{3.14}$$

Then

$$\Omega_X = g_0'\Omega_1 + f_0'\Omega_Z$$
$$\Omega_Z = g_0'\Omega_2 - f_0'\Omega_1. \tag{3.15}$$

Substituting in the above, we obtain

$$Z(s') = g_0 + T\,(g_0'\Omega_2 - f_0'\Omega_1)$$
$$R(s') = \sqrt{f_0^2 + 2\,f_0\,(g_0'\Omega_1 + f_0'\Omega_2)\,T + [1-(g_0'\Omega_2 - f_0'\Omega_1)^2]\,T^2} \tag{3.16}$$

with the following conditions:

$$\Omega_1 \geq 0$$
$$\Omega_1^2 + \Omega_2^2 \leq 1 \tag{3.17}$$

The simultaneous Eqs. 3.16 must have a solution pair (s',T) for each pair (Ω_1,Ω_2) satisfying the conditions of Eqs. 3.17, and s' must lie in the interval in which the particular form given by Eqs. 3.11 or 3.12 is appropriate. As stated above, by choosing the appropriate form for t(s), one and only one solution T for each "triple" s_0, Ω_1, Ω_2 is insured.

For each shield layer, k, the volume, V_k, enclosed, can be calculated from

$$V_k = \pi \int_0^S [R_k(s)]^2 \, Z_k'(s) \, ds \tag{3.18}$$

The shield weight, W, is given by

$$W = \rho_1 (V_1 - V_0) + \rho_2 (V_2 - V_1) + \ldots + \rho_n (V_n - V_{n-1}) \tag{3.19}$$

The optimization problem now consists of minimizing W as a functional of the normal shield layer thicknesses $t_1(s)$, ..., $t_k(s)$, ..., $t_n(s)$, where $t_i(s)$ (i=1, ..., n) is such that the following conditions are satisfied.

- The solution is unique
- $t_1(s) \leq t_2(s) \ldots \leq t_n(s)$ for $0 \leq s \leq S$ (3.20)
- The total aluminum equivalent thickness of the shield at that point $\geq K$, i.e.,

$$A_1 T_1 + A_2 (T_2 - T_1) + \ldots, + A_n (T_n - T_{n-1}) \geq K \tag{3.21}$$

where T_k is a solution of Eq. 3.16 for $t_s = t_k(s)$.

This leads to a problem in the calculus of variations, and since the conditions on the t's are nonlinear, it was decided to attempt an approach which would reduce them to a discrete problem. This, in turn, presents a problem in the minimization of a number of constants, where the constraints are nonlinear.

To solve this reduced problem, the void is first divided into segments according to the sequence $s = s_0, s_1, \ldots, s_p$, where $s_0 = 0$ and $s_p = S$. (See Fig. 18.) Once this is done, the thickness function, $t_k(s)$, for the k^{th} shield layer can be replaced by a sequence of thickness functions, $t_{kp} = t_k(s_p)$ in each interval (see Fig. 19). It is necessary to assume a behavior for the function in the interior of each interval (s_p, s_{p+1}). The simplest assumption which will still permit the sur-

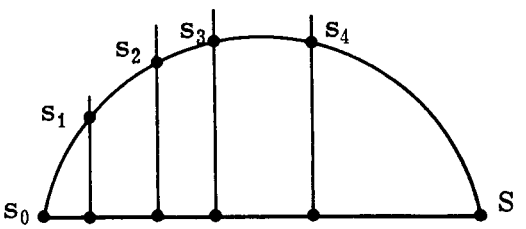

Fig. 18 — Segmentation of the void

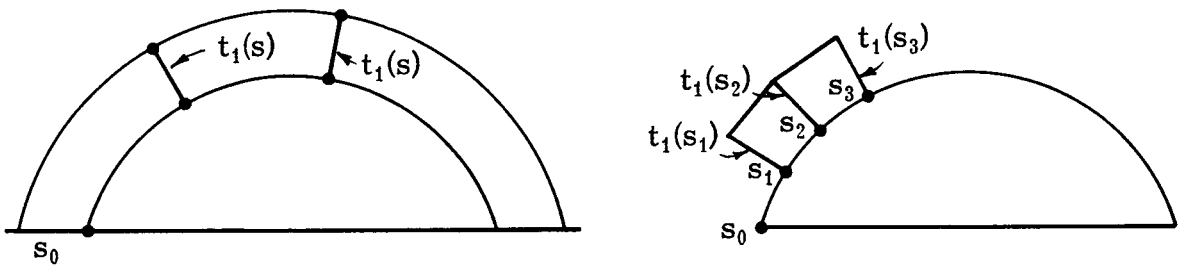

(a) Single thickness function

(b) Sequence of thickness functions

Fig. 19 — Replacement of a single thickness function by a sequence of thickness functions

face, now made up of various sections, to be continuous is a linear one. The relationship in the interval $s_p \leq s \leq s_{p+1}$ is

$$t_k(s) = \frac{(s-s_p)\, t_{k,p+1} + (s_{p+1}-s)\, t_{k,p}}{s_{p+1} - s_p} \tag{3.22}$$

where k denotes the k^{th} shield layer and the initial condition is that

$$t_{k+1,\, p} \geq t_{k,p}.$$

Additional conditions arise as the resulting curves (defined by Eqs. 3.11 or 3.12 depending upon whether a straight line segment or a circular arc is used for the void region or section thereof) are required to give a curve which is concave downward for all values of $0 \leq s \leq S$. The condition given by Eq. 3.21 must also be satisfied. Finally the function $W(t_{1,0} \ldots t_{1,p};\ t_{2,0} \ldots t_{2,p};\ \ldots\ t_{n,0} \ldots t_{n,p})$ must be minimized subject to the conditions which satify $t_{k,p}$.

Another simple approach is to choose t(s) over the interval so that the resulting curve is linear between the two defined points where the thicknesses are known.

If we define

$$\begin{aligned} Z_{k,p} &= Z_k(s_p) \\ R_{k,p} &= R_k(s_p) \end{aligned} \tag{3.23}$$

then the desired condition for convexity is:

$$\frac{R_{k,p+1} - R_{k,p}}{Z_{k,p+1} - Z_{k,p}} \leq \frac{R_{k,p} - R_{k,p-1}}{Z_{k,p} - Z_{k,p-1}} \tag{3.24}$$

This leads to a quadratic condition on $t_{k,p}$. The condition given by Eq. 3.21 still holds, and again the function W must be minimized.

The complete solution to this problem is beyond the scope of this study. The formulation of a method of solution would undoubtedly have to be carried out, partially at least, by means of a digital computer, and a machine program would have to be written to obtain minimum weight shields by this method for cases of interest.

4. EXTENDED AND IMPROVED TREATMENT OF SECONDARY NEUTRONS

In Reference 1 the optimization theory for spherical proton shields was modified to include the production and attenuation of secondary neutrons. Several one-layer shields and one two-layer minimum weight shield were calculated for a single solar flare. Because of a lack of data on (p,n) cross sections, only shields containing aluminum, carbon, and polyethylene (CH_2) could be computed.

In the present study, the cross section data for these materials have been revised according to the latest available data,[2,3,4] and data on several new substances [oxygen, copper, tungsten, and phenol-formaldehyde (C_7H_6O)] have been obtained and they are included in the calculations. Phenol-formaldehyde was included as it is used as an ablative material in many heat shields. Using the computed parameters for all of these materials, a generalized four-dimensional Young diagram has been devised. One-layer spherical shields have been calculated for these substances for two quite different solar flare spectra. Several two-layer minimum weight shields also have been computed.

4.1 REVISION AND EXTENSION OF SECONDARY NEUTRON PARAMETERS

The (p,n) cross sections which are used in this study are the so-called effective values which take into account multiple neutron production. The most recent values were obtained from Bertini's calculations which are available on microfilm from ORNL. A description of the method and the microfilm output are described in References 2 and 3. Besides the cross sections, Bertini also gives the

yield of cascade and evaporation neutrons for proton energies between 25 and 400 Mev. His results are in good agreement with experimental data[4] in the energy ranges where such data are available. The effective cross sections used in this study are shown in Fig. 20 where they have been extrapolated to 500 Mev and then kept constant to 800 Mev.

Bertini has recently reported an error in the code which generated his data.[10] Although this error should have little effect on the (p,n) cross sections themselves, it may affect the yield and, hence, the effective cross sections. However, inasmuch as his data compare favorably with available experiments, it is believed that our results will not be significantly changed by the reported errors.

The four parameters required in a shield optimization theory which is to include secondary neutrons are

- The proton relative stopping power, A
- The material density, ρ
- The neutron attenuation factor, y
- The relative secondary neutron production factor, z.

As pointed out in Section 5 of Reference 1, the parameter z is energy dependent and therefore will vary with the incident proton spectrum. Using the effective (p,n) cross sections, the secondary neutron production was calculated as a function of equivalent aluminum thickness, K, in cm, for the three incident proton spectra given in Table 4. The secondary neutron sources, S(K), (n/cm^2, or $n/cm^2/sec$) thus obtained, are shown in Figs. 21 and 22 for the materials and proton spectra considered. The points on the curves represent the neutron production in aluminum, whereas the spread in the points represents the limits in the deviation of the normalized curves for the materials examined in this study, i.e., C, Cu, O, W, CH_2, C_7H_6O. The relatively small spread in the normalized results for neutron production over the wide range $10^{-3} \leq K \leq 10^2$ makes the use of a single neutron production factor for each of these materials meaningful.

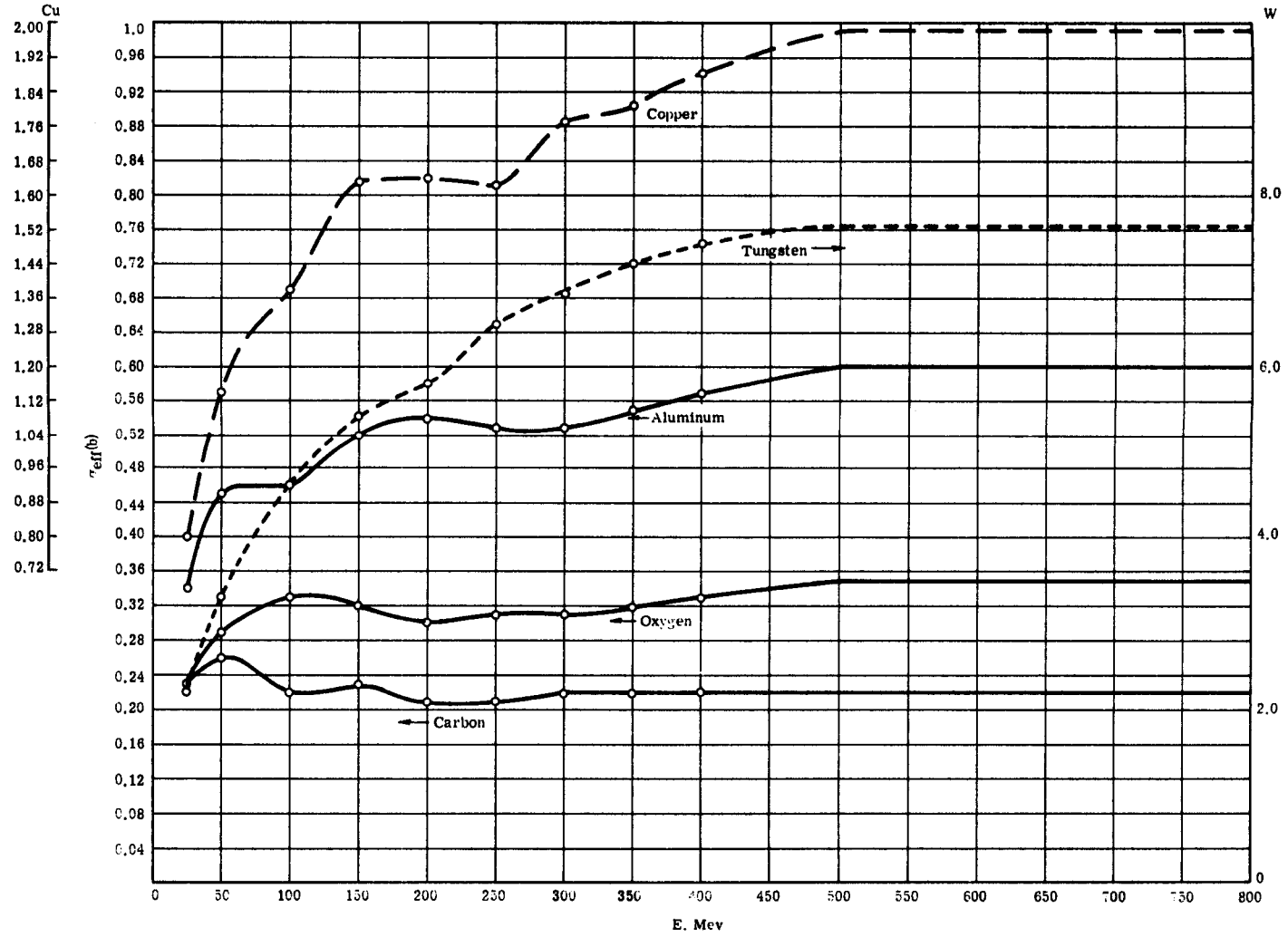

Fig. 20 — Effective neutron production cross sections as a function of incident proton energy

Table 4 — Proton Spectra Used

May 10, 1959 Flare (Protons/cm^2-Mev)

$$P_0 = \frac{3.19 \times 10^{17}}{E^5 + (5 \times 10^6)} \qquad 30 \leq E \leq 800 \text{ Mev}$$

February 23, 1956 Giant Flare (Protons/cm^2-Mev)

$$P_0 = 4.84 \times 10^9 \times E^{-1.27} \qquad 30 \leq E \leq 200 \text{ Mev}$$

$$P_0 = 9.46 \times 10^{11} \times E^{-2.35} \qquad 200 \leq E \leq 800 \text{ Mev}$$

The Van Allen Belt (Protons/cm^2-Mev-sec)

$$P_0 = 1.55 \times 10^2 \times E^{-0.72} \qquad 30 \leq E \leq 80 \text{ Mev}$$

$$P_0 = 7.33 \times 10^3 \times E^{-1.60} \qquad 80 \leq E \leq 400 \text{ Mev}$$

$$P_0 = 1.02 \times 10^5 \times E^{-2.04} \qquad 400 \leq E \leq 800 \text{ Mev}$$

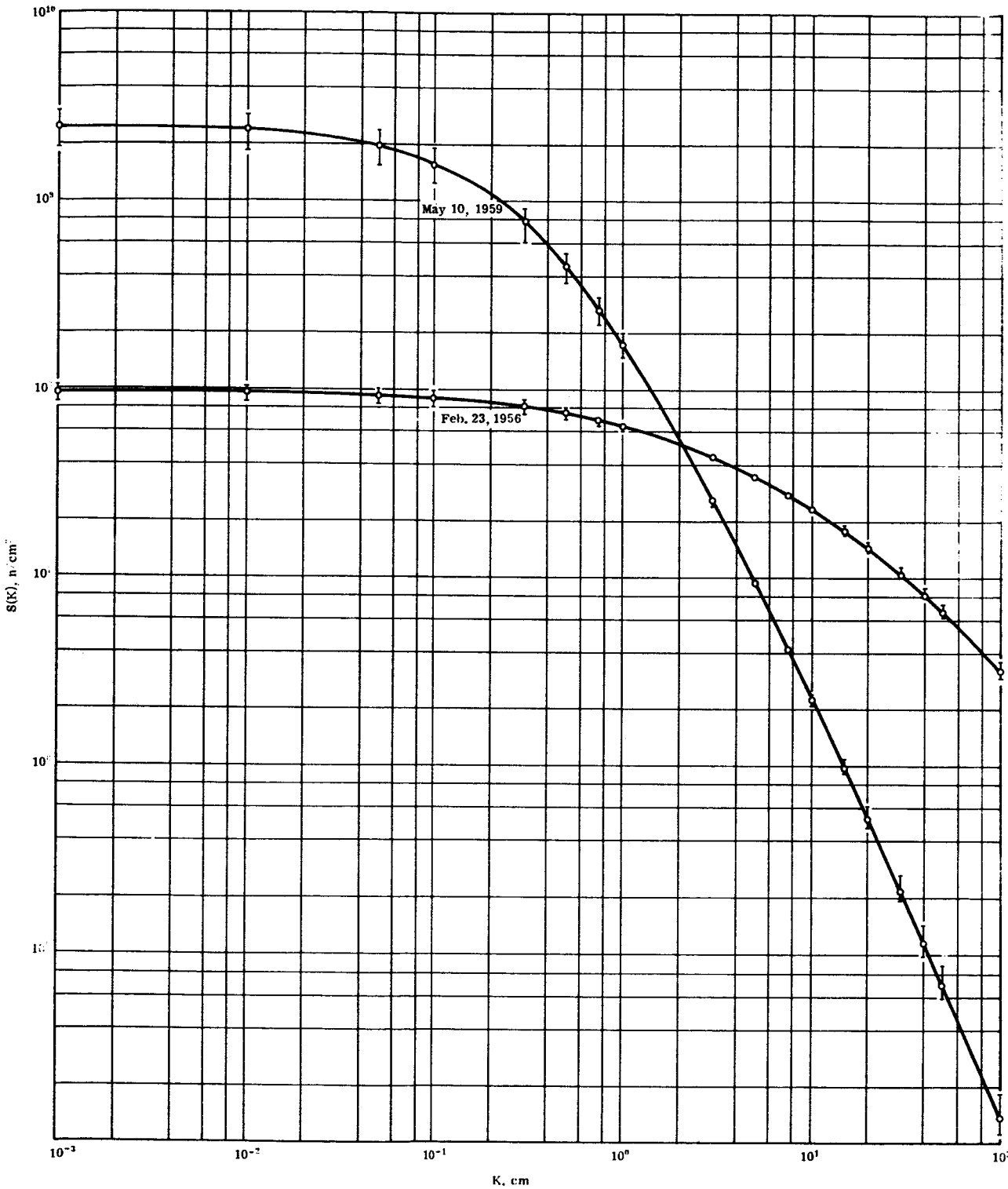

Fig. 21 — Secondary neutron production in several materials as a function of equivalent aluminum thickness for two solar flare spectra

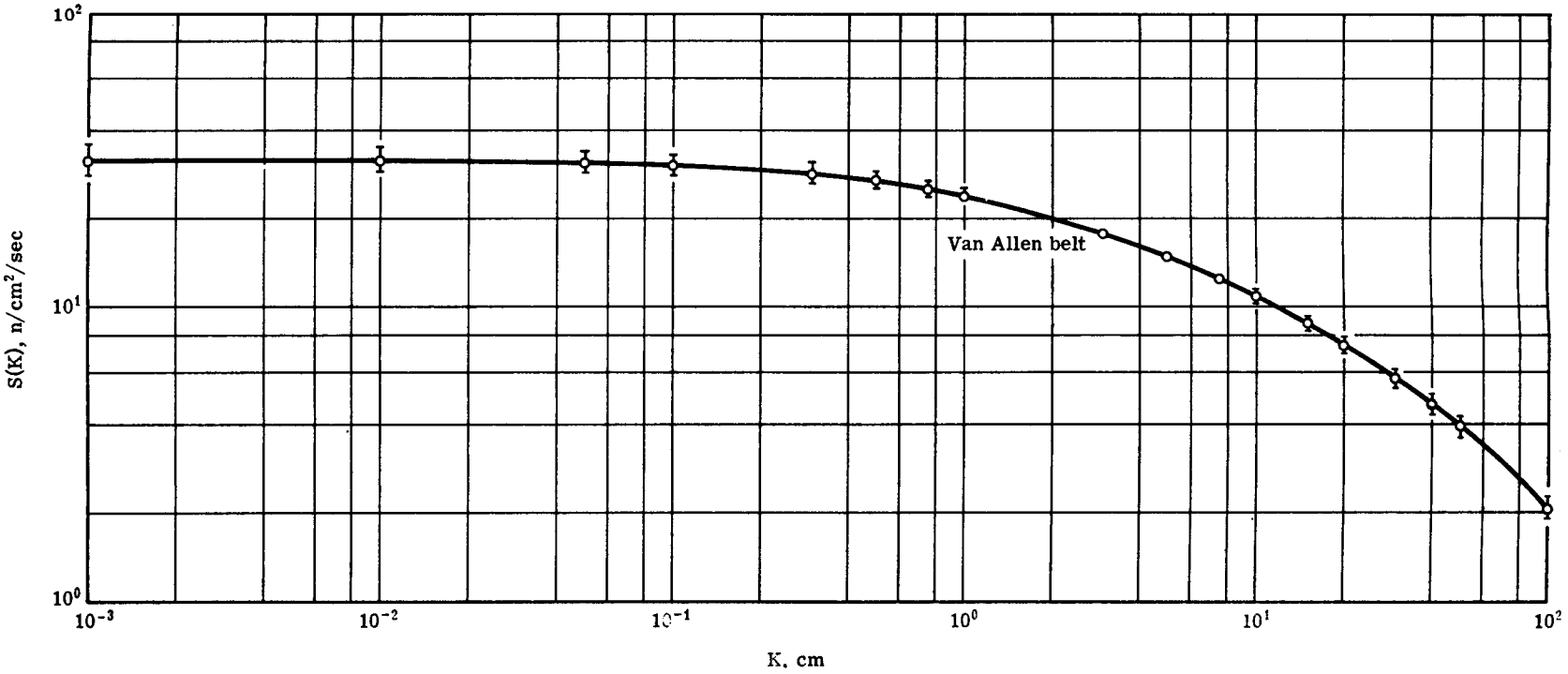

Fig. 22 — Secondary neutron production in several materials as a function of equivalent aluminum thickness for the Van Allen belt spectrum

The parameter used is defined in Eq. 59 of Reference 1 as

$$z = \frac{S(K)}{S_{Al}(K)} \tag{4.1}$$

Values of z for the three proton spectra of Table 4 are given in Table 5.

Table 5 — Primary Proton and Secondary Neutron Material Parameters

Element	Density, ρ, g/cm^3	A	y, cm^{-1}	Z		
				5/10/59	2/23/56	Van Allen
C	2.22	0.934	0.045	0.909	0.833	0.820
Al	2.70	1	0.048	1	1	1
Cu	8.96	2.85	0.13	3.87	4.26	4.26
W	19.3	4.76	0.16	9.52	10.9	11.4
O	0.16	0.0658	0.0030	0.0655	0.0639	0.0621
CH_2	0.92	0.459	0.055	0.323	0.296	0.291
C_7H_6O*	1.27	0.572	0.045	0.539	0.545	0.544

*Phenol-formaldehyde.

It should be noted that the new cross sections, based on Bertini's calculations, result in much higher values of Z for carbon than were obtained in UNC-5049 (0.2 as compared to the present value of 0.9 for May 10, 1959 flare). In fact, carbon now produces almost as many secondary neutrons as does aluminum (for which Z = 1 by definition). This result is reflected in the percentage of the total dose now contributed by neutrons for carbon and CH_2 shields as compared to the percentage given in UNC-5049. (Compare Table 7 of that report with Table 6 of the present report.)

The neutron attenuation factors, y, were computed in the following manner. The results of Bertini's calculations[3,4] were used to obtain the average energy of the

cascade and evaporation neutrons as a function of the incident proton energy and target nucleus. For these average neutron energies, average neutron total cross sections were obtained either from BNL 325[11](for neutron energies <20 Mev) or from experimental results[4] and/or Bertini's calculations (for higher neutron energies). This process was facilitated by the virtual equivalence of neutron and proton total cross sections for energies greater than 100 Mev.

The resulting macroscopic total cross sections were then averaged for each material over the energy range in which neutrons are most likely to be produced in that material in an optimized shield. These averaged cross sections then were used as the parameter y (cm^{-1}) in that material. For example, in materials most likely to be used as the outside layer of the optimum shield, such as CH_2, most neutrons will be produced by low energy protons, and therefore, an average over low energy neutron cross sections is used to obtain y. On the other hand, for inner layer materials, such as copper, most neutrons produced are of higher energy and, therefore, higher energy neutron cross sections were used to yield the neutron attenuation parameter.

It should be noted that this method of calculating y gives only a first approximation to satisfactory values. The y values then could be used in an optimization calculation to compute a shield, and the shield so obtained could then be analyzed (by a computer code) to find the actual neutron production and attenuation. On the basis of this analysis a better guess could be made of the y values and these new values then could be used to reoptimize the shield.

The values of y for the six materials studied are given in Table 5. Finally, the A and ρ values as previously calculated in Table 2 of Reference 1 are also listed in this table. The values of the four parameters listed in Table 5 were used in calculating the generalized Young diagram and in computing the optimized shields listed in Section 4.3.

4.2 THE GENERALIZED YOUNG DIAGRAM

A four-dimensional Young diagram results when the production of secondary neutrons and their subsequent attenuation are included in the shield optimization theory. Although it is not possible to construct such a diagram for visual representation, a mathematical analysis has been made according to the methods presented in Section 9 of Reference 1, using the six materials for which parameters have been calculated. The initial result of such an analysis is a closed hypersurface consisting of 12 tetrahedra. This number was reduced by further analysis to a single tetrahedron which links the materials aluminum, carbon, CH_2, and copper. This is an isolated tetrahedron in four-dimensional space, and what still remains to be determined are its connecting links with the origin of the diagram. This origin represents the air or vacuum which must exist outside of the outermost shield layer. The connecting links can be either triangles (of three materials) or curves (of two materials), but not tetrahedra.

A machine code was used to complete the analysis of the Young diagram. The final result is the generation of that portion of the total hypersurface which includes the materials and mixtures which will make up the minimum weight shield. Although it is not possible to construct the four-dimensional diagram for visual representation, a rough projection in two dimensions is shown in Fig. 23. (It should be noted that because of the nature of the projection the axes cannot be meaningfully labeled.)

From the Young diagram calculated for these six materials (Al, C, Cu, W, CH_2 and C_7H_6O) the following conclusions can be drawn.

1. Phenol-formaldehyde (C_7H_6O) is not included in any optimum shield. This arises from the fact that it is inferior to polyethylene (CH_2) as a shielding material in the region where substances with its values of the four parameters would be used, namely, at the outside of the shield. Therefore, when materials with these characteristics are required, the

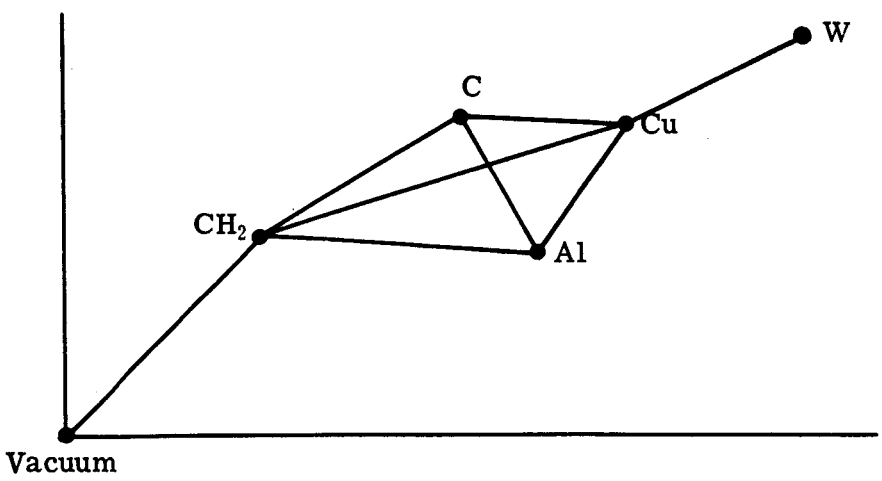

Fig. 23 — Projection in two dimensions of the four-dimensional Young diagram

choice will always fall to CH_2. If phenol-formaldehyde is required for some other reason, it can be used, but a slightly heavier shield will result, i.e., the shield will no longer be optimum.

2. Of the materials considered, only polyethylene may be at the outside of the optimum shield, i.e., only CH_2 connects to vacuum in Fig. 23. Thus, when calculations of a one-layer shield for enclosures 20 cm in radius for the Feb. 23, 1956 flare show that a copper shield gives the lowest weight (Section 4.3), it is concluded that under these conditions a one-layer shield is not the minimum weight shield. Indeed, calculations of two-layer shields show that a Cu-CH_2 shield has a lower weight for that case (see Section 4.3).

3. Tungsten can only be adjacent to a pure region of copper or to a mixed region of tungsten and copper. Thus, the least complex optimum shield containing tungsten would have W, Cu, and CH_2, in that order, starting from the inside.

4. Of the materials considered, three-material mixtures can only consist of combinations of CH_2, C, Al, and/or Cu. (Four-material mixtures are excluded on theoretical grounds.)[1] Two-material mixtures can consist of any two of the above materials with the addition of mixtures of W and Cu as noted above.

As was pointed out in Section 4 of Reference 1, the Young diagram, in a case where four parameters are required, cannot determine the optimum sequence of materials to be used in a minimum weight shield. However, it will restrict the choice to certain materials and certain sequences, and the final choice then can be made by means of actual shield weight comparisons.

4.3 NUMERICAL CALCULATIONS AND RESULTS

Single-layer shields were calculated for all the six materials investigated for void radii of 20 cm and 100 cm, and for the proton spectra of the May 10, 1959 and February 23, 1956 solar flares. The results, for shields which will reduce the total central dose, $\bar{D}$, to 25 rem, are given in Table 6.

The proton dose conversion factor used is $D_p = 2.083 \times 10^{-5}$ rem/Mev/g, which corresponds to an average RBE value of 1.3 rem/rad over the proton energy range. For neutrons, a dose conversion factor of $D_n = 3.8 \times 10^{-8}$ rem/n/cm^2 is used. This corresponds to an average RBE of about 6.5. This is an appropriate conversion factor for neutrons in the energy range 5 to 10 Mev.[12]

It is seen that polyethylene (CH_2) is the best single material of this group, except for cases of small voids and hard incident proton spectra such as the 1956 flare.

It is noteworthy that for all of the shields considered, secondary neutron doses are significant compared with the primary proton doses. For the May 10, 1959 flare, the neutron doses are higher than the proton doses in most cases. This somewhat surprising result can be attributed to several factors.

Table 6 — Single-Layer Shields

(Total Central Dose Constraint: $\bar{D}$ = 25 rem)

May 10, 1959 Flare

Material	Shield Thickness, cm	$\bar{D}$, rem	Proton Dose, rem	Neutron Dose, rem	Void Radius = 20 cm Weight, kg	Void Radius = 100 cm Weight, kg
Al	10.71	25	4.51	20.49	237.0	4.04×10^3
C	11.12	25	4.81	20.19	206.0	3.46
Cu	5.51	25	1.98	23.02	322.8	6.55
W	6.63	25	0.44	24.56	880.5	17.17
CH_2	13.17	25	12.57	12.43	109.8	1.73
C_7H_6O	14.34	25	7.37	17.63	172.8	2.63

February 23, 1956 Flare

Al	46.06	25	16.32	8.68	3170	23.93×10^3
C	48.69	25	16.52	8.48	2940	21.27
Cu	18.65	25	14.29	10.71	1866	25.16
W	16.66	25	9.85	15.15	3336	128.36
CH_2	72.38	25	22.11	2.89	3008	15.89
C_7H_6O	67.59	25	19.21	5.79	3533	19.72

1. Doses are given in rem rather than rad, and the RBE used for neutrons is several times that for protons.
2. A fairly low dose is specified, leading to thick shields which favor a high neutron to proton dose ratio.
3. The spectrum of the May 10, 1959 flare is rather soft, with a great many low energy protons which do not penetrate the shield but do produce secondary neutrons and thereby contribute to the neutron dose.

A series of minimum weight two-layer shields using the materials studied has also been calculated. The calculations were made by means of a machine program written for the CDC-1604-A computer. The results are given in Table 7.

The results show that for the two flares studied, for large enclosure radii (100 cm), the minimum weight spherical shield is composed of a single layer of polyethylene. For smaller void radii (20 cm), such as might be used for a local body shield or a space suit, certain two-layer shields have a lower weight than one composed of CH_2 only. This is particularly true for the February 23, 1956 giant flare, which has a very hard proton spectrum. In this case, the use of a Cu-CH_2 shield results in a 44% weight saving over an all CH_2 shield.

In real space vehicles either structural or ablative material will nearly always comprise the outermost layer of the craft. Similarly, there will be equipment and some sort of cabin liner between the vehicle radiation shield and the astronauts. With these constraints it is no longer obvious that a pure polyethylene shield is best, even for large enclosures.

For example, Table 6 shows that for C and C_7H_6O most of the dose through a one-layer shield comes from neutrons for the May 10, 1959 flare, which has large numbers of low energy protons. Only for CH_2 are the proton and neutron doses about equal. If the shield is composed almost entirely of CH_2, a sizable proton flux will strike the material or equipment closest to the cabin and may produce

Table 7 — Two-Layer Minimum Weight Shields

(Total Central Dose Constraint: $\bar{D}$ = 25 rem)

May 10, 1959 Flare

Materials		Void	Outer Radius of Inner	Outer Radius of Outer	Proton	Neutron	
Inner	Outer	Radius, cm	Material, cm	Material, cm	Dose, rem	Dose, rem	Weight, kg
Al	CH_2	20	20.39	32.70	12.57	12.43	107.50
C	CH_2	20	21.20	32.19	12.14	12.86	106.00
C	CH_2	100	*	*	*	*	*

February 23, 1956 Giant Flare

Cu	CH_2	20	34.15	55.10	15.12	9.88	1.686×10^3
Cu	CH_2	100	*	*	*	*	*
Al	CH_2	20	44.60	80.90	18.08	6.92	2.611×10^3
Al	CH_2	100	*	*	*	*	*
C	CH_2	20	49.80	78.60	18.17	6.83	2.469×10^3
C	CH_2	100	*	*	*	*	*

*Degenerates to a pure CH_2 shield (see Table 6).

a substantial number of secondary neutrons which will then impinge directly on the astronauts. For such a case, it is possible that the lowest total dose may be obtained by including a heavier material in the radiation shield to attenuate the proton flux. Any secondary neutrons produced in this shield material then would be attenuated in a layer of CH_2 located between it and the cabin. Therefore, given such a constraint, it is not at all clear, a priori, what the minimum weight shield would look like, and the synthesis technique could conceivably lead to significant weight savings.

This study is continuing with an investigation of three-layer minimum weight shields. It is planned to write a computer code to solve a number of such cases for the six materials used to date.

5. CONCLUSIONS

The proton shield synthesis technique has been extended to include a number of dose constraints, including average body dose and depth dose, which are of particular importance in shield evaluation. The extended technique leads to several interesting conclusions. For example, for the case of a tissue model which completely fills a shielded spherical enclosure, the theory predicts that all the materials making up the Young diagram must be used in the minimum weight shield. This result can be applied to the design of local body shields.

Analytic expressions have been derived by means of which doses behind given spherical shields in particular proton space environments can be calculated. The sample numerical results obtained agree very well with previous machine calculations made at United Nuclear and with the results of other investigators.[7]

The theory of shield optimization for generalized convex enclosures has been extended along two different lines. By the first approach it is possible to obtain local compositions and layer thicknesses of minimum weight shields for any convex shape specified by two radii of curvatures. Calculations have been carried out which give such compositions and thicknesses over a wide range of parameters. It is then possible, in many cases, to approximate a complete minimum weight shield for an entire vehicle by the combination of a number of local shield results.

The second approach sets forth the theoretical basis for synthesizing analytically an entire minimum weight shield for symmetrical convex enclosures. The complete mathematical formulation of this approach still remains to be worked out.

The work on the inclusion of secondary neutrons in the shield synthesis technique has been extended also by:

1. Improving and expanding the secondary neutron production and attenuation parameters
2. Calculating a generalized four-parameter Young diagram
3. Extending the one- and two-layer shield calculations to other materials and other space proton spectra.

The results of this study substantiate our previous findings that important space shield weight savings are possible by the use of the synthesis technique. It is believed that this method will increase in importance as more shielding is required for longer space voyages or for protection against very high energy proton flares. For these cases the effect of secondaries, particularly neutrons, cannot be ignored.

6. RECOMMENDATIONS FOR FURTHER WORK

In the course of the present study, a machine program to calculate minimum weight spherical shields under a variety of dose constraints was prepared, but it did not become operational. This code should be completed. A method must be found for selecting good enough initial values of the two Lagrange undetermined multipliers to permit the code to converge properly to the final correct solution. Several methods have suggested themselves and it will be necessary to conduct a short "experimental" program on the computer to arrive at the proper procedure. Once the code is completed, a range of problems involving average body dose, depth dose, and various point dose constraints should be solved. These results can be of great importance to the manned space flight program.

As explained in Section 4, a four-parameter Young diagram was calculated and certain useful conclusions were derived from it. The methods used to calculate the Young diagram for these materials should be used to test the usefulness of other likely materials as well as to calculate Young diagrams for other secondary radiations.

As part of the present study, one- and two-layer minimum weight shields designed against protons and secondary neutrons have been computed. The equations for calculating three-layer shields are now being prepared. A machine code should be written to perform the computations. The formulation also should be extended to include more shield layers and to permit the use of mixtures of materials in given layers.

Since all space vehicles must have a designated metal "skin" or ablative material as their outermost layer, this constraint should be included in the shield optimization theory which takes into account both primary protons and secondary neutrons. This special constraint can be looked upon as changing the radiation spectrum which the shield sees, since not only is the proton spectrum changed, but also secondary neutrons may be produced in this outer layer. The inclusion of this constraint in the present theory appears to be feasible and within the present state-of-the-art.

Another important constraint which should be included in this formulation is the presence of equipment and/or a cabin liner between the radiation shield itself and the astronaut's living space. Recently computed minimum weight shields of polyethylene may allow a sizable proton flux to strike this inner material or equipment thus producing substantial numbers of secondary neutrons which then impinge unattenuated directly on the astronauts. With such a system it may be necessary to include a heavier material in the optimum radiation shield to attenuate further the proton flux before it strikes the inner equipment region. Therefore, it would be highly useful to include this constraint in the optimization theory as it could conceivably lead to significant weight savings in cases of real spacecraft.

Although it is usually assumed that secondary protons can be neglected as an important source of tissue dose from space radiation, this problem should be investigated in greater detail. In particular, it may be that low energy secondary protons produced near the inner edge of the shield or in the astronaut himself may affect significantly the total dose received. This is a consequence of the large amount of energy transferred by low energy protons to tissue. The inclusion of secondary protons as well as secondary neutrons in the shield optimization theory still may lead to only a four-parameter system since the same proton relative stopping power, A, may be usable for both primary and secondary protons and the production factor for secondary protons may be proportional to that

for secondary neutrons. Therefore, the problem of incorporating secondary protons into the shield synthesis theory should be investigated.

In the course of the present study a feasible approach to synthesizing an entire minimum weight shield analytically for symmetrical convex enclosures has been formulated and a possible method of solution has been outlined. The mathematical formulation of this approach should be completed and methods of solution should be worked out in enough detail so they can form the basis for a computer program. Such a method, once available, would be of inestimable value in accurately synthesizing minimum weight proton shields for most convex shapes of interest in space work.

The synthesis theory for spherical proton shields has now been formulated in terms of various realistic dose constraints. The next logical step in advancing the method is to include secondary neutrons in the dose constraint theory. It is believed that this is feasible and will lead to an almost complete practical solution to the minimum weight spherical space shield problem.

A final aspect of the continuation of the present shield synthesis work which is considered to be of great importance, is to study the transition from spherical to generalized convex geometry of the dose constraint model. Here, both the local optimization and the complete shield approaches would be investigated to determine which is more likely to give meaningful results without being too complex. The successful conclusion of such a study would go a long way toward the solution of the minimum weight space shield problem for realistic vehicles.

7. APPENDIX A – DERIVATION OF DOSE RELATIONSHIPS

7.1 EQUIVALENT ALUMINUM THICKNESS OF THE SHIELD

Consider a shield consisting of concentric spherical shells of radii r_0, r_1, ..., r_j, where r_0 is the void radius, and containing materials with proton relative stopping powers A_1, A_2, ..., A_j. As shown in Fig. 24, a proton of energy E incident on the shield at angle φ (φ is measured with respect to the inward normal from the surface of the spherical phantom) will penetrate the shield if its energy is greater than the energy, E_0, defined by the following relationship:

$$\frac{1}{\alpha}\int_0^{E_0} E^n \, dE = \sum_{i=1}^{j} A_i t_i(\varphi)$$

or

$$\frac{E_0^{n+1}}{(n+1)\,\alpha} = \sum_{i=1}^{j} A_i t_i(\varphi) \qquad (7.1)$$

where α and n have been defined in Eq. 2.2 and $t_i(\varphi)$ denotes the path length through the i^{th} shell in the φ direction.

The right-hand side of Eq. 7.1 defines the equivalent aluminum thickness of the shield, K, in the φ direction.

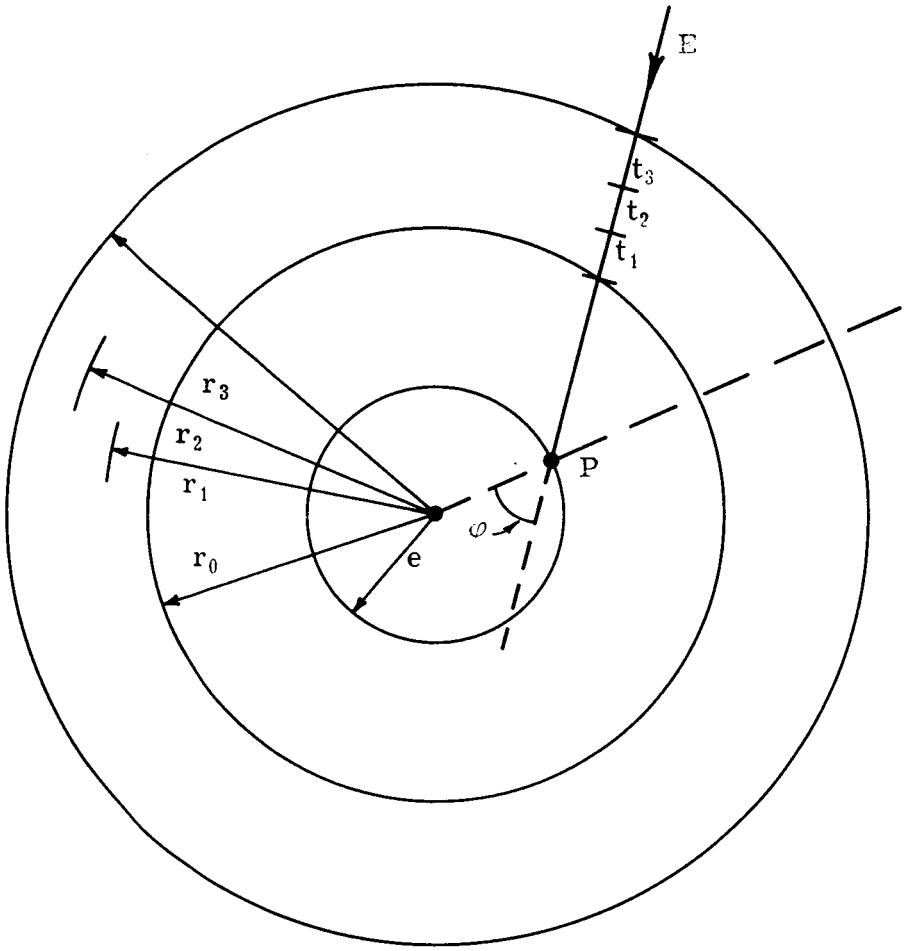

Fig. 24 — Geometry of the dose constraint model

$$K = \sum_{i=1}^{j} A_i t_i(\varphi) \tag{7.2}$$

K, in units of cm of aluminum, will be used frequently to denote the shielding attenuation along given incidence angles.

Since those protons which penetrate the shield and are incident on the spherical phantom are of interest, it is useful to express the path length, $t_i(\varphi)$, as a function of the inner and outer shell radius and the phantom radius, e. Taking the origin at a point P on the phantom surface, one obtains

$$t_i(\varphi) = (r_i^2 - e^2 \sin^2 \varphi)^{1/2} - (r_{i-1}^2 - e^2 \sin^2 \varphi)^{1/2} \tag{7.3}$$

where $0 \leq \varphi \leq \pi/2$.

Hence, Eq. 7.2 can be written

$$K = \sum_{i=1}^{j} A_i \left[(r_i^2 - e^2 \sin^2 \varphi)^{1/2} - (r_{i-1}^2 - e^2 \sin^2 \varphi)^{1/2}\right] \tag{7.4}$$

or

$$K = -A_1 (r_0^2 - e^2 \sin^2 \varphi)^{1/2} + \sum_{i=1}^{j} (A_i - A_{i+1})(r_i^2 - e^2 \sin^2 \varphi)^{1/2} \tag{2.8}$$

with the convention that $A_{j+1} = 0$.

As φ increases from 0 to $\pi/2$, the path length through the shield increases and thus the shielding attenuation increases.

Indeed, the differentiation of Eq. 7.4 gives

$$\frac{\partial K}{\partial \varphi} = e^2 \sin\varphi \cos\varphi \sum_{i=1}^{j} A_i \left[\frac{1}{(r_{i-1}^2 - e^2 \sin^2\varphi)^{1/2}} - \frac{1}{(r_i^2 - e^2 \sin^2\varphi)^{1/2}} \right] \tag{7.5}$$

Since $e \leq r_0 < r_1 < \ldots < r_i < \ldots r_j$, then

$$\frac{1}{(r_{i-1}^2 - e^2 \sin^2\varphi)^{1/2}} > \frac{1}{(r_i^2 - e^2 \sin^2\varphi)^{1/2}}$$

All terms on the right-hand side of Eq. 7.5 are positive. Therefore, K increases with increasing φ (or remains constant if $e = 0$).

The minimum shielding attenuation is given by:

$$K_0 = -A_1 r_0 + \sum_{i=1}^{j} (A_i - A_{i+1})\, r_i \tag{2.9}$$

K_0 is the shielding attenuation constraint used in the previous work[1] in which the protons were assumed to be normally incident to the shield. The use of K_0 is also justified in the case of dose calculation at the center point of the phantom. However, in the general problem, the angle-dependent shielding attenuation, K, must be used. It will be shown in the following sections that analytical expressions of doses can be obtained by using an expansion in series of K.

Since $e \leq r_0 < r_1 < \ldots < r_i < \ldots < r_j$ and $\sin\varphi \leq 1$, Eq. 2.8 can be expanded in series in the following manner

$$K = K_0 + K_1 \sin^2\varphi + K_2 \sin^4\varphi + K_3 \sin^6\varphi + \ldots \tag{2.10}$$

where K_0, K_1, ... are positive, angle-independent coefficients. For example,

$$K_1 = \frac{e^2}{2} \frac{A_1}{r_0} - \sum_{i=1}^{j} \left(\frac{A_i - A_{i+1}}{r_i} \right) \tag{2.11}$$

It can be shown also that the coefficients K_i decrease rapidly, particularly if $e << r_0$.

Also

$$K_0 > K_1 > K_2 \ldots K_n > 0.$$

Thus, if the two first terms of the expansion are retained, i.e., if

$$K = K_0 + K_1 \sin^2 \varphi, \tag{2.12}$$

an approximate equivalent aluminum thickness is being used that is less than, or equal to, the actual equivalent aluminum thickness given by Eq. 2.8. As far as energy deposition in the phantom is concerned, this will be a conservative assumption in the calculations. Using Eq. 2.12 ensures that the calculated energy deposited in the phantom will be greater than the actual one (since, as pointed out, the number of protons incident on the shield and the proton energy loss in aluminum increases rapidly as the energy becomes smaller).

7.2 DETERMINATION OF THE ENERGY OF PROTONS ATTENUATED BY THE SHIELD AND INCIDENT ON THE PHANTOM

A proton of energy E incident on the shield at angle φ will penetrate the shield if its range in aluminum, R(E), is greater than the equivalent aluminum path length through the shield, K (see Fig. 25). Then the emerging proton energy will be a function of E and K.

Consider incident protons with directions passing through a point P on the phantom surface (Fig. 25). Since K increases with increasing φ for $0 \leq \varphi \leq \pi/2$, three cases are possible:

1. $R(E) \leq K_0$, then no protons emerge in the shielded enclosure and hence no protons reach the phantom.
2. $R(E) \geq K_m$, where K_m is the maximum equivalent aluminum thickness of the shield. i.e., if in Eq. 7.4, $\sin \varphi = 1$,

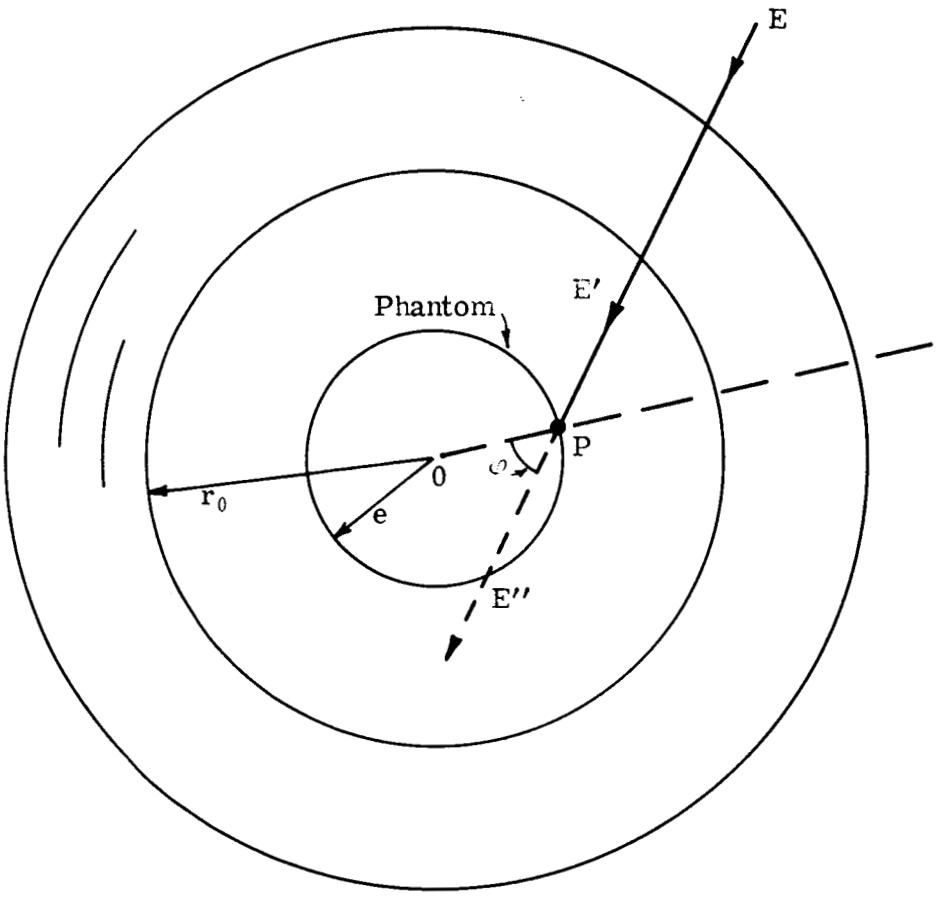

Fig. 25 — Energy attenuation model

$$K_m = \sum_{i=1}^{j} \Delta A_i \, (r_i^2 - e^2)^{1/2} - A_1 \, (r_0^2 - e^2)^{1/2} \qquad (7.6)$$

Then all incident protons of energy E emerge in the shielded enclosure and are incident on the phantom.

3. $K_0 < R(E) < K_{max}$

Then there exists an angle φ_0, $0 < \varphi_0 < \pi/2$, such that

$R(E) = K(\varphi_0)$.

Then only protons incident on the shield with an angle φ less than φ_0 penetrate the shield and reach the phantom.

The emerging proton energy E′ is given by

$$R(E') = R(E) - K(\varphi) \qquad \text{if } R(E) > K(\varphi) \qquad (7.7)$$

Otherwise

$$E' = 0.$$

From Eq. 2.1, the analytical expression for the range in aluminum can be obtained and Eq. 7.7 becomes

$$\frac{E'^{n+1}}{(n+1)\,\alpha} = \frac{E^{n+1}}{(n+1)\,\alpha} - K(\varphi) \qquad (2.13)$$

if

$$\frac{E^{n+1}}{(n+1)\,\alpha} - K(\varphi) > 0$$

otherwise

$$E' = 0$$

7.3 DETERMINATION OF THE ENERGY OF PROTONS LEAVING THE PHANTOM

A proton of energy E′ incident on the spherical phantom with angle φ will penetrate the phantom, emerging with an energy E′′ if its range in aluminum is greater than the equivalent aluminum path length, $\ell(\varphi)$ through the phantom in direction φ,

$$\ell(\varphi) = 2\, A_T e \cos \varphi \tag{7.8}$$

where A_T is the phantom relative stopping power.

Thus, the energy E′′ is determined by the following equations:

$$R(E'') = R(E') - \ell(\varphi) \qquad \text{if } R(E') > \ell(\varphi) \tag{7.9}$$

Otherwise

$$E'' = 0.$$

However, it is shown in the foregoing section that the energy of a proton incident on the phantom, E′, is itself a function of E and φ. If the total aluminum equivalent path length at angle φ through both the shield and the phantom is denoted by $K_T(\varphi)$, i.e.,

$$K_T(\varphi) = K(\varphi) + \ell(\varphi) \tag{7.10}$$

Then, from Eqs. 7.4 and 7.10,

$$K_T(\varphi) = \sum_{i-1}^{j} A_i(\zeta_i - \zeta_{i-i}) + 2\, A_T e \cos \varphi \tag{7.11}$$

where

$$\zeta_i = (r_i^2 - e^2 \sin^2 \varphi)^{1/2}.$$

The behavior of $K(\varphi)$ is not obvious, since as φ increases from 0 to $\pi/2$, $\ell(\varphi)$ decreases while $K(\varphi)$ increases.

It can be shown that if

$$\frac{K_0}{r_0} \leq 2\, A_T \approx 1 \tag{7.12}$$

then $K_T(\varphi)$ is a nonincreasing monotonic function of φ. $K_T(\varphi)$ decreases from $K_T(0) = K_0 + 2\, A_T\, e$ to $K_T\,(\pi/2) = K_m$, the maximum shield path length.

Fig. 26 gives a plot of the variations of $K_T(\varphi)$ and $K(\varphi)$ with φ.

If the approximation (Eq. 2.12) for $K(\varphi)$ is used, then Eq. 7.11 becomes

$$K_T(\varphi) = K_0 + K_1 + 2\, A_T\, e \cos\varphi - K_1 \cos^2\varphi$$

or

$$K_T(\varphi) = K_m + [K_T(0) - K_0] \cos\varphi - (K_m - K_0) \cos^2\varphi \tag{7.13}$$

where

$$K_T(0) = 2\, A_T\, e + K_0$$

is the maximum value of $K_T(\varphi)$, and

$$K_m = K_0 + K_1$$

is the maximum value of $K(\varphi)$.

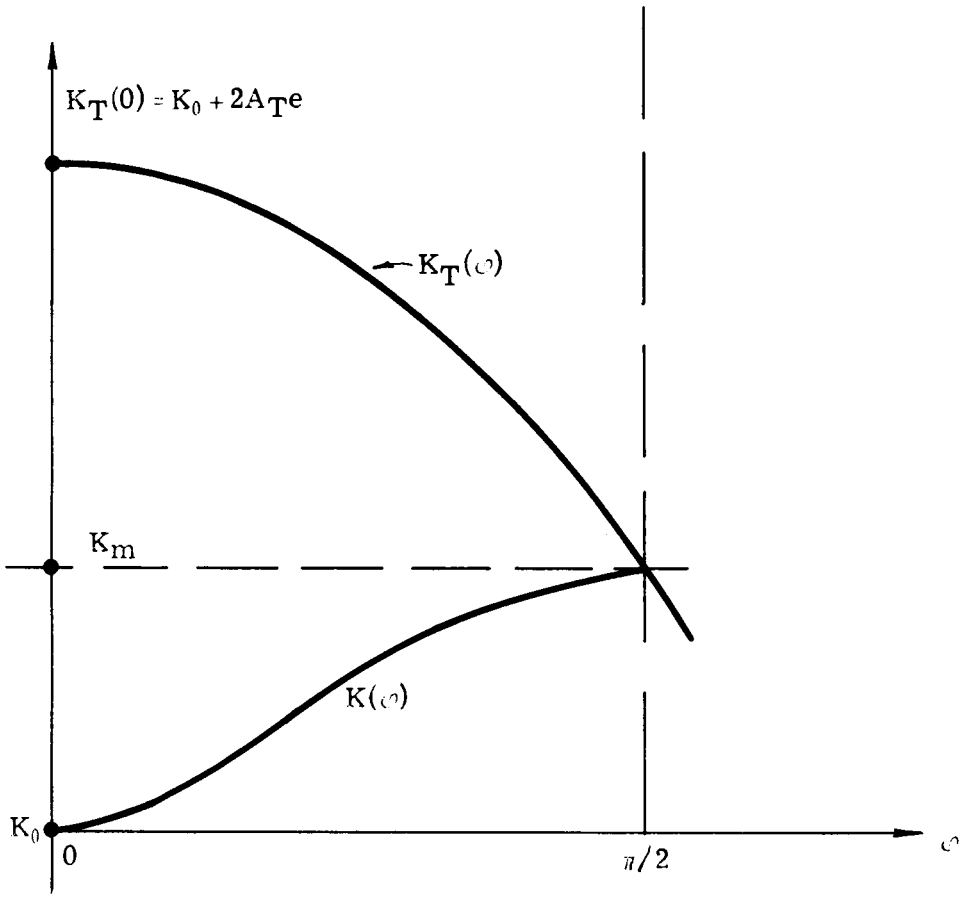

Fig. 26 — Aluminum equivalent path lengths at angle φ, vs φ through: (1) the shield, $K(\varphi)$, (2) the shield and the phantom, $K_T(\varphi)$

7.4 RATE OF ENERGY DEPOSITION PER UNIT MASS OF THE PHANTOM FOR MONOENERGETIC PROTON FLUX

If protons of energy E are isotropically incident on the shielded spherical void, the rate of energy deposition per unit mass of the spherical phantom for a unit flux is given by:

$$F_V(E) = \frac{3}{2 e \rho_T} \left[\int_0^{\varphi_0} E' \sin \varphi \cos \varphi \, d\varphi - \int_{\varphi_1}^{\pi/2} E'' \sin \varphi \cos \varphi \, d\varphi \right] \quad (7.14)$$

where the values of φ_0 and φ_1 depend on the incident proton energy E as shown in Table 2. In Eq. 7.14, $F_V(E)$ is expressed in Mev/g per unit flux (in protons/ cm^2-sec).

Referring to Table 2, it is seen that there are four possible cases.

1. $R \leq K_0$;

   then $\varphi_0 = 0$, and $\varphi_1 = \pi/2$

2. $K_0 < R \leq K_m$;

   then, using Eq. 2.12,

   $$\sin^2 \varphi_0 = \frac{R - K_0}{K_1} = \frac{R - K_0}{K_m - K_0} \quad (7.15)$$

   and $\varphi_1 = \pi/2$

3. $K_m < R \leq K_T(0)$;

   then $\varphi_0 = \pi/2$, and φ_1 is determined by solving the equation

   $$R - K_m - [K_T(0) - K_0] \cos \varphi_1 + (K_m - K_0) \cos^2 \varphi_1 = 0$$

   with $0 < \cos \varphi_1 < 1$.

4. $K_T(0) < R$;

   then $\varphi_0 = \pi/2$, and $\varphi_1 = 0$.

The integration of

$$I_1 = \int_0^{\varphi_0} E' \sin\varphi \cos\varphi \, d\varphi$$

as shown in Appendix B, yields

$$I_1 = \frac{1}{2} \frac{n+1}{n+2} \frac{E_0' R_0'}{K_m - K_0} \qquad \text{if } K_0 < R \leq K_m$$

$$I_1 = \frac{1}{2} \frac{n+1}{n+2} \frac{E_0' R_0' - E_m' R_m'}{K_m - K_0} \qquad \text{if } R > K_m \tag{7.16}$$

where the notation is as follows:

If E and R are the energy and the range in aluminum of protons incident on the shield, $R_0' = R - K_0$ and $R_m' = R - K_m$ represent the range in aluminum of those protons which penetrate the shield and are incident on the phantom normally and tangentially, respectively.

E_0' and E_m' are the proton energies corresponding to R_0' and R_m', respectively, and they are obtained from range-energy tables.

The integration of

$$I_2 = \int_{\varphi_1}^{\pi/2} E'' \sin\varphi \cos\varphi \, d\varphi,$$

also given in Appendix B, is much more complex. The final expressions for I_2 are

$$I_2 = \frac{1}{2}\,\frac{n+1}{n+2}\,\frac{E'_m R'_m}{K_T(0) - K_m} \qquad K_m < R \leq K_T(0)$$

$$I_2 = \frac{1}{2}\,\frac{n+1}{n+2}\,\frac{E'_m R'_m - E''_0 R''_0}{K_T(0) - K_m} \qquad R > K_T(0) \tag{7.17}$$

where E'_m and R'_m have been defined in the foregoing discussion for I_1, $R''_0 = R - K_T(0)$ is the range in aluminum of a proton which emerges from the phantom along a normal and E''_0 is the proton energy corresponding to the range R''_0.

Introducing Eqs. 7.16 and 7.17 into Eq. 7.14 yields the expressions for the energy deposition per unit body mass and unit proton flux as a function of R (or E). These results have been summarized in Table 3.

7.5 DOSE CALCULATION FOR GIVEN PROTON SPECTRA – AVERAGE BODY DOSE

The dose or dose rate per unit mass of the spherical crew man per unit proton flux for an isotropic proton flare incident on the shielded void is given by

$$D = \int_0^\infty F_V(E)\, P(E)\, dE \tag{7.18}$$

where P(E) is the energy distribution of the incident proton flux given in Eq. 2.5 and Table 1, and $F_V(E)$ is given in Table 3. If P(E) is in protons/cm^2-sec-Mev, D is expressed in Mev/g-sec. If P(E) is the time-integrated proton flux, D is expressed in Mev/g.

If the proton range, R, is used as variable rather than the proton energy, E, Eq. 7.18 becomes (Appendix C)

$$D = \frac{1}{e}\left\{\frac{\int_0^{\infty} \beta \frac{(R-K_0)^{a-1}}{R^{a+b}}\,dR - \int_{K_m}^{\infty} \beta \frac{(R-K_m)^{a-1}}{R^{a+b}}\,dR}{K_m - K_0}\right.$$

$$\left. - \frac{\int_{K_m}^{\infty} \beta \frac{(R-K_m)^{a-1}}{R^{a+b}}\,dR - \int_{K_T(0)}^{\infty} \beta \frac{[R-K_T(0)]^{a-1}}{R^{a+b}}\,dR}{K_T(0) - K_m}\right\} \tag{7.19}$$

where

$$a = \frac{1}{n+1} + 2 > 0 \tag{7.20}$$

$$a + b = \frac{m+n}{n+1} > 0 \tag{7.21}$$

$$\beta = \frac{3\,C_1}{4\rho_T} \frac{[\alpha(n+1)]^{-\frac{m-2}{n+1}}}{n+2} \tag{7.22}$$

As shown in Section 2, C_1 and m are constants in given energy ranges (Table 1). Further, a single power fit for the aluminum stopping power may not be enough. Hence, it may be necessary to subdivide all integrals in Eq. 7.19 into partial integrals in which a, b, and β are constants.

7.5.1 Single Power Fit

The case of a single power fit for both the energy distribution of incident protons and stopping power of aluminum is of great interest since even a 4 g/cm^2-thick aluminum shield stops all protons of energy less than 60 Mev. Since $R \geq K_0$ in Eq. 7.19, C_1 and m may be considered as constants in all the domain of integration. In addition, the number of protons of energy higher than 10^3 Mev is relatively small. Therefore, n and α can be considered as constants for all values of R.

In Appendix C we show that in this case Eq. 7.19 becomes

$$D = \frac{\beta}{e}\left[\frac{K_0^{-b} - K_m^{-b}}{K_m - K_0} - \frac{K_m^{-b} - K_T(0)^{-b}}{K_T(0) - K_m}\right]\int_0^\infty \frac{y^{a-1}}{(1+y)^{(a+b)}}\,dy \qquad (7.23)$$

where, from Eqs. 7.20 and 7.21,

$$b = \frac{m-n-3}{n+1} \qquad (7.24)$$

Since n = 0.786 and the range of the m values as given in Table 1 is

$$0.7 \leq m \leq 5,$$

then b can take negative values, viz.,

$$-1.73 \leq b \leq 0.68.$$

If b > 0,

$$\int_0^\infty \frac{y^{(a-1)}}{(1+y)^{(a+b)}}\,dy = \frac{\Gamma(a)\,\Gamma(b)}{\Gamma(a+b)} = B(a,b) \qquad (7.25)$$

where B(a,b) is called the complete beta function often found in statistics, and $\Gamma(x)$ is the tabulated gamma function.

Eq. 7.13 then becomes

$$D = \frac{\beta\, B(a,b)}{e}\left[\frac{K_0^{-b} - K_m^{-b}}{K_m - K_0} - \frac{K_m^{-b} - K_T(0)^{-b}}{K_T(0) - K_m}\right] \qquad (2.15)$$

Although the beta function is discontinuous for b = 0, −1, it is shown in Appendix C that the dose given by Eq. 2.15 is a positive continuous function of b if b is greater than −2.

When b tends to zero either positively, or negatively, D tends to the value D_0

$$D_0 = \frac{\beta}{e}\left[\frac{\log K_m/K_0}{K_m - K_0} - \frac{\log K_T(0)/K_m}{K_T(0) - K_m}\right] \tag{2.16}$$

When b tends to -1, D tends to the value D_{-1}

$$D_{-1} = (a-1)\, D_0 = \frac{n+2}{n+1} D_0 \tag{2.17}$$

where D_0 is given in Eq. 2.16.

In conclusion, if the energy distribution of the incident protons and the stopping power of aluminum can be represented by single power fits, the average body dose is given by

$$D = \frac{C}{e} f(K_0, K_m) \tag{7.26}$$

where C is a constant which depends only on the characteristics of the spectrum distribution fit (m, C_1) and the aluminum stopping power fit (α, n), so that

$$C = \beta\, B(a,b)$$

and

$$f(K_0, K_m) = \frac{K_0^{-b} - K_m^{-b}}{K_m - K_0} - \frac{K_m^{-b} - (2A_T e + K_0)^{-b}}{K_0 + 2A_T e - K_m} \tag{7.27}$$

depends on the maximum and minimum shield attenuations, K_m and K_0 and the man size, e.

7.5.2 General Case

It may be necessary to divide the energy range into several portions in each of which the energy distribution of the incident protons can be represented by a power

function of the energy. This would be the case if one considers protons from the Van Allen belt or the February 23, 1956 flare as being incident on the shield. Hence, a general solution for the average body dose is of interest.

Assume that the energy distribution of the incident proton flare can be represented by ℓ power fits as follows

$$P_j(E) = C_1^j E^{-m_j} \tag{7.28}$$

when $E_{j-1} < E \leq E_j$ (or $R_{j-1} < R < R_j$ if the proton range in aluminum is used as a variable), $j = 1, 2, \ldots, \ell$; $E_0 = R_0 = 0$, and E_ℓ and R_ℓ are infinite.

Then, in each energy range, the following quantities can be defined

$$b_j = \frac{m_j - n - 3}{n+1}$$

$$\beta_j = \frac{3\, C_1^j}{4 \rho_T} \frac{[\alpha(n+1)]^{-\frac{m_j-2}{n+1}}}{n+2}$$

$$a = \frac{1}{n+1} + 2$$

and

$$B_{x_j}(a,b) = \int_0^{x_j} u^{(b-1)} (1-u)^{(a-1)}\, du.$$

By convention, when $x \geq 1$, $B_x(a,b)$ equals the complete beta function, $B(a,b)$, and when $x < 1$, it becomes the incomplete beta function often found in mathematical statistics.[13] When $x = 0$, $B_x(a,b) = 0$. Numerous approximations to the incomplete beta function, $B_x(a,b)$ are available.[14] Most tables[15] use the "standardized" form which is called the incomplete-beta-function ratio:

$$I_X(a,b) = \frac{B_X(a,b)}{B(a,b)}$$

Then, the average body dose is given by

$$D = \frac{1}{e} \sum_{j=1}^{\ell} \beta_j f_j(K_0,K_m) \tag{2.18}$$

where

$$\begin{aligned} f_j(K_0,K_m) = \frac{1}{K_m - K_0} \Bigg\{ & K_0^{-b_j} \left[B_{\frac{K_0}{R_{j-1}}}(a,b_j) - B_{\frac{K_0}{R_j}}(a,b_j) \right] \\ & - K_m^{-b_j} \left[B_{\frac{K_m}{R_{j-1}}}(a,b_j) - B_{\frac{K_m}{R_j}}(a,b_j) \right] \Bigg\} \\ & - \frac{1}{K_T(0) - K_m} \Bigg\{ K_m^{-b_j} \left[B_{\frac{K_m}{R_{j-1}}}(a,b_j) - B_{\frac{K_m}{R_j}}(a,b_j) \right] \\ & - K_T(0)^{-b_j} \left[B_{\frac{K_T(0)}{R_{j-1}}}(a,b_j) - B_{\frac{K_T(0)}{R_j}}(a,b_j) \right] \Bigg\} \end{aligned} \tag{7.29}$$

Eq. 2.18 reduces to Eq. 2.15 if a single power fit for the energy spectrum is valid when $R \geq K_0$.

7.6 DOSE CALCULATION FOR PARTICULAR CASES

7.6.1 Specified Dose at Phantom Center without Self-Shielding

When the phantom radius tends to zero, only protons normally incident on the shield may impinge on the phantom. Then

$$K_m = K_0 + K_1 = K_0 + e^2 k_1$$

with

$$k_1 = \frac{1}{2} \sum_{i=1}^{j} \left(\frac{1}{r_{i-1}} - \frac{1}{r_i} \right) \quad \text{(see Eq. 2.11)}$$

Also,

$$K_m^{-b} = K_0^{-b} \left(1 + e^2 \frac{k_1}{K_0} \right)^{-b} \approx K_0^{-b} \left[1 - \frac{b k_1}{K_0} e^2 + \frac{b(b+1)}{2} \frac{k_1^2}{K_0^2} e^4 \right]$$

when $e << 1$.

Similarly,

$$K_T(0)^{-b} = K_0^{-b} \left(1 + 2A_T \frac{e}{K_0} \right)^{-b} \approx K_0^{-b} \left[1 - b \frac{2A_T}{K_0} e + \frac{b(b+1)}{2} \frac{4A_T^2}{2} e^2 \right]$$

when $e << 1$.

When e tends to zero, Eq. 2.15 becomes

$$D = D(0) = b(b+1) \beta A_T \frac{B(a,b)}{K_0^{b+2}} = b(b+1) A_T \frac{C}{K_0^{b+2}} \qquad (2.20)$$

which is the dose rate at the center of the void.

7.6.2 The Case of Very Large Void Radius

Assuming that

$$K_m = K_0(1+\delta)$$

where δ is a small number, then even if the phantom radius is large, when δ tends

to 0, Eq. 2.15 becomes

$$D = \frac{\beta}{e} B(a,b) \left[bK_0^{-(b+1)} - \frac{K_0^{-b} - (K_0 + 2 A_T e)^{-b}}{2 A_T e} \right] \tag{7.30}$$

which is the dose when $r_0 >> e$.

If

$$x = \frac{K_0}{2 A_T e} ,$$

then

$$D = \frac{\beta}{e} \frac{B(a,b)}{K_0^{(b+1)}} \left\{ b - x \left[1 - \left(\frac{x}{1+x} \right)^b \right] \right\} \tag{7.31}$$

Then, when $x << 1$,

$$D = b \frac{\beta}{e} \frac{B(a,b)}{K_0^{b+1}} ,$$

and when $x >> 1$,

$$D = b(b+1) \beta A_T \frac{B(a,b)}{K_0^{b+2}}$$

which is the case of $e << 1$ studied in Section 7.6.1 (Eq. 2.20).

7.6.3 Case of Normal Incidence

Assuming that all protons from the flare penetrate the shield and the phantom at zero angle, the average body dose becomes

$$D = b \frac{\beta}{e} B(a,b) \left[K_0^{-(b+1)} - (K_0 + 2 A_T e)^{-(b+1)} \right] \tag{7.32}$$

where a, b, β have been defined in Eqs. 7.20, 7.24, and 7.22, respectively.

When e tends to zero, Eq. 7.32 becomes

$$D = 2\,b(b+1)\,A_T\beta\,\frac{B(a,b)}{K_0^{b+2}} \tag{7.33}$$

7.6.4 Specified Dose at the Phantom Center with Self-Shielding

If the average body dose is desired in a concentric spherical tissue region inside the phantom of radius e′ (e′ < e), Eq. 2.15 applies by replacing e by e′,

$$K_0 \quad \text{by} \quad \sum_{i=1}^{j} \Delta A_i r_i - A_1 r_0 + A_T(e-e')$$

$$K_m \text{ by } \sum_{i=1}^{j} \Delta A_i\,(r_i^2 - e'^2)^{1/2} - A_1(r_0^2 - e'^2)^{1/2} + A_T(e^2 - e'^2)^{1/2}$$

$$K_T(0) \text{ by } \sum_{i=1}^{j} \Delta A_i r_i - A_1 r_0 + A_T(e+e').$$

As e′ tends to zero, it can be shown that Eq. 2.18 holds if we replace

K_0 by $K_0 + A_T e$.

Hence, the dose in an infinitesimally small sample of tissue located at the phantom center is given by

$$D(\text{center}) = b(b+1)\,\beta A_T\,\frac{B(a,b)}{(K_0+A_T e)^{b+2}} \tag{2.21}$$

7.6.5 Depth Dose

The specific requirement in this case is to evaluate the proton energy per gram of tissue deposited in a shell of thickness de′ located at r = e′ ($0 \leq e' \leq e$) when de′ tends to zero. The radius of phantom is e. If $D_v(e')$represents the average body dose in a sphere of radius e′, then the depth dose, D_p, at r = e′, is given by

$$4\pi\rho_T e'^2\, de'\, D_p(e') = \frac{4}{3}\pi\rho_T \frac{d}{de'}\left[e'^3 D_v(e')\right] de'$$

or

$$D_p(e') = \frac{1}{3e'^2}\frac{d}{de'}\left[e'^3 D_v(e')\right] \tag{7.34}$$

The analytical expression for the average body dose, D_v, is obtained from Eq. 7.26 and can be written as

$$D_v(e') = \frac{C}{e'} f(K_0', K_m') \tag{7.35}$$

Substituting Eq. 7.35 into Eq. 7.31 gives

$$D_p(e') = \frac{C}{3e'^2}\frac{d}{de'}\left(e'^2 f\right)$$

or

$$D_p(e') = \frac{C}{3}\left[\frac{2f}{e'} + \frac{df}{de'}\right] \tag{7.36}$$

To obtain a compact expression for the depth dose, K_m' is expanded in series, assuming e′ small compared to r_i, and using the two first terms of the expansion in the calculations. Thus,

$$K'_m = K_0 + A_T e + \frac{e'^2}{2}\left(\frac{A_1}{r_0} - \sum_{i=1}^{j}\frac{\Delta A_i}{r_i} - \frac{A_T}{e}\right) \tag{7.37}$$

and

$$\frac{dK'_m}{de'} = \frac{2(K'_m - K'_0)}{e'} - 2A_T \tag{7.38}$$

or

$$\frac{dK'_m}{de'} = \frac{2[K'_m - (K'_0 + 2A_T e')]}{e'} + 2A_T \tag{7.39}$$

Hence, it can be shown that

$$D_p(e') = \frac{A_T C}{3}\left\{\left[\frac{K_0^{-b} - K_m'^{-b}}{(K'_m - K'_0)^2} - \frac{K_m'^{-b} - (K'_0 + 2A_T e')^{-b}}{(K'_0 + 2A_T e' - K'_m)^2}\right]\right.$$

$$\left. + b\left[\frac{K_0'^{-(b+1)} - 2K_m'^{-(b+1)}}{K'_m - K'_0} + \frac{2K_m'^{-(b+1)} - (K'_0 + 2A_T e')^{-(b+1)}}{K'_0 + 2A_T e' - K'_m}\right]\right\} \tag{2.22}$$

In particular, if $e' = e$, the skin dose, $D_p(e)$ is obtained. Thus, in Eq. 2.22, K'_0 would equal K_0, the aluminum equivalent shield thickness and $K'_0 + 2A_T e' = K_0 + 2A_T e$, the aluminum equivalent shield and tissue thickness. Also,

$$K'_m = K_m = \sum_{i=1}^{j} \Delta A_i (r_i^2 - e^2)^{1/2} - A_1 (r_0^2 - e^2)^{1/2}$$

which is the aluminum equivalent path length through the shield in the direction tangent to the man volume.

If $e' = 0$, $K'_0 = K'_m = K'_0 + 2A_T e' = K_0 + A_T e$, Eq. 2.22 shows that $D_p(0)$ is undetermined for $e' = 0$.

However, for $e' << 1$, the following expansions can be used for $K_0'^{-n}$, $(K_0' + 2A_T e')^{-n}$ and $(K_m')^{-n}$.

$$K_0'^{-n} = (K_0 + A_T e)^{-n} \left[1 + \frac{nA_T}{K_0 + A_T e} e' + \frac{n(n+1)}{2} \left(\frac{A_T e'}{K_0 + A_T e} \right)^2 + \ldots \right] \quad (7.40)$$

$$(K_0' + 2A_T e')^{-n} = (K_0 + A_T e)^{-n} \left[1 - n \frac{A_T e'}{K_0 + A_T e} + \frac{n(n+1)}{2} \left(\frac{A_T e'}{K_0 + A_T e} \right)^2 + \ldots \right] \quad (7.41)$$

$$K_m'^{-n} = (K_0 + A_T e)^{-n} \left[1 - n \frac{k_1 e'^2}{2(K_0 + A_T e)} + \frac{n(n+1)}{2} \left(\frac{k_1 e'^2}{2(K_0 + A_T e)} \right)^2 + \ldots \right] \quad (7.42)$$

where

$$k_1 = \frac{A_1}{r_0} - \sum_{i=1}^{j} \frac{A_i}{r_i} - \frac{A_T}{e}$$

Introducing Eqs. 7.40, 7.41, and 7.42 into Eq. 2.22 yields for the center dose ($e' \to 0$)

$$D_p(0) = b(b+1)\, A_T C\, (K_0 + A_T e)^{-(b+2)} \quad (2.21)$$

This is exactly the analytical expression found directly in Section 7.6.4 (Eq. 2.21). Indeed, $D_p(0)$ can be considered as the average body dose in an infinitesimally small spherical volume of tissue located at the phantom center.

8. APPENDIX B – THE INTEGRATION OF I_1 AND I_2

8.1 THE INTEGRATION OF I_1

$$I_1 = \int_0^{\varphi_0} E' \sin \varphi \cos \varphi \, d\varphi \tag{8.1}$$

where

$$E' = [(n+1)\alpha]^{\frac{1}{n+1}} \, [R-K(\varphi)]^{\frac{1}{n+1}} , \tag{8.2}$$

with

$$K(\varphi) = K_0 + K_1 \sin^2 \varphi$$

or

$$K(\varphi) = K_0 + (K_m - K_0) \sin^2 \varphi \tag{8.3}$$

and

$\varphi_0 = \frac{\pi}{2}$ if $R \geq K_m$, and

$0 < \varphi_0 < \pi/2$ if $R < K_m$.

The limit of the integral is then obtained by solving the following equation

$$R = K_0 + (K_m - K_0) \sin^2 \varphi \tag{8.4}$$

If in Eq. 8.1 the variables are changed so that

$$u = R - K(\varphi) \tag{8.5}$$

then

$$I_1 = \frac{[(n+1)\alpha]^{\frac{1}{n+1}}}{2(K_m - K_0)} \int_{u_0}^{R-K_0} u^{\frac{1}{n+1}} \, du \tag{8.6}$$

where $u_0 = R - K_m$ if $\varphi_0 = \pi/2$

otherwise $u_0 = 0$.

Integrating Eq. 8.6 yields

$$I_1 = \frac{1}{2} \frac{n+1}{n+2} \frac{[(n+1)\alpha]^{\frac{1}{n+1}}}{K_m - K_0} \left[(R - K_0)^{\frac{1}{n+1} + 1} - u_0^{\frac{1}{n+1} + 1} \right] \tag{8.7}$$

Now, $R_0' = R - K_0$ and $R_m' = R - K_m$ represent the range in aluminum of protons incident on the phantom normally and tangentially, respectively. From the energy-range relationship Eq. 2.14, if E_0' and E_m' are the energies corresponding to R_0' and R_m' respectively, Eq. 8.7 can be written as

$$\begin{aligned} I_1 &= \frac{1}{2} \frac{n+1}{n+2} \frac{E_0' R_0'}{K_m - K_0} && \text{if } R \leq K_m \text{ (or } \varphi_0 < \pi/2) \\ I_1 &= \frac{1}{2} \frac{n+1}{n+2} \frac{E_0' R_0' - E_m' R_m'}{K_m - K_0} && \text{if } R > K_m \text{ (or } \varphi_0 = \pi/2) . \end{aligned} \tag{8.8}$$

8.2 THE INTEGRATION OF I_2

$$I_2 = \int_{\varphi_1}^{\pi/2} E'' \sin \varphi \cos \varphi \, d\varphi \tag{8.9}$$

where

$$E'' = [(n+1)]^{\frac{1}{n+1}} \; [R - K_T(\varphi)]^{\frac{1}{n+1}} \tag{8.10}$$

with

$$K_T(\varphi) = K_m + 2A_T e \cos \varphi - (K_m - K_0) \cos^2 \varphi$$

or

$$K_T(\varphi) = K_m + [K_T(0) - K_0] \cos \varphi - (K_m - K_0)\cos^2 \varphi \tag{8.11}$$

and

$$\varphi_1 = 0 \qquad \text{if } R \geq K_T(0)$$

$$0 < \varphi_1 < \pi/2 \qquad \text{if } R < K_T(0)$$

ϕ_1 is obtained by solving the equation

$$R - K_m - 2A_T e \cos \varphi_1 + (K_m - K_0) \cos^2 \varphi_1 = 0 \tag{8.12}$$

where $0 < \cos \varphi_1 < 1$.

Since $K_T(\varphi)$ was shown to be monotonic in all practical cases, there is just one solution to Eq. 8.12.

Upon the change of variables, $x = \cos \varphi$, Eq. 8.9 becomes

$$I_2 = [(n+1)\alpha]^{\frac{1}{n+1}} \int_0^{\cos \varphi_1} [R - K_m - 2A_T e + (K_m - K_0)x^2]^{\frac{1}{n+1}} x\,dx \qquad (8.13)$$

Eq. 8.13 can be written as follows:

$$I_2 = \frac{[(n+1)\alpha]^{\frac{1}{n+1}}}{2(K_m - K_0)} \int_0^{\cos \varphi_1} [R - K_m - 2A_T e\,x + (K_m - K_0)x^2]^{\frac{1}{n+1}}$$

$$\times [-2A_T e + 2(K_m - K_0)x]\,dx + [(n+1)\alpha]^{\frac{1}{n+1}} \frac{A_T e}{K_m - K_0}$$

$$\times \int_0^{\cos \varphi_1} [R - K_m - 2A_T e\,x + (K_m - K_0)x^2]^{\frac{1}{n+1}}\,dx \qquad (8.14)$$

The first term on the right-hand side of Eq. 8.14 can be integrated, and since $2A_T e = K_T(0) - K_0$,

$$I_2 = \frac{1}{2} \frac{n+1}{n+2} \frac{[(n+1)\alpha]^{\frac{1}{n+1}}}{K_m - K_0} \left\{ [R - K_T(\varphi_1)]^{\frac{n+2}{n+1}} - (R - K_m)^{\frac{n+2}{n+1}} + \frac{n+2}{n+1} [K_T(0) - K_0] I_3 \right\} \qquad (8.15)$$

where

$$I_3 = \int_0^{\cos \varphi_1} [R - K_m - 2A_T e\,x + (K_m - K_0)\,x^2]^{\frac{1}{n+1}}\,dx \qquad (8.16)$$

If $\overline{K}_T(\varphi)$ is used rather than $K_T(\varphi)$ in Eq. 8.16 where

$$\overline{K}_T(\varphi) = K_m + [K_T(0) - K_m] \cos \varphi$$

I_3 becomes

$$I_3 = \int_0^{\cos \varphi_1} \{R - K_m - [K_T(0) - K_m]x\}^{\frac{1}{n+1}} \, dx$$

$$I_3 = \frac{n+1}{n+2} \frac{1}{K_T(0) - K_m} (R - K_m)^{\frac{n+2}{n+1}} - [R - \overline{K}_T(\varphi_1)]^{\frac{n+2}{n+1}} \tag{8.17}$$

Introducing Eq. 8.17 into Eq. 8.16, and assuming $K_T(\varphi_1) = \overline{K}_T(\varphi_1)$ within a good approximation,

$$I_2 = \frac{1}{2} \frac{n+1}{n+2} \frac{[(n+1)\alpha]^{\frac{1}{n+1}}}{K_T(0) - K_m} \left\{ (R - K_m)^{\frac{n+2}{n+1}} - [R - K_T(\varphi_1)]^{\frac{n+2}{n+1}} \right\} \tag{8.18}$$

Now $R''_m = R'_m = R - K_m$ and $R''_0 = R - K_T(0)$ represent the range in aluminum of protons emerging along a normal and tangent to the phantom, respectively. If E'_m and E''_0 are the energies corresponding to R'_m and R''_0, respectively, using Eq. 2.14 I_2 becomes

$$I_2 = \frac{1}{2} \frac{n+1}{n+2} \frac{E'_m R'_m}{K_T(0) - K_m} \qquad \text{if } K_m < R \leq K_T(0)$$

$$I_2 = \frac{1}{2} \frac{n+1}{n+2} \frac{E'_m R'_m - E''_0 R''_0}{K_T(0) - K_m} \qquad \text{if } R > K_T(0). \tag{8.19}$$

9. APPENDIX C – EVALUATION OF THE AVERAGE BODY DOSE

The average body dose, D, is given by

$$D = \int_0^\infty F_V(E)\, P(E)\, dE \tag{9.1}$$

where $P(E) = C_1 E^{-m}$ is the incident proton spectrum and $F_V(E)$ is the energy deposition rate in the body.

If the range, R, is used as a variable rather than the energy, E, from Eq. 2.14

$$E = [\alpha(n+1)]^{\frac{1}{n+1}}\, R^{\frac{1}{n+1}} \tag{9.2}$$

$$dE = [\alpha(n+1)]^{\frac{1}{n+1}}\, \frac{R^{-\frac{1}{n+1}}}{n+1}\, dR \tag{9.3}$$

Hence,

$$P(E)dE = C_1 \frac{[\alpha(n+1)]^{\frac{m-1}{n+1}}}{n+1}\, R^{-\frac{m+n}{n+1}}\, dR \tag{9.4}$$

Using the expressions of $F_V(R)$ in Table 3, Eq. 1 can be written as

$$D = \frac{\epsilon C_1}{K_m - K_0} \frac{\alpha(n+1)^{-\frac{m-2}{n+1}}}{n+1} \left[\int_{K_0}^{\infty} \frac{(R-K_0)^{\frac{n+2}{n+1}}}{R^{\frac{m+n}{n+1}}} dR - \int_{K_m}^{\infty} \frac{(R-K_m)^{\frac{n+2}{n+1}}}{R^{\frac{m+n}{n+1}}} dR \right]$$

$$- \frac{\epsilon C_1}{K_T(0) - K_m} \frac{\alpha(n+1)^{-\frac{m-2}{n+1}}}{n+1} \left[\int_{K_m}^{\infty} \frac{(R-K_m)^{\frac{n+2}{n+1}}}{R^{\frac{m+n}{n+1}}} dR \right.$$

$$\left. - \int_{K_T(0)}^{\infty} \frac{[R-K_T(0)]^{\frac{n+2}{n+1}}}{R^{\frac{m+n}{n+1}}} dR \right] \tag{9.5}$$

Let

$$\beta = \frac{\epsilon C_1}{n+1} [\alpha(n+1)]^{-\frac{m-2}{n+1}} = \frac{3C_1}{4e\rho_T} \frac{[\alpha(n+1)]^{-\frac{m-2}{n+1}}}{n+2} \tag{9.6}$$

where

$$a = \frac{n+2}{n+1} + 1 \tag{9.7}$$

$$b = \frac{m-n-3}{n+1} . \tag{9.8}$$

In each integral, we change variables such that the limits of integration are 0 and ∞, then we obtain

$$D = \beta \left[\frac{K_0^{-b} - K_m^{-b}}{K_m - K_0} - \frac{K_m^{-b} - K_T(0)^{-b}}{K_T(0) - K_m} \right] \quad (I) \tag{9.9}$$

where

$$I = \int_0^{\infty} \frac{y^{(a-1)}}{(y+1)^{(a+b)}}\, dy \tag{9.10}$$

which is by definition the beta function if $a > 0$ and $b > 0$, i.e.,

$$I = B(a,b) = \frac{\Gamma(a)\,\Gamma(b)}{\Gamma(a+b)} \tag{9.11}$$

Now and and $a+b = (m+n)/(n+1)$ are always positive. However, b is positive only if $m > n + 3$. As b tends toward 0, I becomes infinite. Now show that D tends toward a finite value when $b \to 0$.

$$[\Gamma(b)]_{b\to 0} \approx \frac{1}{b}$$

$$K_0^{-b} - K_m^{-b} \approx b\,(\log K_m - \log K_0) = b \log \frac{K_m}{K_0}$$

$$K_m^{-b} - K_T(0)^{-b} \approx b\,[\log K(0) - \log K_m] = b \log \frac{K_T(0)}{K_0}$$

Therefore, as b approaches 0, D tends to the value D_0 where

$$D_0 = \beta \left[\frac{\log(K_m/K_0)}{K_m - K_0} - \frac{\log(K_T(0)/K}{K_T(0) - K_m} \right] \tag{9.12}$$

If b is negative and tends to zero by negative values, I tends to $-\infty$, but D still tends toward D_0. Hence, D is continuous at $b = 0$. When

$$-1 < b < 0, \quad I < 0,$$

and

$$\left[\frac{K_0^{-b} - K_m^{-b}}{K_m - K_0} - \frac{K_m^{-b} - K_T(0)^{-b}}{K_T(0) - K_0}\right] \qquad < 0$$

such that D remains positive.

Now, from the values of m in Table 1, b cannot be less than -2, since if b = -2, then m = 1 - n = 1 - 0.786 = 0.214. For all flares, m > 0.7. Therefore, we have to show that Eq. 9.11 gives a finite value for the dose as b tends toward -1 by higher and lower values and that the dose is positive for $-2 < b < -1$.

Let $b = -1 + \delta$, where δ is a small positive or negative number.

Then

$$\frac{\Gamma(a)\,\Gamma(b)}{\Gamma(a+b)} = \frac{\Gamma(a)\,\Gamma(-1+\delta)}{\Gamma(a+\delta-1)} = \frac{\Gamma(a)\,\Gamma(\delta)}{\Gamma(a+\delta)} \times \frac{a+\delta-1}{\delta-1}$$

and as $\delta \to 0$,

$$I = \frac{\Gamma(a)\,\Gamma(b)}{\Gamma(a+b)} \quad [-(a-1)]\,. \tag{9.13}$$

On the other hand,

$$K_0^{-b} = K_0\, e^{-\delta \log K_0} \approx K_0(1 - \delta \log K_0)$$

$$K_m^{-b} = K_m\, e^{-\delta \log K_m} \approx K_m(1 - \delta \log K_m) \tag{9.14}$$

$$K_T(0)^{-b} = K_m\, e^{-\delta \log K_T(0)} \approx K_T(0)\ [1 - \delta \log K_T(0)]$$

Substituting Eqs. 9.13 and 9.14 into Eq. 9.9 yields the following, as $\delta \to 0$ and D tends toward D_{-1}

$$D_1 = +(a-1)\beta \left\{ \frac{\log (K_m/K_0)}{K_m - K_0} - \frac{\log [K_T(0)/K_0]}{K_T(0) - K_0} \right\} \tag{9.15}$$

which does not depend on the sign of δ, and D_{-1} is positive since from Eq. 9.7 $a > 1$.

Let b equal a number between -1 and -2. Then $\Gamma(b)$ is positive and therefore $B(a,b) > 0$.

Since

$$K_T(0) > K_m > K_0,$$

then

$$\frac{K_0^{-b} - K_m^{-b}}{K_m - K_0} - \frac{K_m^{-b} - K_T(0)^{-b}}{K_T(0) - K_0} > 0 \qquad \text{if } -2 < b < -1.$$

Therefore,

$$D > 0$$

when

$$-2 < b < -1.$$

10. APPENDIX D – THE SOLUTION OF THE LAGRANGE MULTIPLIER EQUATION

The equation to be solved is

$$r_i^2 - \nu \frac{\Delta A_i}{\Delta \rho_i} - \eta \frac{\Delta A_i}{\Delta \rho_i} \left(\frac{r_2}{\sqrt{r_i^2 - e^2}} - 1 \right) = 0 \tag{10.1}$$

in which

$$r_i \geq e > 0. \tag{10.2}$$

Also, from Eq. 2.27 we have

$$\nu = \nu' + \eta > \eta > 0 \tag{10.3}$$

If we define

$$x = r_i^2$$

$$x_0 = \frac{\Delta A_i}{\rho_i}$$

$$S = \eta \frac{\Delta A_i}{\rho_i} ,$$

Eq. 10.1 can be written as

$$\frac{x - x_0}{S} = \frac{1}{\left(1 - \frac{e^2}{x}\right)^{1/2}} \tag{10.4}$$

From Eq. 10.2, it can be shown that the left hand side of Eq. 10.4 is positive. Therefore,

$$x \geq x_0 > 0 \tag{10.5}$$

where $x = x_0$ if $e = 0$.

On the other hand, from Eq. 10.3 we can write

$$x_0 - S > 0 \tag{10.6}$$

Eq. 10.4 now can be transformed as follows:

$$(x - x_0 + S)^2 \ (x - e^2) = S^2 x$$

or

$$x(x-x_0) \ (x-x_0+2S) = e^2(x-x_0+S)^2. \tag{10.7}$$

The solutions of Eq. 10.7 are given by the intersections of the parabola $y_1 = e^2(x - x_0 + s)^2$ and the cubic $y_2 = x(x - x_0) \ (x - x_0 + 2S)$. But, from Eq. 10.5, the desired solution must be greater than x_0. Since $x_0 - S > 0$, two cases are possible in view of the zeros of the cubic: $x_0 - 2S < 0$ and $x_0 - 2S > 0$. y_1 and y_2 are plotted for both cases in Fig. 27.

The plots show that there are up to three real and positive solutions for Eq. 10.7 but that one and only one solution is such that $x > x_0$.

Hence, if one makes the change of variable, $X = x - x_0$ in Eq. 10.7, and solves the cubic equation in X, one gets only one real root such that $X > 0$.

Eq. 10.7 then becomes

$$X(X+x_0) \ (X+2S) = e^2(X+S)^2 = 0$$

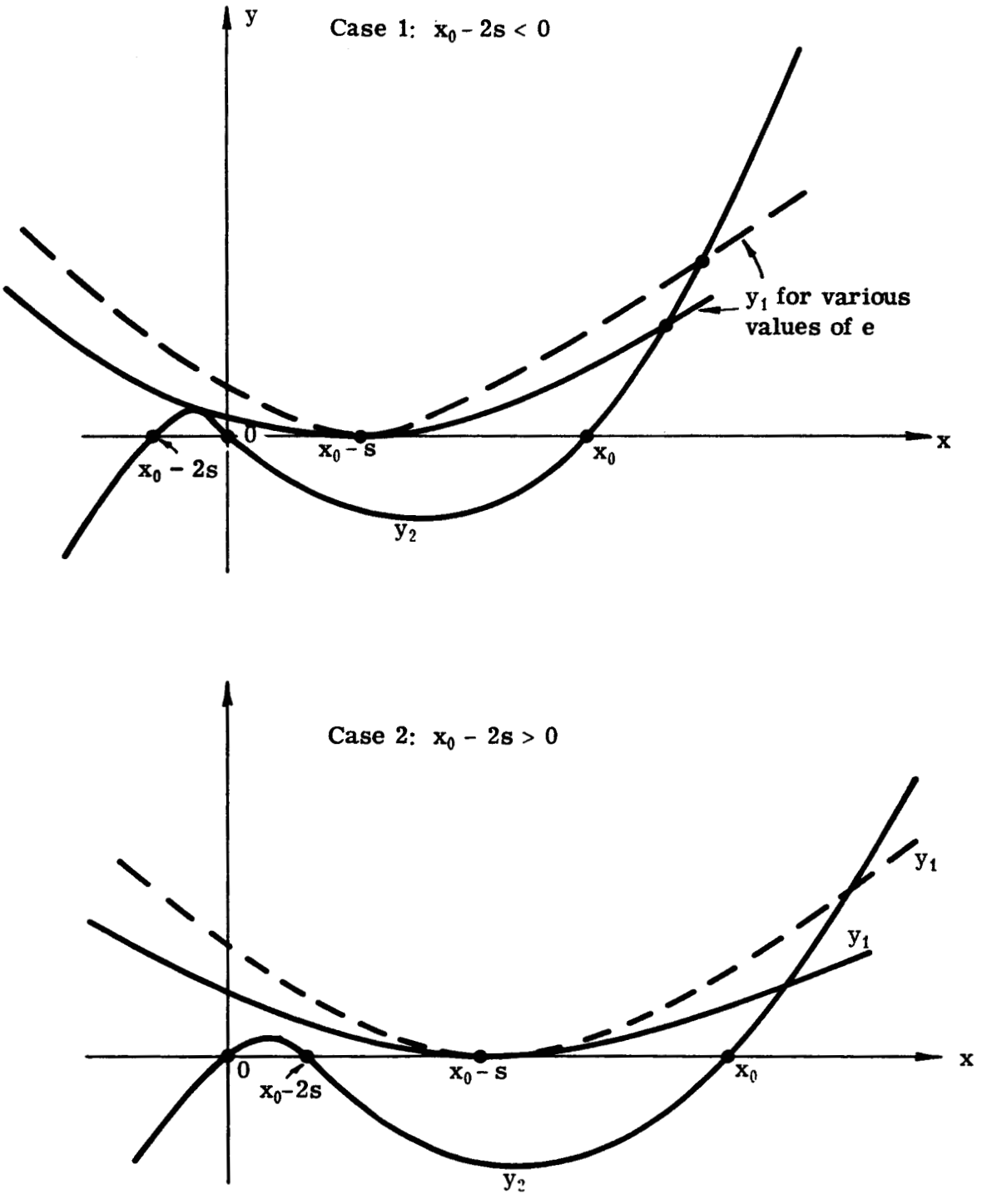

Fig. 27 — Solutions of Eq. 10.7

or

$$X^3 + (x_0 + 2S - e^2)\, X^2 + 2S(x_0 - e^2)X + e^2S^2 = 0. \tag{10.8}$$

Now let

$$\begin{aligned} p &= x_0 - e^2 + 2S \\ q &= 2S(x_0 - e^2) \\ t &= e^2S^2 \end{aligned} \tag{10.9}$$

and

$$\begin{aligned} a &= 1/3\ (3q - p^2) \\ b &= 1/27\ (2p^3 - 9pq + 27t) \end{aligned} \tag{10.10}$$

One can then compute the discriminant

$$\Delta = \frac{b^2}{4} + \frac{a^3}{27} \tag{10.11}$$

If $\Delta > 0$, there will be only one real root

$$X = \frac{p}{3} + \left(\sqrt{\Delta} - \frac{b}{2}\right)^{1/3} - \left(\sqrt{\Delta} + \frac{b}{2}\right)^{1/3} \tag{10.12}$$

If $\Delta < 0$, there will be three real roots. The desired solution will then be obtained as follows:

Compute

$$\cos\varphi = \left(\frac{b^2/4}{|a^3/27|}\right)^{1/2} \tag{10.13}$$

Compute the value of the angle φ. Then the solution is given by

$$X = \frac{p}{3} + 2\left|\frac{a}{3}\right|^{1/2} \cos\frac{\varphi}{3}. \tag{10.14}$$

11. REFERENCES

1. A.D. Krumbein, et al., Synthesis of Minimum Weight Proton Shields, UNC-5049 (Feb. 25, 1963).
2. H.W. Bertini, Monte Carlo Calculations on Intranuclear Cascades, ORNL-3383 (May 1963).
3. H.W. Bertini, Description of Printed Output from Intranuclear Cascade Calculations, ORNL-TM-480 (Feb. 1963).
4. H.W. Bertini, A Literature Survey of Nonelastic Reactions for Nucleons and Pions Incident on Complex Nuclei at Energies Between 20 Mev and 33 Bev, ORNL-3455 (Aug. 1963).
5. D. Halliday, "Introductory Nuclear Physics," 2nd Ed., p. 155, John Wiley and Sons, Inc., New York 1958.
6. J.R. Winckler and P.S. Bhavsar, J. of Geophys. Res., 65:2647 (1960).
7. H.J. Schaefer, A Note on the Influence of Shield Geometry on Air Dose and Tissue Dose from Protons Within a Space Vehicle, Fig. 6, NASA-CR-50780 (Apr. 1963).
8. M. Slater, Lagrange Multipliers Revisited, Cowles Foundation Discussion Paper, Math-403 (Nov. 1950); Reprinted as Cowles Foundation Discussion Paper No. 80 (Oct. 1959).
9. E.S. Troubetzkoy, Shield Weight Minimizing Equation, UNC Phys/Math-2621 (Sept. 21, 1962).
10. H.W. Bertini, Private Communication.
11. D.J. Hughes and R.B. Schwartz, Neutron Cross Sections, 2nd Ed., BNL-325 (July 1958).
12. H. Goldstein, "Fundamental Aspects of Reactor Shielding," Addison-Wesley Publishing Co., Cambridge, Mass., 1959.

13. H. Bateman, Higher Transcendental Functions, p. 85, Vol. I, McGraw Hill Book Co., (1953).

14. J.A. Greenwood and H.O. Hartley, "Guide to Tables in Mathematical Statistics," pp. 197-202, Princeton University Press, Princeton, N.J., 1962.

15. K. Pearson, Tables of the Incomplete Beta Function, pp. 423-426, Biometrika 38 (1934).

DISTRIBUTION

	No. of Copies
George C. Marshall Space Flight Center National Aeronautics and Space Administration Huntsville, Alabama	40 *

*Plus 1 reproducible.